

DOCTORAL THESIS

Design of Composite Pulse Sequences for Quantum Technologies

Author:

Hayk L. GEVORGYAN

Supervisor:

Acad. Prof. DSc.
Nikolay V. VITANOV

A thesis submitted in fulfillment
of the requirements for the degree of
Doctor of Philosophy

Department of Theoretical Physics
Group of Quantum Optics and Quantum Information



SOFIA UNIVERSITY ST. KLIMENT OHRIDSKI
Sofia, Bulgaria

May 2023

Design of Composite Pulse Sequences for Quantum Technologies, © May 2023

Author:

Hayk L. GEVORGYAN

Supervisor:

Acad. Prof. DSc. Nikolay V. VITANOV

Institute:

SOFIA UNIVERSITY ST. KLIMENT OHRIDSKI, Sofia, Bulgaria

CONTENTS

List of Figures	vi
List of Tables	ix
Abstract	xiii
Declaration of Authorship	xv
Acknowledgments	xvii
Acronyms	xxi
1 INTRODUCTION	1
1.1 Quantum coherent control techniques	1
1.2 Rotations on the Bloch sphere	1
1.2.1 Rotation gate	2
1.2.2 Phase-shift gate	4
1.3 Composite pulses in nuclear magnetic resonance	5
1.4 Thesis Outline	8
2 COMPOSITE PULSES FOR ROBUST ULTRAHIGH-FIDELITY ROTATION	
GATES	11
2.1 Introduction	11
2.2 SU(2) Approach	14
2.2.1 Quantum gate fidelity	16
2.2.2 Composite pulse sequences	17
2.3 X (NOT) gate	18
2.3.1 First-order error compensation	19
2.3.2 Second-order error compensation	20
2.3.3 Higher-order error compensation	22
2.4 Hadamard gate	23
2.4.1 First-order error correction	24
2.4.2 Second-order error correction	25
2.4.3 Higher-order error correction	25
2.5 General rotation gate	27

2.5.1	First-order error correction	27
2.5.2	More than three pulses	27
2.6	Comments and conclusions	28
3	COMPOSITE PULSES FOR ROBUST ULTRAHIGH-FIDELITY PHASE GATES	37
3.1	Introduction	37
3.2	SU(2) Approach	39
3.3	Broadband composite phase gates	40
3.3.1	Design for composite phase gates	40
3.3.2	General Phase-shift gate	40
3.4	Comments and conclusions	53
4	NARROWBAND AND PASSBAND COMPOSITE PULSES: APPLICATION TO QUANTUM SENSING	55
4.1	Introduction	55
4.2	Derivation	57
4.2.1	Narrowband composite pulses	57
4.2.2	Passband composite pulses	59
4.2.3	Performance measures	60
4.3	X gate	61
4.3.1	Narrowband	61
4.3.2	Passband	62
4.4	Hadamard gate	64
4.4.1	Narrowband	64
4.4.2	Passband	65
4.5	General rotation gate	65
4.5.1	Narrowband	65
4.5.2	Passband	67
4.6	Conclusions	68
5	DETERMINISTIC GENERATION OF ARBITRARY ULTRASMALL EXCITATION OF QUANTUM SYSTEMS BY COMPOSITE PULSE SEQUENCES	85
5.1	Introduction	85
5.2	The method	88
5.3	Small-probability composite sequences	89
5.3.1	Two-pulse composite sequences	89
5.3.2	Three-pulse composite sequences	91
5.3.3	Four-pulse composite sequences	95
5.3.4	Higher number of pulses	96
5.4	Quantum gates for ultrasmall rotations	99

5.4.1	First-order error compensation	99
5.4.2	Second-order error compensation	100
5.5	Conclusions	101
6	COMPOSITE PULSES FOR ULTRAROBUST OR ULTRASENSITIVE CONTROL	103
6.1	Introduction and motivation	103
6.2	Jones matrices and on the quantum-classical analogy	104
6.3	Derivation Method	105
6.3.1	Ultra-BB, ultra-NB and ultra-PB	107
6.4	Ultrabroadband rotational $\theta = \pi$ pulses	108
6.5	Ultranarrowband rotational $\theta = \pi$ pulses	109
6.6	Ultrabroadband phasal $\zeta = \pi$ pulses	110
6.7	Comments and conclusions	111
7	BROADBAND COMPOSITE NONRECIPROCAL POLARIZATION WAVE PLATES AND OPTICAL ISOLATORS	117
7.1	Introduction	117
7.2	Background	118
7.3	Composite wave plate	119
7.4	Broadband optical isolator	120
7.5	Numerical calculations	121
7.6	Conclusions	124
8	GENERAL CONCLUSIONS AND PERSPECTIVES	127
	APPENDICES	129
A	PUBLICATIONS AND PRESENTATIONS	129
A.1	Publications	129
A.2	Presentations	129
	BIBLIOGRAPHY	130

LIST OF FIGURES

Figure 2.1	Frobenius distance fidelity \mathcal{F} (solid) and trace distance fidelity \mathcal{F}_T (dashed) of composite X gates. The numbers N on the curves refer to composite sequences XN listed in Table 2.1.	20
Figure 2.2	Frobenius distance fidelity F (top) and infidelity (bottom) of composite X gates. The infidelity is in logarithmic scale in order to better visualize the high-fidelity (low-infidelity) range. The numbers N on the curves refer to composite sequences XN listed in Table 2.1.	30
Figure 2.3	Frobenius distance fidelity (top) and infidelity (bottom) of composite Hadamard gates produced by using the symmetric composite sequences HN s from Table 2.2.	31
Figure 3.1	Frobenius distance fidelity F (top) and infidelity (bottom) of composite Z gates. The infidelity is in logarithmic scale in order to better visualize the high-fidelity (low-infidelity) range. The numbers N on the curves refer to Composite Pulse (CP) sequences ZN listed in the Table 3.1.	46
Figure 3.2	Frobenius distance fidelity F (top) and infidelity (bottom) of composite S gates. The infidelity is in logarithmic scale in order to better visualize the high-fidelity (low-infidelity) range. The numbers N on the curves refer to Composite Pulse (CP) sequences SN listed in the Table 3.2.	47
Figure 3.3	Frobenius distance fidelity F (top) and infidelity (bottom) of composite T gates. The infidelity is in logarithmic scale in order to better visualize the high-fidelity (low-infidelity) range. The numbers N on the curves refer to Composite Pulse (CP) sequences TN listed in the Table 3.3.	48
Figure 4.1	Frobenius distance fidelity (top) and infidelity (bottom) of composite narrowband Hadamard gates produced by the four families of composite sequences from the Table 4.3.	64
Figure 4.2	Frobenius distance fidelity (top) and infidelity (bottom) of composite narrowband X gates produced by the antisymmetric composite sequences AN s (3,7,11 pulses) and WN s (5,9,13 pulses) from the Table 4.1.	69

Figure 4.3	Frobenius distance fidelity (top) and infidelity (bottom) of composite X gates produced by the antisymmetric composite sequences AN-m designed by the regularization method from the Table 4.2.	70
Figure 4.4	Frobenius distance fidelity (top) and infidelity (bottom) of composite passband X gates produced by PN (pari passu) sequences from the Table 4.4.	71
Figure 4.5	Frobenius distance fidelity (top) and infidelity (bottom) of composite passband X gates produced by DN (diversis passuum) sequences from the Table 4.6.	72
Figure 4.6	Frobenius distance fidelity (top) and infidelity (bottom) of composite passband Hadamard gates produced by PN (pari passu) sequences from the Table 4.5.	73
Figure 4.7	Frobenius distance fidelity (top) and infidelity (bottom) of composite passband Hadamard gates produced by DN (diversis passuum) sequences from the Table 4.7.	74
Figure 5.1	Performance of the two-pulse composite sequences (5.7) (red dashed) and (5.11) (blue solid) for the transition probability $p = 10^{-4}$. The dotted curves show the single pulse excitation probability for comparison.	92
Figure 5.2	Performance of the three-pulse composite sequences (5.14) (red dashed) and (5.22) (blue solid) for the transition probability $p = 10^{-4}$. The dotted curves show the single pulse excitation probability for comparison.	94
Figure 5.3	Performance of the four-pulse symmetric composite sequences (5.24) (red dashed), (5.26) (purple long-dashed) and the asymmetric sequence (5.28) (blue solid) for the transition probability $p = 10^{-4}$. The dotted curves show the single pulse excitation probability for comparison.	97
Figure 6.1	Transition probability $p(\epsilon)$ of ultrabroadband rotational π pulses. The numbers N on the curves refer to Composite Pulse (CP) sequences UBN listed in the Table 6.1. As noted above, the curves have $k = N - 1$ alternations on the top of the plot, unlike the BB2 sequence, which has 2 alternations, so it's worse than our five- π UB5.	109

Figure 6.2	Transition probability $p(\epsilon)$ of ultranarrowband rotational π pulses. The numbers N on the curves refer to Composite Pulse (CP) sequences UNN listed in the Table 6.2. As noted above, the curves have $k = N - 1$ alternations on the bottom of the plot, unlike the NB2 sequence, which has 2 alternations, so it's worse than our five- π UN5.	110
Figure 6.3	Trace fidelity $z(\epsilon)$ of ultrabroadband phasal π pulses. The numbers N on the curves refer to Composite Pulse (CP) sequences UBPhN listed in the Table 6.3. As noted above, the curves have $k = N - 2$ alternations on the top of the plot.	111
Figure 7.1	Scheme of the broadband optical isolator. ARQWP stands for the achromatic reciprocal quarter-wave plate, while ANRQWP stands for the achromatic nonreciprocal quarter-wave plate.	121
Figure 7.2	Fidelity versus systematic deviation for the composite waveplates designed by using three configurations: Eq. (7.5) is depicted by the blue dashed line, Eq. (7.6) by the black dotted line, and Eq. (7.7) by the red solid line. The gray dotted line is for a quarter-wave plate with a single Faraday rotator for easy reference.	122
Figure 7.3	Transmission and isolation properties of the optical isolators with different numbers of wave plates in the series, compared to the isolator based on a single rotator (blue line), vs the systematic deviation ϵ . The other three curves refer to the sequences of Eqs. (7.5) depicted by a purple line, (7.6) by a red line, and (7.7) by a black line.	123
Figure 7.4	The same as Figure 7.3 but instead of systematic deviation ϵ we use the wavelength parameter.	124

LIST OF TABLES

Table 2.1	Phases of symmetric composite sequences of $N = 2n + 1$ nominal π pulses, which produce the X gate with a pulse area error compensation up to order $O(\epsilon^n)$. The last column gives the high-fidelity range $[\pi(1 - \epsilon_0), \pi(1 + \epsilon_0)]$ of pulse area error compensation wherein the Frobenius distance fidelity is above the value 0.9999, i.e. the fidelity error is below 10^{-4}	32
Table 2.2	Phases of symmetric composite sequences of $N = 2n + 1$ nominal π pulses, which produce the X gate with a pulse area error compensation up to order $O(\epsilon^n)$. The last column gives the high-fidelity range $[\pi(1 - \epsilon_0), \pi(1 + \epsilon_0)]$ of pulse area error compensation wherein the Frobenius distance fidelity is above the value 0.9999, i.e. the fidelity error is below 10^{-4}	33
Table 2.3	Pulse area α and phases of composite pulse sequences which produce rotation gates of angle θ (according to (5.33)). The area α and all phases are given in units π . The case of $\theta = \frac{1}{2}\pi$ repeats the symmetric Hadamard gate already presented in Sec. 2.4; they are given here for the sake of comparison and completeness.	35
Table 3.1	Phases of asymmetric composite sequences of $N = 2n + 2$ nominal π pulses, which produce the Z gate with a pulse area error compensation up to order $O(\epsilon^n)$. The last column gives the high-fidelity range $[\pi(1 - \epsilon_0), \pi(1 + \epsilon_0)]$ of pulse area error compensation wherein the Frobenius distance fidelity is above the value 0.9999, i.e. the fidelity error is below 10^{-4}	49

Table 3.2	Phases of asymmetric composite sequences of $N = 2n + 2$ nominal π pulses, which produce the S gate with a pulse area error compensation up to order $O(\epsilon^n)$. The last column gives the high-fidelity range $[\pi(1 - \epsilon_0), \pi(1 + \epsilon_0)]$ of pulse area error compensation wherein the Frobenius distance fidelity is above the value 0.9999, i.e. the fidelity error is below 10^{-4}	50
Table 3.3	Phases of asymmetric composite sequences of $N = 2n + 2$ nominal π pulses, which produce the T gate with a pulse area error compensation up to order $O(\epsilon^n)$. The last column gives the high-fidelity range $[\pi(1 - \epsilon_0), \pi(1 + \epsilon_0)]$ of pulse area error compensation wherein the Frobenius distance fidelity is above the value 0.9999, i.e. the fidelity error is below 10^{-4}	51
Table 3.4	Phases of composite pulse sequences which produce phase gates of angle ϕ (according to (3.3)). The all phases are given in units π . The cases of $\phi = \pi$, $\phi = \frac{1}{2}\pi$ and $\phi = \frac{1}{4}\pi$ repeat the asymmetric Z, S and T gates respectively, already presented in Subsec. 3.3.2; they are given here for the sake of comparison and completeness.	52
Table 4.1	Phases of antisymmetric composite sequences of $N = 2n_s + 1$ nominal π pulses, which produce the π rotation with a pulse area error sensitivity up to order $O(\epsilon^{n_s})$. The last column gives the half-fidelity range or, so called, FWHM (full width at half maximum) $[\pi(1 - \epsilon_0), \pi(1 + \epsilon_0)]$ of pulse area error sensitivity wherein the Frobenius distance fidelity is above the value 0.5, i.e. the infidelity is below $\text{HM} = \frac{\text{MAX} + \text{MIN}}{2} = \frac{1 + 0}{2} = 0.5$	75
Table 4.2	Phases of antisymmetric composite sequences of $N = 2n_s + 1$ nominal π pulses, which produce the π rotation with a pulse area error sensitivity up to order $O(\epsilon^{n_s})$. The last column gives the half-fidelity range or, so called, FWHM (full width at half maximum) $[\pi(1 - \epsilon_0), \pi(1 + \epsilon_0)]$ of pulse area error sensitivity wherein the Frobenius distance fidelity is above the value 0.5, i.e. the infidelity is below $\text{HM} = \frac{\text{MAX} + \text{MIN}}{2} = \frac{1 + 0}{2} = 0.5$	76

Table 4.3	Phases of AN: antisymmetric composite sequences of $N - 2$ nominal π pulses, sandwiched by two pulses of areas $\pi/4$, and WN: asymmetric Wimperis-kind composite sequences of $N - 1$ nominal π pulses, preceded (or succeeded) by a pulse of area $\theta = \pi/2$; which produce the $\theta = \pi/2$ rotation with a pulse area error sensitivity up to order $O(\epsilon^{ns})$. The last column gives FWHM (full width at half maximum) $[\pi(1 - \epsilon_0), \pi(1 + \epsilon_0)]$ of pulse area error sensitivity wherein the Frobenius distance fidelity is above the value $\frac{1+(1-\sqrt{1-1/\sqrt{2}})}{2}$, i.e. the infidelity is below $HM = \frac{MAX+MIN}{2} = \frac{1+(1-\sqrt{1-1/\sqrt{2}})}{2} \approx 0.7294$, where the minimum (at $\epsilon = \pm 1$) Frobenius distance fidelity for $\pi/2$ rotations is $MIN = 1 - \sqrt{1 - 1/\sqrt{2}} \approx 0.4588$	77
Table 4.4	Phases of pari passu passband pulses for X gate. PB1-like pulse structure is used (2π pulses with single π).	80
Table 4.5	Phases of pari passu passband pulses for Hadamard gate. PB1-like pulse structure is used (2π pulses with single $\pi/2$).	81
Table 4.6	Phases of diversis passuum passband pulses for X gate.	82
Table 4.7	Phases of diversis passuum passband pulses for Hadamard gate.	83
Table 5.1	Pulse areas and phases (in units of π) for the composite sequence (5.11) (in units of π) for a few values of the transition probability. All composite sequences have the error order $O(\epsilon^3)$	91
Table 5.2	Pulse areas and phases (in units of π) for the composite sequences of 3 pulses (5.22) for a few values of the transition probability p . All composite sequences have the error order $O(\epsilon^5)$	93
Table 5.3	Pulse areas and phases (in units of π) for the composite sequences of 4 pulses (5.28). All composite sequences have the error order $O(\epsilon^7)$	98
Table 5.4	Parameters of the composite sequence G3 of Eq. (5.39) for different transition probabilities p	100

Table 6.1	Phases of symmetric, altering, ultrabroadband composite rotational $\theta = \pi$ sequences of $N = k + 1$ nominal π pulses, which produce ultrarobust population transfer in the ultrabroadband pulse area error correction range. The last column gives the high-transition probability range $[\pi(1 - \epsilon_0), \pi(1 + \epsilon_0)]$ of pulse area error compensation wherein the errant transition probability is above the value 0.9.	113
Table 6.2	Phases of asymmetric, altering, ultranarrowband composite rotational $\theta = \pi$ sequences of $N = k + 1$ nominal π pulses, which produce ultrasensitive population transfer in the ultranarrowband pulse area error sensitivity range. The last column gives the full width at half maximum range $[\pi(1 - \epsilon_0), \pi(1 + \epsilon_0)]$ of pulse area error sensitivity wherein the errant transition probability is above the value 0.5. Note that the full population transfer occurs at the center for zero pulse area error $p(\epsilon = 0) = 1$	114
Table 6.3	Phases of asymmetric, altering, ultrabroadband composite phasal $\zeta = \pi$ sequences of $N = k + 2$ nominal π pulses, which produce ultrarobust Z phase gate in the ultrabroadband pulse area error correction range. The last column gives the high-fidelity range $[\pi(1 - \epsilon_0), \pi(1 + \epsilon_0)]$ of pulse area error compensation wherein the trace fidelity is above the value 0.9.	115
Table 7.1	Calculated angles of rotation (in radians) for the three sequences of Eqs. (7.5), (7.6), and (7.7).	120

ABSTRACT

Composite pulses occupies an honorable place in the range of quantum control techniques, and has an advantage among them to be suitable for robust, sensitive or any high-precision manipulation of quantum systems. The goal is to expand the scope of the methodology born in nuclear magnetic resonance, and modernize its applications. We present the leverage of this flexible method in quantum computing, quantum sensing, quantum information processing, and polarization optics. The latter point to the existence of a quantum-classical analogy due to the underlying analogous mathematics.

The possibility to design robust quantum gates via broadband composite pulses with ultrahigh-fidelity exceeding the quantum computation benchmark is remarkable for quantum computing. Derivation of the narrowband and passband composite pulses for quantum sensing applications imposes the use of $SU(2)$ and novel regularization approaches of optimization. Interestingly, composite pulses is also capable of robust transitions of ultrasmall probability, and can have potential applications to deterministic single-photon emission and the DLCZ protocol well-known in quantum information processing. Another modification leads to ultrarobust and ultrasensitive quantum controls of transition probability via composite pulses, which may have essential applications for creation of ultrabroadband and ultranarrowband conversion efficiency polarization half-wave plates. Also the similar optimization method can be applied to design ultrarobust Z quantum gates, equivalent to polarization π rotators in polarization optics. Composite pulses parameters can be utilised for construction of broadband composite nonreciprocal polarization wave plates and optical isolators.

We cover a wide range of research disciplines and provide a deep and broad understanding of the interdisciplinarity, flexibility and possibilities of the technique. In this sense, composite pulses is powerful and has great prospects.

STATEMENT OF AUTHORSHIP

I, Hayk L. Gevorgyan, born November 27, 1995 in Yerevan, Armenia, declare that this thesis titled *Design of Composite Pulse Sequences for Quantum Technologies* and the work presented in it are my own. I confirm that this work was done mainly while in candidature for a research degree at Sofia University St. Kliment Ohridski.

Except where reference is made in the text of the thesis, this thesis contains no material published elsewhere or extracted in whole or in part from a thesis accepted for the award of any other degree or diploma. No other person's work has been used without due acknowledgment in the main text of the thesis. This thesis has not been submitted for the award of any degree or diploma in any other tertiary institution.

Hayk L. Gevorgyan

May 24, 2023

ACKNOWLEDGMENTS

I wish to thank the H2020-MSCA-ITN-ETN (Horizon 2020 - Marie Skłodowska-Curie actions - Innovative Training Networks - European Training Networks), *Light-Matter Interfaces for Quantum Enhanced Technologies* project (LIMQUET - Contract No. 765075), funded by the European Commission, for the financial support.

I express my sincere gratitude to my supervisor **Acad. Prof. DSc. Nikolay V. Vitanov** for his professional guide during my Ph.D. study. It was an honor for me to get to know him and the members of his group *Quantum Optics and Quantum Information*, in the department of theoretical physics at the University of Sofia. Thank you all of you for fruitful discussions and support.

I would like to thank Prof. Stéphane Guerin for inviting me to the project after my master's degree at the Université Bourgogne-Franche-Comté, Dijon, France, and for welcoming and supervising me during my secondment in his laboratory.

DEDICATION

to my father-scientist Lekdar A. Gevorgian and mother-scientist Anahit H. Shamamian

ACRONYMS

CP	Composite Pulse
CPs	Composite Pulses
NMR	Nuclear Magnetic Resonance
PO	Polarization Optics
QC	Quantum Computing
QI	Quantum Information
QIP	Quantum Information Processing
QS	Quantum Sensing

INTRODUCTION

1.1 QUANTUM COHERENT CONTROL TECHNIQUES

A huge variety of quantum control techniques are used in many areas of physics to manipulate the physical system. Among them few are appreciable as resonant excitation, adiabatic passage, shaped pulses, optimal control theory, Composite Pulses (CPs). It is also entertaining that they can be adapted to obtain new control methods such as composite adiabatic passage and shortcut to adiabaticity. In general, coherent control techniques differ from each other by the choice of targeted cost parameters, hence, the resulting quality indicators are different.

Resonant excitation is the artless manipulation of the system, sensitive to the experimental errors, providing the smallest operation run-time. Optimal control theory and shaped pulses with proper temporal shaping of experimental parameters target the minimization of the operation run-time (fast) and robust evolution of the system. CPs, although a little slower (moderate), occupies an honorable place between resonant excitation and adiabatic passage (slow), due to its flexibility to shape the precision measure (fidelity or transition probability) in essentially any desired manner, which is impossible with a single resonant pulse or adiabatic technique, being the versatile tool for both robust or/and sensitive operation of the system. No wonder that the method is sometimes called magic CPs, noteworthy that it can provide ultrahigh accuracy even for ultrasmall probability transitions of the system, which is discussed in detail in thesis.

1.2 ROTATIONS ON THE BLOCH SPHERE

The propagator of a coherently driven qubit is the solution of the Schrödinger equation,

$$i\hbar\partial_t\mathbf{U}(t, t_i) = \hat{H}(t)\mathbf{U}(t, t_i), \quad (1.1)$$

subject to the initial condition $\mathbf{U}(t_i, t_i) = \hat{I}$, the identity matrix. If the Hamiltonian is Hermitian, the propagator is unitary. If the Hamiltonian is also traceless, then the propagator has the SU(2) symmetry and can be represented as

$$\mathbf{U}_0 = \begin{bmatrix} a & b \\ -b^* & a^* \end{bmatrix}, \quad (1.2)$$

where a and b are the complex-valued Cayley-Klein parameters satisfying $|a|^2 + |b|^2 = 1$. A traceless Hermitian Hamiltonian has the form $\hat{H}(t) = \frac{1}{2}\hbar[\Omega(t)\cos(\phi)\hat{\sigma}_x + \Omega(t)\sin(\phi)\hat{\sigma}_y + \Delta\hat{\sigma}_z]$, where $\Omega(t)$ (assumed real and positive) is the Rabi frequency quantifying the coupling, ϕ is its phase, and Δ is the field-system detuning.

On exact resonance ($\Delta = 0$) and for $\phi = 0$, we have $a = \cos(A/2)$, $b = -i\sin(A/2)$, where A is the temporal pulse area $A = \int_{t_i}^{t_f} \Omega(t) dt$. For a system starting in state $|1\rangle$, the single-pulse transition probability is $p = |b|^2 = \sin^2(A/2)$.

1.2.1 Rotation gate

Basically starting from TDSE (a time-dependent Schrödinger equation) for a two-level system, one can reach the evolution operator for a single-qubit, which is called Rabi rotation gate from AMO (atomic, molecular and optical) devices in experimental Quantum Computing (QC) [1, 2], or theta pulse in Nuclear Magnetic Resonance (NMR) [3]. Thus, each pulse in a Composite Pulse (CP) sequence is considered resonant and hence it generates the propagator

$$\mathbf{U}(A, \phi) = \begin{bmatrix} \cos(A/2) & -ie^{i\phi}\sin(A/2) \\ -ie^{-i\phi}\sin(A/2) & \cos(A/2) \end{bmatrix}, \quad (1.3)$$

where ϕ is the phase of the coupling. SU(2) symmetry is a character for physical-level gates [1, 4] in QC devices in contrast to U(2) quantum gates [2] in theoretical QC. However, from a physical point of view it is more natural to use SU(2) gates, which have $\det = 1$ (while the determinant of the Hadamard gate is -1). The reason is that in a closed qubit (with only two states and no ancilla states) the Hamiltonian is symmetric, and then the propagator (i.e., the gate) is SU(2) symmetric.

Our objective is to construct the qubit rotation gate $\hat{R}_y(\theta) = e^{i(\theta/2)\hat{\sigma}_y}$, where θ is the rotation angle and $\hat{\sigma}_y$ is the Pauli's y matrix. In matrix form,

$$\mathbf{R}_y(\theta) = \begin{bmatrix} \cos(\theta/2) & \sin(\theta/2) \\ -\sin(\theta/2) & \cos(\theta/2) \end{bmatrix}. \quad (1.4)$$

The rotation gate (1.4) is equivalent to the rotation gate $\hat{R}_x(\theta) = e^{i(\theta/2)\hat{\sigma}_x}$, or in matrix form,

$$\mathbf{R}_x(\theta) = \begin{bmatrix} \cos(\theta/2) & i \sin(\theta/2) \\ i \sin(\theta/2) & \cos(\theta/2) \end{bmatrix}. \quad (1.5)$$

We shall use the gate (1.4) because it is real and because it coincides with the ubiquitous definition of the rotation matrix. Therefore, hereafter we drop the subscript y for the sake of brevity.

The X or NOT gate is defined as

$$\begin{bmatrix} 0 & 1 \\ 1 & 0 \end{bmatrix} = \hat{\sigma}_x, \quad (1.6)$$

Because the determinant of this matrix is -1 , it is not of SU(2) type. Instead, we shall construct the SU(2) gate

$$\mathbf{X} = \begin{bmatrix} 0 & 1 \\ -1 & 0 \end{bmatrix}, \quad (1.7)$$

which is related to the gate (1.6) by a phase transformation and it is equivalent to it. The gate (1.7) is also equivalent to the often used gate

$$e^{i(\pi/2)\hat{\sigma}_x} = \begin{bmatrix} 0 & i \\ i & 0 \end{bmatrix}, \quad (1.8)$$

which can be obtained from Eq. (1.7) by a phase transformation too. However, we prefer to use the gate (1.7) because it is real and also because it is a special case of the general rotation gate (1.4).

We shall use the following form of the Hadamard gate (known as pseudo-Hadamard form),

$$\mathbf{H} = \mathbf{R}_y(\pi/2) = e^{i(\pi/4)\hat{\sigma}_y} = \frac{1}{\sqrt{2}} \begin{bmatrix} 1 & 1 \\ -1 & 1 \end{bmatrix}. \quad (1.9)$$

It is SU(2) symmetric and it is equivalent to the more common Walsh-Hadamard form

$$\frac{1}{\sqrt{2}} \begin{bmatrix} 1 & 1 \\ 1 & -1 \end{bmatrix}, \quad (1.10)$$

which is not SU(2) symmetric. The gate (1.9) is equivalent to the often used SU(2) symmetric gate (known as the Splitter gate)

$$\mathbf{H}_x = e^{i(\pi/4)\hat{\sigma}_x} = \frac{1}{\sqrt{2}} \begin{bmatrix} 1 & i \\ i & 1 \end{bmatrix}, \quad (1.11)$$

which is related to it by a phase transformation.¹

A single resonant pulse of temporal area $A = \theta_\epsilon = \theta(1 + \epsilon)$ produces the propagator $\hat{R}(\theta_\epsilon) = e^{i[\theta(1+\epsilon)/2]\hat{\sigma}_y} = \hat{R}(\theta)[1 + O(\epsilon)]$, i.e. it is accurate up to zeroth order $O(\epsilon^0)$ in the pulse area error ϵ . Our approach is to replace the single θ pulse with a CP sequence of pulses of appropriate pulse areas and phases, such that the overall propagator produces the rotation gate (1.4) with an error of higher order, i.e. $\hat{R}(\theta)[1 + O(\epsilon^{n+1})]$. Then we say that the corresponding composite rotation gate is accurate up to, and including, order $O(\epsilon^n)$.

1.2.2 Phase-shift gate

Indeed, $\hat{R}_x(\theta)$ can be obtained from $\hat{R}_y(\theta)$ by simple phase transformation, $\hat{R}_x(\theta) = \hat{F}(\pi/2)\hat{R}_y(\theta)\hat{F}(-\pi/2)$. Here $\hat{F}(\phi) = e^{-i(\phi/2)\hat{\sigma}_z}$ is a phase-shift gate (up to a global phase factor), or in matrix form,

$$\mathbf{F}(\phi) = \mathbf{R}_z(\phi) = \begin{bmatrix} e^{-i\phi/2} & 0 \\ 0 & e^{i\phi/2} \end{bmatrix} := \begin{bmatrix} 1 & 0 \\ 0 & e^{i\phi} \end{bmatrix}, \quad (1.12)$$

which is equivalent to it up to an inefficient global factor of $e^{-i\phi/2}$. It cannot be obtained via a single theta pulse (5.1), and thus requires a circuit with two or more $\theta = \pi$ rotation gates

$$\mathbf{F}(\phi) = \mathbf{U}(\pi, \nu + \pi - \phi/2)\mathbf{U}(\pi, \nu) = \mathbf{U}(\pi, \nu)\mathbf{U}(\pi, \nu + \pi + \phi/2). \quad (1.13)$$

¹ In the Quantum Information (QI) literature it is often preferred to use U(2), rather than SU(2) gates, e.g. the Hadamard, S and T gates are all U(2) but not SU(2) gates. In a quantum circuit it does not matter as long as the same type of gates are used in the same circuit. The reason is that the Hadamard gate is involutory, i.d. it is equal to its inverse, and it is very convenient to write a quantum circuit in terms of \hat{H} only, rather than with \hat{H} and $\hat{H}^\dagger = \hat{H}^T$. However, from a physical point of view it is more natural to use SU(2) gates, which have $\det = 1$ [while the determinant of the Hadamard gate is -1]. The reason is that in a closed qubit (with only two states and no ancilla states) the Hamiltonian is symmetric, $\hat{H}(t) = \frac{1}{2}\hbar[\Omega(t) + \Delta\hat{\sigma}_z]$, and then the propagator (i.e. the gate) is SU(2) symmetric.

We shall use the following forms for the Pauli-Z gate,

$$\mathbf{Z} = \mathbf{F}(\pi) = \begin{bmatrix} i & 0 \\ 0 & -i \end{bmatrix} = e^{i(\pi/2)\hat{\sigma}_z} := \begin{bmatrix} 1 & 0 \\ 0 & -1 \end{bmatrix} = \hat{\sigma}_z, \quad (1.14)$$

for the phase gate S (or P)

$$\mathbf{S} = \mathbf{F}(\pi/2) = \frac{1}{\sqrt{2}} \begin{bmatrix} 1-i & 0 \\ 0 & 1+i \end{bmatrix} := \begin{bmatrix} 1 & 0 \\ 0 & i \end{bmatrix}, \quad (1.15)$$

and for the gate T (or $\pi/8$)

$$\mathbf{T} = \mathbf{F}(\pi/4) = \begin{bmatrix} e^{-i(\pi/8)} & 0 \\ 0 & e^{i(\pi/8)} \end{bmatrix} := \begin{bmatrix} 1 & 0 \\ 0 & e^{i(\pi/4)} \end{bmatrix}. \quad (1.16)$$

1.3 COMPOSITE PULSES IN NUCLEAR MAGNETIC RESONANCE

CPs have been developed in NMR in the 1980s. However, similar ideas have been introduced in Polarization Optics (PO) much earlier, in the 1940s [5–8]: by stacking several ordinary wave plates at specific angles with respect to their fast polarization axes one can design either achromatic (broadband) polarization retarders and rotators or (narrowband) polarization filters [5–14]. In the last two decades, CPs have spread out to most experimental QI platforms far beyond NMR. Applications include qubit control in trapped ions [15–22], neutral atoms [23], doped solids [24–26], quantum dots [27–32], and NV centers in diamond [33], high-accuracy optical clocks [34], cold-atoms interferometry [35–37], optically dense atomic ensembles [38], magnetometry [39], optomechanics [40], etc.

CPs are classified in NMR by Wimperis [3] into broadband, narrowband and passband classes, where he defined 1st type and 2nd type of pulses BB_1 , NB_1 , PB_1 and BB_2 , NB_2 , PB_2 respectively. It is common to use abbreviation from the left to the right when the overall evolution matrix is the chronological multiplication of the single evolutions from the right to the left.

BB_1 and BB_2 pulses follow

$$BB_1(\theta) : (\pi)_{\phi_1}(2\pi)_{\phi_2}(\pi)_{\phi_1}(\theta)_0, \quad (1.17)$$

with $\phi_1 = \arccos(-\theta/4\pi)$ and $\phi_2 = 3\phi_1$,

$$BB_2(\theta) : (\pi)_{\pi/2}(2\pi)_{\phi_2}(\pi)_{\pi/2}(\theta)_0, \quad (1.18)$$

with $\phi_2 = 3\pi/2 + \theta/4$.

NB_1 and NB_2 pulses follow

$$NB_1(\theta) : (\pi)_{\phi_1}(2\pi)_{\phi_2}(\pi)_{\phi_1}(\theta)_0, \quad (1.19)$$

with $\phi_1 = \arccos(-\theta/4\pi)$ and $\phi_2 = -\phi_1$,

$$NB_2(\theta) : (\pi)_{\pi/2}(2\pi)_{\phi_2}(\pi)_{\pi/2}(\theta)_0, \quad (1.20)$$

with $\phi_2 = 3\pi/2 - \theta/4$.

NB_1 and NB_2 pulses follow

$$PB_1(\theta) : (2\pi)_{\phi_1}(4\pi)_{\phi_2}(2\pi)_{\phi_1}(\theta)_0, \quad (1.21)$$

with $\phi_1 = \arccos(-\theta/8\pi)$ and $\phi_2 = -\phi_1$,

$$PB_2(\theta) : (2\pi)_{\pi/2}(4\pi)_{\phi_2}(2\pi)_{\pi/2}(\theta)_0, \quad (1.22)$$

with $\phi_2 = 3\pi/2 - \theta/8$.

A first approach to use average Hamiltonian theory and Magnus expansion of the propagator pioneered by Tycko [41], and used by Wimperis. BB_1 , NB_1 , PB_1 CPs have flat fidelity, while BB_2 , NB_2 , PB_2 have alternations in fidelity and show better property (broader or/and narrower) at the expense of precision measure.

Besides these asymmetric sequences, Jones and co-workers [42] develop time-symmetric sequence called SCROFULOUS (Short composite rotation for undoing length over and under shoot),

$$SCROFULOUS(\theta) : (\theta_1)_{\phi_1}(\pi)_{\phi_2}(\theta_1)_{\phi_1}, \quad (1.23)$$

with $\theta_1 = \arcsinc(2 \cos(\theta/2)/\pi)$, $\phi_1 = \arccos(-\pi \cos \theta_1 / (2\theta_1 \sin \theta/2))$, $\phi_2 = \phi_1 - \arccos(-\pi/2\theta_1)$, where unnormalized sinc function is defined as $\text{sinc}(\theta) = \sin \theta / \theta$.

In the case of π rotation, one can choose $\theta_1 = \arcsinc(0) = \pi$ and $\arccos(-\pi/2\theta_1) = -4\pi/3$,

$$SCROFULOUS(\pi) : (\pi)_{\pi/3}(\pi)_{5\pi/3}(\pi)_{\pi/3}. \quad (1.24)$$

Thus $\phi_2 - \phi_1 = 4\pi/3$, and Tycko's and co-workers' [43] result can be recovered

$$Tycko(N=3) : (\pi)_0(\pi)_{2\pi/3}(\pi)_0, \quad (1.25)$$

for the broadband excitation without phase distortion. This leads to the division of the broadband CPs into two sub-classes, named variable and constant rotations [44–46].

Variable-rotation CPs (sometimes called class B) compensate parameter errors only in the transition probability p (or the population inversion $w = 2p - 1$). Recently in [47], several classes of arbitrarily accurate analytic CP sequences for variable rotations have been presented. Constant-rotation, or phase-distortionless [43], CPs (sometimes called class A) compensate parameter errors in both the transition probability and the phases of the created superposition state (i.e., in the Bloch vector coherences u and v). The latter are obviously more demanding and require longer sequences for the same order of compensation. However, in QC and QI wherein phase relations are essential, constant rotations are clearly the ones to be used for quantum rotation gates [42].

SCROFULOUS is the shortest constant rotation with the first order of pulse area error compensation. BB_1 is the second order constant rotation, which is outperformed by our shorter X5 and H5s symmetric sequences [48].

SK1 is the shortest passband CP [49], being geometric rotation gate [50], as SCROFULOUS, also consists of three elementary pulses

$$SK1 : (\theta)_0(2\pi)_{\phi_1}(2\pi)_{-\phi_1}, \quad (1.26)$$

with parameter $\phi_1 = \arccos(-\theta/4\pi)$.

In [49], two methods have been used to construct arbitrarily accurate CPs. The Trotter-Suzuki sequences [49, 51] recover $B2 = BB_1$, $N2 = NB_1$ and $P2 = PB_1$ sequences and generalize them as arbitrary accurate B_n , N_n and P_n sequences. The Solovay-Kitaev method uses elements of the proof of the Solovay Kitaev theorem [49, 52], relies on general properties of Hamiltonians and gives SK_n sequences. Interestingly, it was also possible to output combined broadband and SK sequences SB_n in [49].

Wimperis analytically derived two sub-families of broadband phase-distortionless CP sequences, F_n [53, 54] and G_n [54, 55], targeting π rotations. Both consist of the sequence of π pulses, one has no alternation in fidelity and is flat-top, and another is family of alternating² CPs.

Antisymmetric passband APB_n sequences [56] target π rotations, proposed by Odedra and Wimperis.

² This means that the measure of accuracy is no longer flat and wiggles occur. Such a mechanism can be used to enhance the property of the CP by changing the required precision benchmark.

Possibility to derive equiangular CPs [57] can be interesting from the point of view of optimal control. In our opinion, from the aspects of the stable and systematic optimization the π sequences in the CP are required.

Although concatenated pulses [58, 59] can compensate both off-resonance error and pulse area error, there is an alternative mechanism, which provides better performance pattern, and consists of CPs with precisely chosen detuning, pulse area and composite phase parameters³.

Although these theoretical approaches (derivation, nesting or concatenating) for arbitrary accurate CPs exist, they require very long sequences and operation run-time. In this thesis we propose analytical and numerical methods for systematic derivation of CPs, to obtain the required property with better trade-off between operation run-time and property measure.

1.4 THESIS OUTLINE

The remainder of this thesis is organized as follows.

Chapter 1 provides background information relevant to the field of research, viz., a detailed discussion of the major existing contributions of CPs technique in the literature.

Chapter 2 details the application of the technique into QC, especially for the design of ultrahigh-fidelity composite rotation gates [48], and our proposed SU(2) approach, viz., Newton's error correction (optimization of the sum of the absolute squares of the errors, i.e. overall-gate error) with Monte-Carlo simulation method (free parameters are chosen from the set of random solutions).

Chapter 3 details the application of the technique for the design of ultrahigh-fidelity composite phase gates [60] with the same method in QC.

Chapter 4 summarizes the results of narrowband and passband CP sequences, applicable to Quantum Sensing (QS).

Chapter 5 modernizes the properties of the technique, opening new horizons for the development of robust ultrasmall probability transitions with the application to deterministic single-photon emission in Quantum Information Processing (QIP).

³ Unfortunately, this is not included in the dissertation.

Chapter 6 examines the capability of the technique for ultrarobust or ultrasensitive control at the little-expense of the precision due to a novel derivation method. These novel CPs are suitable for PO applications such as ultrabroadband and ultranarrowband composite polarization half waveplates [61].

Chapter 7 presents the use of the methodology for the development of optical devices, namely broadband nonreciprocal polarization waveplates and optical isolators [62] in PO.

Chapter 8 concludes this thesis. First, we summarize our work. Then, we highlight interesting aspects that we did not fully cover and provide a thorough discussion of potential topics and areas, that may be interesting for future research activities.

COMPOSITE PULSES FOR ROBUST ULTRAHIGH-FIDELITY ROTATION GATES

CP sequences, which produce arbitrary pre-defined rotations of a qubit on the Bloch sphere, are presented. The composite sequences contain up to 17 pulses and can compensate up to eight orders of experimental errors in the pulse amplitude and the pulse duration. Composite sequences for three basic quantum gates — X (NOT), Hadamard and arbitrary rotation — are derived. Three classes of composite sequences are presented — one symmetric and two asymmetric. They contain as their lowest members two well-known composite sequences — the three-pulse symmetric SCROFULOUS pulse and the four-pulse asymmetric BB1 pulse, which compensate first and second-order errors, respectively. The shorter sequences are derived analytically, and the longer ones numerically (instead by nesting and concatenation, as usually done hitherto). Consequently, the composite sequences derived here match or outperform the existing ones in terms of either speed or accuracy, or both. For example, we derive a second-order composite sequence, which is faster (by about 13%) than the famous BB1 sequence. For higher-order sequences the speed-up becomes much more pronounced. This is important for QIP as the sequences derived here provide more options for finding the sweet spot between ultrahigh fidelity and high speed.

2.1 INTRODUCTION

Quantum rotation gates, such as the Hadamard gate and the X (or NOT) gate are central elements in any quantum circuit [2, 63, 64]. Traditionally, a general rotation at an angle θ is implemented by a resonant pulsed field with a temporal area of θ , hence the name θ pulses. In particular, the Hadamard gate is implemented by a resonant $\pi/2$ pulse, and the X gate is implemented by a resonant π pulse, which are the theoretically fastest means for producing these gates. However, resonant driving is prone to errors in the experimental parameters, e.g. the pulse amplitude, duration, and detuning.

Various proposals have been made in order to generate rotation gates that are resilient to experimental errors, at the expense of being longer, and hence slower. Adiabatic techniques are the traditional remedy for tackling such errors [65]. Ever since 1932 [66–69], adiabatic evolution via a level crossing is the ubiquitous adiabatic method to produce complete population inversion and hence the X gate. More recently, adiabatic evolution via a half crossing has gained popularity as a means for producing half excitation, and hence the Hadamard gate [70–74]. This idea has been used in a technique known as half-SCRAP (Stark-chirped rapid adiabatic passage) [70] and the closely related two-state STIRAP (stimulated Raman adiabatic passage) [71], which has been successfully implemented in a trapped-ion experiment [72]. In both cases, pulse shaping and chirping are designed such that their time dependences resemble the delayed-pulse ordering of conventional STIRAP [75]. In a variation of these, an adiabatic technique has been proposed [73] which generates arbitrary coherent superpositions of two states, which is controlled by the initial and final ratios of the field’s amplitude and its detuning. An extension of this half-crossing technique to three states has been experimentally demonstrated in a trapped-ion experiment, with an error of about 1.4×10^{-4} , i.e. close to the quantum computation benchmark level [74], which was achieved by using pulse shaping. Another proposal used a sequence of two half-crossing adiabatic pulses split by a phase jump, which serves as a control parameter to the created superposition state [76].

In three-state Raman-coupled qubits, a very popular technique is fractional STIRAP [77–79], in which the Stokes pulse arrives before the pump pulse but the two pulses vanish simultaneously. This leads to the creation of a coherent superposition of the two end states of the chain. Tripod-STIRAP [80–82], an extension of STIRAP wherein a single state is coupled to three other states, has also been used for the generation of coherent superpositions of these three states or two of them. We also note a technique for creation of coherent superposition states and for navigation between them by quantum Householder reflections [83, 84].

While adiabatic techniques provide great robustness to parameter errors, in general they struggle to deliver the ultrahigh fidelity required in quantum computation. A powerful alternative to achieve ultrahigh fidelity while featuring robustness to parameter errors is the technique of CPs [44, 45]. The CP sequence is a finite train of pulses with well-defined relative phases between them. These phases are control parameters, which are determined by the desired excitation profile. CPs can shape the excitation profile in essentially any desired manner, which is impossible with a single resonant pulse or adiabatic techniques. In particular, one can create a broadband composite π pulse, which delivers transition probability of 1 not only for a pulse area $A = \pi$ and zero detuning $\Delta = 0$, as a single resonant π pulse,

but also in some ranges around these values [3, 24, 44, 45, 85–93]. Alternatively, narrowband CPs [3, 46, 89, 91, 94–99] squeeze the excitation profile around a certain point in the parameter space: they produce excitation that is more sensitive to parameter variations than a single pulse, with interesting applications to sensing, metrology and spatial localization. A third family of CPs — passband pulses — combine the features of broadband and narrowband pulses: they provide highly accurate excitation inside a certain parameter range and negligibly small excitation outside it [3, 98, 100–103].

CPs have been developed in NMR in the 1980's. However, similar ideas have been introduced in PO much earlier, in the 1940's [5–8]: by stacking several ordinary wave plates at specific angles with respect to their fast polarization axes one can design either achromatic (broadband) polarization retarders and rotators or polarization filters [5–14, 104, 105]. In the last two decades, CPs have spread out to most experimental QI platforms far beyond NMR. Applications include qubit control in trapped ions [15–22], neutral atoms [23], doped solids [24–26], quantum dots [27–32], and NV centers in diamond [33], high-accuracy optical clocks [34], cold-atoms interferometry [35–37], optically dense atomic ensembles [38], magnetometry [39], optomechanics [40], etc.

There are no universally applicable CPs to all kinds of problems and physical platforms because the requirements in different applications are different. For instance, in NMR, CPs which compensate errors in very broad parameter ranges with only modest accuracy are ubiquitous. On the contrary, in QI, very high accuracy is required within some moderately large parameter ranges. CPs are particularly suitable for QI because they are quite unique in providing both ultrahigh fidelity and resilience to experimental errors. No other quantum control method offers this combination of high fidelity and robustness to errors and therefore, CPs might be the key enabling control technology for high-fidelity qubit operations which are mandatory in scalable QC.

In this chapter, we present several sets of single-qubit rotation quantum gates constructed with CP sequences. There are two classes of composite rotations, named variable and constant rotations [44, 45]. *Variable-rotation* CPs (sometimes called *Class B*) compensate parameter errors only in the transition probability p (or the population inversion $w = 2p - 1$). Recently [47], several classes of arbitrarily accurate analytic composite sequences for variable rotations have been presented. *Constant-rotation*, or *phase-distortionless* [43], CPs (sometimes called *Class A*) compensate parameter errors in both the transition probability and the phases of the created superposition state (i.e., in the Bloch vector coherences u and v). The latter are obviously more demanding and require longer sequences for the same order

of compensation. However, in QIP wherein phase relations are essential, constant rotations are clearly the ones to be used for quantum rotation gates [42].

In this chapter, we focus at the derivation of ultrahigh-fidelity composite rotation gates, including the X, Hadamard and general rotation, which compensate pulse-area errors up to eighth order. The X and Hadamard gates are special cases of general rotations but they are treated separately due to their importance in QI. Our results extend earlier results on some of these gates using shorter pulse sequences. The first phase-distortionless CP was designed by Tycko [94] which produces a composite X gate. It consists of three pulses of total nominal area of 3π and provides a first-order error compensation. A second-order error compensation CP was constructed by Wimperis, the well-known BB1 (broadband of type 1) pulse [3, 90]. It consists of four pulses with a total nominal pulse area of $4\pi + \theta$ and it produces a constant rotation at an arbitrary angle θ . More recently, Wimperis and co-workers developed several phase-distortionless anti-symmetric composite π pulses designed for rephasing of coherence [53, 56, 106]. Jones and co-workers have devoted a great deal of attention to composite X gates, with an emphasis of geometric approaches for derivation of such sequences, which work up to 5 and 7 pulses [42, 55, 107, 108]. We point out that our results supplement earlier results by our and other groups on different gates, i.e. composite quantum phase gate [109], the CNOT [110–116], Toffoli [117], and C^n -NOT gates [117].

Composite rotation gates with a pulse area error compensation of third and higher order have been constructed using nesting and concatenation of shorter composite sequences. For larger error order, this procedure produces (impractical) composite sequences of extreme length. Here we use analytic approaches and brute-force numerics to derive three classes of composite sequences for X, Hadamard and rotation gates which achieve error compensation of up to 8th order with much shorter sequences than before.

This chapter is organized as follows. In Sec. 2.2 we explain the derivation method. Composite π rotations, representing the X gate are presented in Sec. 2.3. Composite implementations of the Hadamard gate are given in Sec. 2.4, and composite rotation gates in Sec. 2.5. Finally, Sec. 2.6 presents the conclusions.

2.2 SU(2) APPROACH

The derivation of the composite rotation gates is done in the following manner. A phase shift ϕ imposed on the driving field, $\Omega(t) \rightarrow \Omega(t) e^{i\phi}$, is imprinted onto the propagator (1.2) as

$$\mathbf{U}_\phi = \begin{bmatrix} a & b e^{i\phi} \\ -b^* e^{-i\phi} & a^* \end{bmatrix}. \quad (2.1)$$

A train of N pulses, each with area A_k and phase ϕ_k (applied from left to right),

$$(A_1)_{\phi_1} (A_2)_{\phi_2} (A_3)_{\phi_3} \cdots (A_N)_{\phi_N}, \quad (2.2)$$

produces the propagator (acting, as usual, from right to left)

$$\mathcal{U} = \mathbf{U}_{\phi_N}(A_N) \cdots \mathbf{U}_{\phi_3}(A_3) \mathbf{U}_{\phi_2}(A_2) \mathbf{U}_{\phi_1}(A_1). \quad (2.3)$$

Let us assume that the nominal (i.e. for zero error) pulse areas A_k have a systematic error ϵ , i.e. $A_k \rightarrow A_k(1 + \epsilon)$. If all nominal pulse areas are the same, as it is the case for many CP sequences, this is the natural assumption because the apparatus will produce possibly imperfect but identical pulses. If the pulse areas are different, this is also a reasonable assumption in many cases. For example, if a trapped ion is addressed by an imperfectly pointed laser beam then it will “see” the same systematic deviation from the perfect field amplitude (and hence pulse area) for any chosen target pulse area. Atoms in atomic clouds in magneto-optical or dipole traps or ions in doped solids (e.g. for optical memories) addressed by electromagnetic fields offer another example: they will “see” different field amplitude due to spatial inhomogeneity depending on their position in the sample, but this field amplitude will deviate from the optimal one by the same relative systematic error ϵ regardless of the value of the optimal amplitude if the atoms do not move much during the duration of the CP sequence.

Our objective in this chapter is to construct the qubit rotation gate $\hat{R}_y(\theta) = e^{i(\theta/2)\hat{\sigma}_y}$ (1.4). Under the assumption of a single systematic pulse area error ϵ , we can expand the composite propagator (2.3) in a Taylor series versus ϵ . Because of the SU(2) symmetry of the overall propagator, it suffices to expand only two of its elements, say $\mathcal{U}_{11}(\epsilon)$ and $\mathcal{U}_{12}(\epsilon)$. We set their zero-error values to the target values,

$$\mathcal{U}_{11}(0) = \cos(\theta/2), \quad \mathcal{U}_{12}(0) = \sin(\theta/2), \quad (2.4)$$

and we set as many of their derivatives with respect to ϵ , in the increasing order, as possible,

$$\mathcal{U}_{11}^{(m)}(0) = 0, \quad \mathcal{U}_{12}^{(m)}(0) = 0, \quad (m = 1, 2, \dots, n), \quad (2.5)$$

where $\mathcal{U}_{jl}^{(m)} = \partial_\epsilon^m \mathcal{U}_{jl}$ denotes the m th derivative of \mathcal{U}_{jl} with respect to ϵ . The largest derivative order n satisfying Eqs. (2.5) gives the order of the error compensation $O(\epsilon^n)$.

Equations (2.4) and (2.5) generate a system of $2(n+1)$ algebraic equations for the nominal pulse areas A_k and the composite phases ϕ_k ($k = 1, 2, \dots, N$). The equations are complex-valued and generally we have to solve $4(n+1)$ equations with the $2N$ free parameters (nominal pulse areas and phases). Because of the normalization condition $|\mathcal{U}_{11}|^2 + |\mathcal{U}_{12}|^2 = 1$, an error compensation of order n requires a CP sequence of $N = 2n + 1$ pulses (or $N = 2n$ in some lucky cases).

As stated above, the derivation of the CP sequences requires the solution of Eqs. (2.4) and (2.5). For a small number of pulses (up to about five), the set of equations can be solved analytically. For longer sequences, Eqs. (2.4) and the first two equations ($n = 1$) of Eqs. (2.5) can still be solved analytically, but the higher orders in Eqs. (2.5) they are solved numerically. We do this by using standard routines in MATHEMATICA[©].

2.2.1 Quantum gate fidelity

If Eqs. (2.4) and (2.5) are satisfied, then the overall propagator can be written as

$$\mathbf{U}(\epsilon) = \mathbf{R}(\theta) + O(\epsilon^{n+1}), \quad (2.6)$$

with $\mathbf{R}(\theta) = \mathbf{U}(0)$. Then the *Frobenius distance fidelity*,

$$\mathcal{F} = 1 - \|\mathbf{U}(\epsilon) - \mathbf{R}(\theta)\| = 1 - \sqrt{\frac{1}{4} \sum_{j,k=1}^2 |\mathcal{U}_{jk} - R_{jk}|^2}, \quad (2.7)$$

is of the same error order $O(\epsilon^n)$ as the propagator, $\mathcal{F} = 1 - O(\epsilon^{n+1})$. As shown by Jones and co-workers [64] for the composite X gates, the *trace fidelity*,

$$\mathcal{F}_T = \frac{1}{2} \text{Tr} [\mathbf{U}(\epsilon) \mathbf{R}(\theta)^\dagger], \quad (2.8)$$

has a factor of 2 higher error order $O(\epsilon^{2n})$, i.e. $\mathcal{F}_T = 1 - O(\epsilon^{2n+1})$. The reason is that in the Frobenius distance, all information of the actual propagator is involved, while in the trace distance some of this information is lost. Therefore, throughout this chapter we shall use the Frobenius distance fidelity (2.7), which is a much more strict and unforgiving to errors fidelity measure; moreover, its error is of the same order as the propagator error.

We note here that for variable rotations, Eqs. (2.4) and (2.5) have to be satisfied for only one of the propagator elements, say \mathcal{U}_{12} . This means that with the same number of pulses one can achieve a factor of 2 higher order of error compensation for variable rotations than for constant rotations. However, this error compensation applies to the transition probability only, but not to the propagator phases. For

variable rotations the overall propagator cannot be written in the form of Eq. (2.6), and consequently, neither of the fidelities (2.7) or (2.8) is of the form $1 - O(\epsilon^{n+1})$.

2.2.2 Composite pulse sequences

We have performed extensive numeric simulations which have returned numerous solutions. We have categorized them in three types of composite sequences, one symmetric and two asymmetric.

- Each symmetric sequence consists of a sequence of $2n - 1$ nominal π pulses, sandwiched by two pulses of areas α , with symmetrically ordered phases,

$$\alpha_{\phi_1} \pi_{\phi_2} \pi_{\phi_3} \cdots \pi_{\phi_{n-1}} \pi_{\phi_n} \pi_{\phi_{n-1}} \cdots \pi_{\phi_3} \pi_{\phi_2} \alpha_{\phi_1}. \quad (2.9)$$

These sequences generalize the three-pulse SCROFULOUS sequence [42], which is of this type, to more than three pulses.

- The first type of asymmetric sequences consists of a sequence of nominal π pulses, preceded (or superseded) by a pulse of area θ ,

$$\pi_{\phi_1} \pi_{\phi_2} \pi_{\phi_3} \cdots \pi_{\phi_{N-1}} \theta_{\phi_N}. \quad (2.10)$$

These sequences generalize the five-pulse BB1 sequence [3], which is of this type, to more than five pulses.

- The second type of asymmetric sequences consists of a sequence of $N - 2$ nominal π pulses, preceded (or superseded) by single pulses of areas α and β ,

$$\alpha_{\phi_1} \pi_{\phi_2} \pi_{\phi_3} \cdots \pi_{\phi_{N-1}} \beta_{\phi_N}. \quad (2.11)$$

To the best of our knowledge, this type of composite sequences has not been reported in the literature hitherto.

Below we consider these three classes of composite sequences and test their performance by using the Frobenius distance (2.7). We consider three figures of merit to be essential.

- The most important parameter is the order of error compensation $O(\epsilon^n)$. The larger n , the broader the high-fidelity range and the larger the errors ϵ , which can be compensated.
- The second most important parameter is the total pulse area $\mathcal{A}_{\text{tot}} = \sum_{k=1}^N |\mathcal{A}_k|$. It determines the length of the sequences and hence the speed of the gates.

Usually, the peak Rabi frequency is limited either by the experimental apparatus or by the qubit properties, e.g., too large Rabi frequency can cause unwanted couplings to other levels or to other qubits (cross-talk). Therefore, for a fixed peak Rabi frequency, the total pulse area determines the total duration of the composite sequence.

- Another consideration is the number of pulses N in the sequence. Unless there are issues with the implementation of the phase jumps, this argument is of far less importance than the other two. However, if the phase jumps require some time to implement or cannot be implemented with high accuracy, then sequences of fewer pulses are preferable. For this reason, we often give several different CPs for each error order.

2.3 X (NOT) GATE

As it is well known, such a gate (1.7) can be produced by a resonant pulse of temporal area π . The propagator of a π pulse reads

$$\mathbf{U} = \begin{bmatrix} \cos(\pi(1 + \epsilon)/2) & \sin(\pi(1 + \epsilon)/2) \\ -\sin(\pi(1 + \epsilon)/2) & \cos(\pi(1 + \epsilon)/2) \end{bmatrix}, \quad (2.12)$$

where ϵ is the pulse area error. The Frobenius distance fidelity (2.7) reads

$$\mathcal{F} = 1 - \sqrt{2} \left| \sin \frac{\pi\epsilon}{4} \right|. \quad (2.13)$$

For comparison, the trace fidelity is

$$\mathcal{F}_T = 1 - 2 \sin^2 \frac{\pi\epsilon}{4} = \cos \frac{\pi\epsilon}{2}. \quad (2.14)$$

Obviously the error stemming from the Frobenius distance fidelity (2.13), which is of order $O(\epsilon)$, is far greater than the value of the error stemming from the trace fidelity (2.14), which is of order $O(\epsilon^2)$, as noted by Jones and co-workers [42].

The three types of composite sequences (5.33), (2.10), and (2.11) coalesce into a single type, a sequence of π pulses. Below we consider these sequences, in the increasing order of error compensation.

2.3.1 First-order error compensation

The careful analysis of Eqs. (2.4) and (2.5) shows that the shortest possible CP which can compensate first-order errors consists of three pulses, each with a pulse area of π , and symmetric phases,

$$\pi_{\phi_1} \pi_{\phi_2} \pi_{\phi_1}. \quad (2.15)$$

Solving Eq. (2.4) along with Eq. (2.5) for the first derivatives gives two solutions for the phases,

$$\pi_{\frac{1}{6}\pi} \pi_{\frac{5}{6}\pi} \pi_{\frac{1}{6}\pi}, \quad (2.16a)$$

$$\pi_{\frac{5}{6}\pi} \pi_{\frac{1}{6}\pi} \pi_{\frac{5}{6}\pi}. \quad (2.16b)$$

These two sequences generate the same propagator and hence the same fidelity.

The Frobenius distance and trace distance fidelities read

$$\mathcal{F} = 1 - \mathcal{I}_1, \quad (2.17a)$$

$$\mathcal{F}_T = 1 - \mathcal{I}_1^2, \quad (2.17b)$$

where the Frobenius distance infidelity is

$$\mathcal{I}_1 = \sqrt{2 \left(1 + 2 \cos^2 \frac{\pi\epsilon}{4}\right)} \sin^2 \frac{\pi\epsilon}{4}. \quad (2.18)$$

Obviously, the Frobenius distance infidelity \mathcal{I}_1 is of order $O(\epsilon^2)$ and it is much larger than the trace distance infidelity \mathcal{I}_1^2 , which is of order $O(\epsilon^4)$.

The Frobenius distance fidelity and the trace fidelity are plotted in Figure 2.1 for X gates produced by a single pulse and composite sequences of 3 and 5 (see below) pulses. The three-pulse composite X gate (2.16) produces much higher fidelity than the single-pulse X gate. Obviously, the trace distance fidelity is much higher than the Frobenius distance fidelity: compare the curves with labels 1 and 1_T ; 3 and 3_T ; 5 and 5_T . In fact, as seen in the figure, the trace distance fidelity for a single pulse (label 1_T) almost coincides with the Frobenius distance fidelity for the three-pulse composite sequence (label 3). With respect to the quantum computation benchmark fidelity value of $1 - 10^{-4}$, the Frobenius distance fidelity (2.17a) for the three-pulse composite X gates of Eqs. (2.16) remains above this value in the pulse area interval $(0.992\pi, 1.008\pi)$, i.e. for relative errors up to $|\epsilon| < 0.008$. For comparison, the trace distance fidelity (2.17b) remains above this value in the pulse area interval $(0.919\pi, 1.081\pi)$, i.e. for relative errors up to $|\epsilon| < 0.081$, a factor of

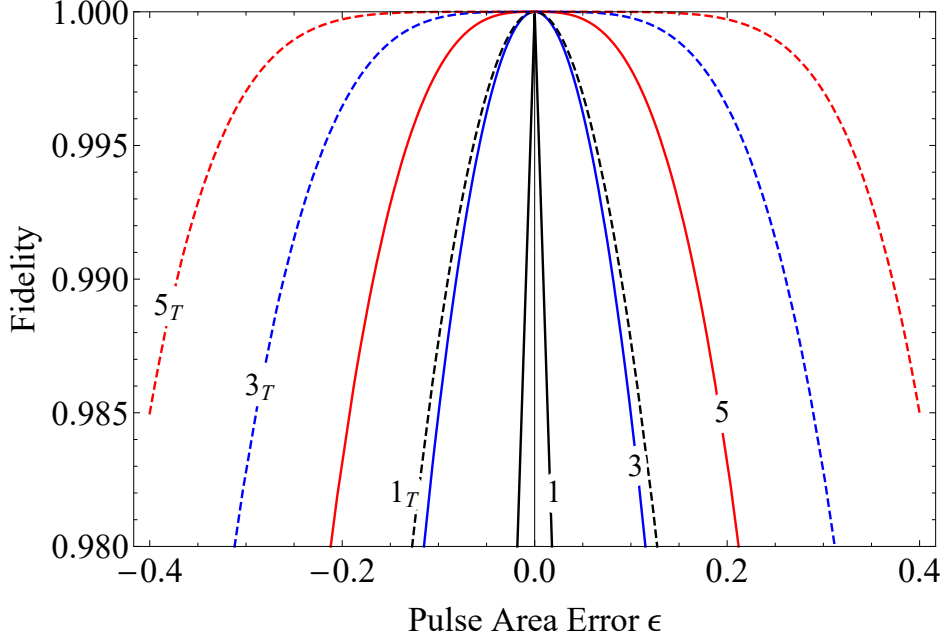


Figure 2.1: Frobenius distance fidelity \mathcal{F} (solid) and trace distance fidelity \mathcal{F}_T (dashed) of composite X gates. The numbers N on the curves refer to composite sequences XN listed in Table 2.1.

10 larger. This is the reason why in this chapter, we will use the much more severe Frobenius distance fidelity.

2.3.2 Second-order error compensation

For sequences of four pulses, it becomes possible to annul the second-order derivatives in Eq. (2.5). A number of solutions exist, some of which are

$$(2\pi)_{3\chi}\pi_{\pi+\chi}\pi_{\frac{1}{2}\pi}\pi_{-\chi}, \quad (2.19a)$$

$$\pi_{\pi+\chi}(2\pi)_{3\chi}\pi_{\pi+\chi}\pi_{\frac{1}{2}\pi}, \quad (2.19b)$$

$$\pi_{\frac{1}{2}\pi}\pi_{\pi+\chi}(2\pi)_{3\chi}\pi_{\pi+\chi}, \quad (2.19c)$$

$$\pi_{-\chi}\pi_{\frac{1}{2}\pi}\pi_{\pi+\chi}(2\pi)_{3\chi}, \quad (2.19d)$$

where $\chi = \arcsin\left(\frac{1}{4}\right) \approx 0.0804\pi$. The second and third sequences are related to the BB1 sequence of Wimperis [3]. Note that all these sequences have a total nominal pulse area of 5π , and can be considered as five-pulse sequences because the effect of $(2\pi)_{3\chi}$ is the same as $\pi_{3\chi}\pi_{3\chi}$.

The Frobenius fidelity for all these sequences reads $\mathcal{F} = 1 - \mathcal{I}_2$, with the infidelity

$$\mathcal{I}_2 = \sqrt{8 + 9 \cos \frac{\pi\epsilon}{2} + 3 \cos^2 \frac{\pi\epsilon}{2}} \left| \sin \frac{\pi\epsilon}{4} \right|^3. \quad (2.20)$$

Obviously, this fidelity is accurate up to order $O(\epsilon^2)$, as the error is of order $O(\epsilon^3)$. The trace fidelity reads $\mathcal{F}_T = 1 - \mathcal{I}_2^2$. The trace fidelity is accurate up to order $O(\epsilon^5)$, as the error is of order $O(\epsilon^6)$. Obviously, the trace infidelity is much smaller than the Frobenius distance infidelity, as for the three-pulse composite sequences.

The same second-order error compensation, and the same fidelity, can be obtained by composite sequences of five pulses of area π each,

$$\pi_{\phi_1} \pi_{\phi_2} \pi_{\phi_3} \pi_{\phi_4} \pi_{\phi_5}. \quad (2.21)$$

Hence the total pulse area is 5π , the same as the four-pulse sequences above. Because of the additional phase compared to the four-pulse sequences, various phase choices are possible. For example, an asymmetric sequence of the kind (2.21) has the phases $\phi_1 = 0$, $\phi_2 = \arcsin\left(\frac{14+\sqrt{31}}{20}\right) \approx 0.4337\pi$, $\phi_3 = \pi + \arcsin\left(\frac{9\sqrt{31}-19}{80}\right) \approx 1.1271\pi$, $\phi_4 = \arcsin\left(\frac{9\sqrt{31}+19}{80}\right) \approx 0.3320\pi$, $\phi_5 = \arcsin\left(\frac{14-\sqrt{31}}{20}\right) \approx 0.1385\pi$.

We have derived also the symmetric sequence

$$\pi_{\phi_1} \pi_{\phi_2} \pi_{\phi_3} \pi_{\phi_2} \pi_{\phi_1}, \quad (2.22)$$

with $\phi_1 = \arcsin(1 - \sqrt{5/8}) \approx 0.0672\pi$, $\phi_2 = \arcsin((3\sqrt{10} - 2)/8) \approx 0.3854\pi$, $\phi_3 = 2\phi_2 - 2\phi_1 + \pi/2 \approx 1.1364\pi$. For these five-pulse sequences the Frobenius infidelity \mathcal{I}_2 is given again by Eq. (2.20), and the trace infidelity by \mathcal{I}_2^2 . The respective fidelities are plotted in Figure 2.1. Obviously, they are much larger than the respective fidelities for a single pulse and the three-pulse composite sequence (2.16).

The Frobenius distance infidelity (2.20) remains below the quantum computation fidelity threshold 10^{-4} in the pulse area interval $(0.964\pi, 1.036\pi)$, i.e. for relative errors up to $|\epsilon| < 0.036$. On the other hand, the trace distance infidelity \mathcal{I}_2^2 remains above this value in the pulse area interval $(0.832\pi, 1.168\pi)$, i.e. for relative errors up to $|\epsilon| < 0.168$, a factor of almost 5 larger. As for the three-pulse composite X gate, as seen in Figure 2.1, the Frobenius distance fidelity is much more demanding error measure as its error is much larger than the error of the trace distance fidelity.

Hereafter we will leave out the trace distance fidelity (2.8) and will use only the Frobenius distance fidelity (2.7), because it is a much stricter measure of the gate error.

We conclude this subsection by noting that the availability of various four- and five-pulse symmetric and asymmetric sequences which produce the same fidelity is not a redundancy because they may have rather different sensitivity to phase errors, as has been shown recently for other composite sequences [118].

2.3.3 Higher-order error compensation

For composite sequences of more than 5 pulses, the equations for the composite phases quickly become very cumbersome and impossible to solve analytically. They repeat the pattern of the sequences of four and five pulses above: the composite sequences of $2n$ and $2n + 1$ pulses have a total pulse area of $(2n + 1)\pi$, with all pulses in the sequence being nominal π pulses, with the exception of one of the pulses in the $2n$ -pulse sequence which has a nominal pulse area of 2π . Either sequences of $2n$ and $2n + 1$ pulses produce error compensation of the order $O(\epsilon^n)$ and identical fidelity profiles.

The $2n + 1$ -pulse sequences have an additional free phase which can be used to make the composite sequence *symmetric* as in Eq. (5.33), viz.

$$\pi_{\phi_1} \pi_{\phi_2} \pi_{\phi_3} \cdots \pi_{\phi_{n-1}} \pi_{\phi_n} \pi_{\phi_{n-1}} \cdots \pi_{\phi_3} \pi_{\phi_2} \pi_{\phi_1}. \quad (2.23)$$

The propagators generated by the symmetric composite sequences (2.23) feature two important properties:

1. All even-order derivatives $\mathcal{U}_{11}^{(2k)}(0)$ of the diagonal elements in Eq. (2.5) vanish, and so do all odd-order derivatives $\mathcal{U}_{12}^{(2k+1)}(0)$ of the off-diagonal elements.
2. The remaining nonzero derivatives in Eq. (2.5) are either real or imaginary: $\mathcal{U}_{11}^{(2k+1)}(0)$ are real, whereas $\mathcal{U}_{12}^{(2k)}(0)$ are imaginary.

Therefore, Eqs. (2.4) and (2.5) reduce to a set of $n + 1$ real trigonometric equations for $n + 1$ free phases. There are multiple solutions for the phases for every $(2n + 1)$ -pulse composite sequence.

Two of the phases can be found analytically. The solution of the zeroth-order Eqs. (2.4) reads

$$\phi_{n+1} = \frac{\pi}{2} + 2[\phi_n - \phi_{n-1} + \phi_{n-2} - \phi_{n-3} + \cdots + (-)^n \phi_1]. \quad (2.24)$$

Given this relation, the equation $\mathcal{U}_{11}^{(1)}(0) = 0$ reduces to

$$2 \sum_{k=1}^n \sin(\Phi_k) = (-)^{n+1}, \quad (2.25)$$

with

$$\begin{aligned}\Phi_k &= 2 \sum_{j=1}^{k-1} (-)^{j+1} \phi_j + (-)^{k+1} \phi_k \\ &= 2[\phi_1 - \phi_2 + \phi_3 + \cdots + (-)^k \phi_{k-1}] + (-)^{k+1} \phi_k,\end{aligned}\quad (2.26)$$

from where we can find ϕ_n . For example, for 3, 5, and 7 pulses we have, respectively,

$$\sin(\phi_1) + \sin(2\phi_1 - \phi_2) = -\frac{1}{2}, \quad (2.27a)$$

$$\sin(\phi_1) + \sin(2\phi_1 - \phi_2) + \sin(2\phi_1 - 2\phi_2 + \phi_3) = \frac{1}{2}, \quad (2.27b)$$

$$\begin{aligned}\sin(\phi_1) + \sin(2\phi_1 - \phi_2) + \sin(2\phi_1 - 2\phi_2 + \phi_3) \\ + \sin(2\phi_1 - 2\phi_2 + 2\phi_3 - \phi_4) = -\frac{1}{2}.\end{aligned}\quad (2.27c)$$

From each of these we can find two solutions for the phase with the largest subscript.

The remaining $n - 1$ phases $\phi_1, \phi_2, \dots, \phi_{n-1}$ can be determined numerically.

We have derived numerically the composite phases of symmetric sequences of an odd number of pulses, Eq. (2.23). They are presented in Table 2.1. The fidelity of these composite X gates is plotted in Figure 2.2. It is clear from the table and the figure that a single pulse has very little room for errors as the high-fidelity X gate allows for pulses area errors of less than 0.01%. The three-pulse composite X gate offers some leeway, with the admissible error of 0.8%. The real pulse area error correction effect is achieved with the composite sequences of 5 to 9 pulses, for which the high-fidelity range of admissible errors increases from 3.6% to 11.7%. Quite remarkably, errors of up to 25% can be eliminated, and ultrahigh fidelity maintained, with the 17-pulse composite X gate. Note that these error ranges are calculated by using the rather tough Frobenius distance fidelity (2.7). Had we use the much more relaxed trace distance fidelity (2.8), these ranges would be much broader, see the numbers for 1, 3 and 5 pulses above.

That said, very long sequences are barely practical because the gate is much slower. Moreover, it is hard to imagine a quantum computer operating with 25% pulse area error. Therefore, the composite sequences of 5, 7 and 9 pulses seems to offer the best fidelity-to-speed ratio.

2.4 HADAMARD GATE

The Hadamard gate (1.9) can be generated by an ideal resonant $\pi/2$ pulse, which is, however, prone to experimental errors. In order to construct the composite

Hadamard gate we have considered all three types of composite sequences (5.33), (2.10), and (2.11). Below we consider these sequences, in the increasing order of error compensation.

2.4.1 First-order error correction

The shortest pulse sequence that can provide a first-order error compensated Hadamard gate consists of three pulses,

$$\alpha_{\phi_1} \pi_{\phi_2} \alpha_{\phi_1}. \quad (2.28)$$

Equations (2.4) result in the equations

$$-\sin(\alpha) \cos(\phi_1 - \phi_2) = \frac{1}{\sqrt{2}}, \quad (2.29a)$$

$$e^{-i\phi_1} [\sin(\phi_1 - \phi_2) - i \cos(\alpha) \cos(\phi_1 - \phi_2)] = \frac{1}{\sqrt{2}}. \quad (2.29b)$$

The first derivatives of Eqs. (2.5) are annulled by the single equation

$$2\alpha \cos(\phi_1 - \phi_2) + \pi = 0. \quad (2.29c)$$

From Eqs. (2.29a) and (2.29c) we find

$$\frac{\sin \alpha}{\alpha} = \frac{\sqrt{2}}{\pi}. \quad (2.30)$$

Therefore the value of the pulse area α is given by an inverse sinc function of $\sqrt{2}/\pi$, which gives $\alpha \approx 0.6399\pi$. Given α , we can find $\phi_1 - \phi_2$ from Eq. (2.29a) or (2.29c), and then ϕ_1 from

$$\sqrt{2} \sin(\phi_1 - \phi_2) = \cos(\phi_1), \quad (2.31)$$

which is the real part of Eq. (2.29b) [after multiplying it by $e^{i\phi_1} \sqrt{2}$]. The values are $\phi_1 \approx 1.8442\pi$ and $\phi_2 \approx 1.0587\pi$. Therefore, this CP reads

$$(0.6399\pi)_{1.8442\pi} \pi_{1.0587\pi} (0.6399\pi)_{1.8442\pi}. \quad (2.32)$$

In term of degrees, it reads $115^\circ_{332^\circ} 180^\circ_{191^\circ} 115^\circ_{332^\circ}$. This composite sequence is related to the well-known sequence SCROFULOUS [42]: $115^\circ_{62^\circ} 180^\circ_{281^\circ} 115^\circ_{62^\circ}$; the two sequences can be obtained from each other by adding 90° to all phases in our sequence.

2.4.2 Second-order error correction

Second-order error compensation is obtained by a composite sequence of at least 4 pulses. A popular CP is the BB1 pulse of Wimperis [3],

$$\text{BB1} = (\pi/2)_0 \pi_\chi (2\pi)_{3\chi} \pi_\chi, \quad (2.33)$$

which produces the gate (1.11), with a total pulse area of 4.5π . It can be viewed as identical to the five-pulse sequence

$$(\pi/2)_0 \pi_\chi \pi_{3\chi} \pi_{3\chi} \pi_\chi. \quad (2.34)$$

We have derived a different, asymmetric four-pulse CP,

$$\text{H4a} = \alpha_{\phi_1} \pi_{\phi_2} \pi_{\phi_3} \beta_{\phi_4}, \quad (2.35)$$

where $\alpha = 0.7821\pi$, $\beta = 1.3914\pi$, $\phi_1 = 1.8226\pi$, $\phi_2 = 0.6492\pi$, $\phi_3 = 1.2131\pi$, $\phi_4 = 0.3071\pi$. This pulse has a total area of about 4.17π , i.e. it is faster than the BB1 pulse. It is accurate up to the same order $O(\epsilon^2)$ and produces essentially the same fidelity profile as BB1.

We have also derived a five-pulse composite Hadamard gate by using the symmetric sequence

$$\text{H5s} = \alpha_{\phi_1} \pi_{\phi_2} \pi_{\phi_3} \pi_{\phi_2} \alpha_{\phi_1}, \quad (2.36)$$

with $\alpha = 0.45\pi$, $\phi_1 = 1.9494\pi$, $\phi_2 = 0.5106\pi$, $\phi_3 = 1.3179\pi$. It delivers again the second-order error compensation $O(\epsilon^2)$, however, with a total pulse area of just about 3.9π . Therefore it is considerably faster than the BB1 pulse, by over 13%, while having a similar performance.

2.4.3 Higher-order error correction

Similarly to the second order, the *third-order error compensation* is obtained in several different manners, requiring at least 6 pulses. The 6-pulse sequence with the minimal pulse area of about 5.72π reads

$$\text{H6a} = \alpha_{\phi_1} \pi_{\phi_2} \pi_{\phi_3} \pi_{\phi_4} \pi_{\phi_5} \beta_{\phi_6}, \quad (2.37)$$

with $\alpha = 0.5917\pi$, $\beta = 1.1305\pi$, and the phases given in Table 2.2. The same error correction order is achieved with the symmetric seven-pulse sequence

$$\text{H7s} = \alpha_{\phi_1} \pi_{\phi_2} \pi_{\phi_3} \pi_{\phi_4} \pi_{\phi_3} \pi_{\phi_2} \alpha_{\phi_1}, \quad (2.38)$$

with $\alpha = 0.2769\pi$, and the phases given in Table 2.2. It produces the same fidelity profile as the 6-pulse sequence but it is a little faster as its pulse area is about 5.55π . Another seven-pulse composite sequence is built similarly to the BB1 sequence (2.33),

$$\text{H7w} = (\pi/2)_{\pi/2}\pi_{\phi_2}\pi_{\phi_3}\pi_{\phi_4}\pi_{\phi_5}\pi_{\phi_6}\pi_{\phi_7}, \quad (2.39)$$

with the phases given in Table 2.2. It achieves the same error order compensation $O(\epsilon^3)$, however, with a larger total pulse area of 6.5π compared to the previous two CPs.

Fourth-order error compensation is obtained by at least 8 pulses. The 8-pulse sequence with the minimal pulse area of about 7.40π reads

$$\text{H8a} = \alpha_{\phi_1}\pi_{\phi_2}\pi_{\phi_3}\pi_{\phi_4}\pi_{\phi_5}\pi_{\phi_6}\pi_{\phi_7}\beta_{\phi_8}, \quad (2.40)$$

with $\alpha = 0.4954\pi$, $\beta = 0.9028\pi$, and the phases are given in Table 2.2. The same error correction order is achieved with the symmetric nine-pulse sequence

$$\text{H9s} = \alpha_{\phi_1}\pi_{\phi_2}\pi_{\phi_3}\pi_{\phi_4}\pi_{\phi_5}\pi_{\phi_4}\pi_{\phi_3}\pi_{\phi_2}\alpha_{\phi_1}, \quad (2.41)$$

with $\alpha = 0.2947$, with the phases in Table 2.2. Its total pulse area is 7.59π . The BB1-like nine-pulse composite sequence,

$$\text{H9w} = (\pi/2)_{\pi/2}\pi_{\phi_2}\pi_{\phi_3}\pi_{\phi_4}\pi_{\phi_5}\pi_{\phi_6}\pi_{\phi_7}\pi_{\phi_8}\pi_{\phi_9}, \quad (2.42)$$

with the phases in Table 2.2, achieves the same fourth-order error compensation $O(\epsilon^4)$, however, with the largest total pulse area of 8.5π compared to the previous two CPs.

The same pattern is repeated for the longer pulse sequences presented in Table 2.2: for the same order of pulse area error compensation, the fastest sequences, with the smallest total pulse area are either the asymmetric HNa or symmetric HNs sequences, and the BB1-like sequences HNw are the slowest ones.

The fidelity and the infidelity of the composite Hadamard gates of up to seventh-order error compensation are plotted in Figure 2.3. Obviously, as the number of pulses in the composite sequences, and hence the compensated error order, increase the fidelity and infidelity profiles improve and get broader.

2.5 GENERAL ROTATION GATE

2.5.1 First-order error correction

The shortest pulse sequence that can provide a first-order error compensation, as for the X and Hadamard gates, consists of three pulses,

$$\alpha_{\phi_1} \pi_{\phi_2} \alpha_{\phi_1}. \quad (2.43)$$

Equations (2.4) result in the equations

$$-\sin(\alpha) \cos(\phi_1 - \phi_2) = \cos(\theta/2), \quad (2.44a)$$

$$e^{-i\phi_1} [\sin(\phi_1 - \phi_2) - i \cos(\alpha) \cos(\phi_1 - \phi_2)] = \sin(\theta/2). \quad (2.44b)$$

The first derivatives of Eqs. (2.5) are annulled by the single equation

$$2\alpha \cos(\phi_1 - \phi_2) + \pi = 0. \quad (2.44c)$$

From Eqs. (2.44a) and (5.41a) we find

$$\frac{\pi \sin(\alpha)}{\alpha} = 2 \cos(\theta/2). \quad (2.45)$$

Therefore the value of the pulse area α is given by an inverse sinc function of $(2/\pi) \cos(\theta/2)$. Given α , we can find $\phi_1 - \phi_2$ from Eq. (2.44a) or (5.41a), and then ϕ_1 from

$$\sin(\phi_1 - \phi_2) = \sin(\theta/2) \cos(\phi_1), \quad (2.46)$$

which is obtained from Eq. (2.44b).

This composite sequence is related to the SCROFULOUS CP [42], as mentioned above. The values of the pulse area and the composite phases are given in Table 2.3.

2.5.2 More than three pulses

The five-pulse sequence,

$$\alpha_{\phi_1} \pi_{\phi_2} \pi_{\phi_3} \pi_{\phi_2} \alpha_{\phi_1}, \quad (2.47)$$

provides a second-order error compensation. The sequences with 7, 9, etc. pulses have the same structure and deliver an error compensation of order 3, 4, etc. Generally, a $2n + 1$ -pulse symmetric sequence of this structure delivers an error compensation up to order $O(\epsilon^n)$. Unfortunately, analytic expressions for the composite parameters for more than three pulses are hard to obtain, if possible at all. Hence

we have derived them numerically and their values are listed in Table 2.3. The fidelity of these sequences behave similarly to the ones for the X and Hadamard gates.

2.6 COMMENTS AND CONCLUSIONS

In this chapter we presented a number of CP sequences for three basic quantum gates — the X gate, the Hadamard gate and arbitrary rotation gates. The composite sequences contain up to 17 pulses and can compensate up to eight orders of experimental errors in the pulse amplitude and duration. The short composite sequences are calculated analytically and the longer ones numerically.

Three classes of composite sequences have been derived — one symmetric and two asymmetric. For the X gate, the three classes coalesce into a single set of symmetric sequences of nominal π pulses presented in Table 2.1. For the Hadamard gate, cf. Table 2.2, two of the classes contain as their lowest members two well-known composite sequences: the three-pulse symmetric SCROFULOUS pulse [42] and the four-pulse asymmetric BB1 pulse [3], which compensate first and second-order pulse area errors, respectively. The third, asymmetric class of composite sequences, does not contain members published before. All three classes produce essentially identical fidelity profiles for the same order of error compensation. In general, the SCROFULOUS-like symmetric sequences HN and the asymmetric sequences HN_a require the least total pulse area and hence are the fastest, whereas the asymmetric BB1-like sequences HN_w are the slowest. For the general rotation gates, the three classes behave similarly, although we have presented only the symmetric sequences in Table 2.3 for the sake of brevity.

The composite rotations derived here outperform the existing composite rotations in terms of either speed, or accuracy, or both. Although we could not improve the first-order SCROFULOUS sequence, we have derived second-order composite sequences which are faster (by over 13%) than the famous BB1 sequence [3]: our second-order error compensated Hadamard gate has a total nominal pulse area of about 3.9π , which is substantial improvement over the BB1 pulse, which delivers the same error order with a total pulse area of 4.5π [3]. The longer composite sequences are derived by brute numerics and they are much shorter than previous sequences with the same order of error compensation obtained by nesting and concatenation of short sequences. For example, our n th order error-compensated X gates are constructed by $2n + 1$ nominal π pulses, which is much shorter than the concatenated composite sequences. For example, the 5th order error compensation is produced by a concatenated 15-pulse sequence, whereas we achieve this by an 11-pulse sequence. Similar scaling applies to the Hadamard and the rotation gates.

The results presented in this chapter demonstrate the remarkable flexibility of **CPs** accompanied by extreme accuracy and robustness to errors — three features that cannot be achieved together by any other coherent control technique. We expect these composite sequences, in particular the **X** and Hadamard gates, to be very useful quantum control tools in **QI** applications because they provide a variety of options to find the optimal balance between ultrahigh fidelity, error range and speed, which may be different in different physical systems.

We note that in this chapter we have assumed an exact resonance. In many experiments, this condition is well justified because the qubit frequency and the frequency of the driving field are controlled extremely accurately. The fluctuations in the Rabi frequency, deriving from fluctuations in the radiation intensity, either due to source instabilities (typical for lasers) or spatial inhomogeneities (e.g. pointing errors in laser-controlled trapped ions, spatial intensity variations in rf- or microwave-controlled doped solids, etc.) are much more significant sources of errors. Nonetheless, in certain situations it may be necessary to compensate detuning errors too and one should use **CPs** with double error compensation.

Besides all, the results presented in this chapter can be applied in **PO** to obtain broadband polarization retarders, viz., broadband half-, quarter- and arbitrary-wave plates with an arbitrary phase retardation. This is possible to accomplish due to quantum-classical analogy of composite rotations on the Bloch and the Poincaré spheres (cf. 6.2). A simple transformation between the parameters in the rotation gate and in the Jones matrix applies and the results can be compared¹. We see the difficulty to practically construct fractional- π pulses (the first and the last pulses, viz. α parameter in the symmetric sequences or α and β parameters in the asymmetric sequences), which is necessary to overcome in the design of quarter- and arbitrary-wave plates.

¹ Composite phases in the rotation matrix and in the Jones matrix are related. Let's compare the results in Table 2.1 and in the article [119]. Using symmetric **XN** sequences $\varphi_i \rightarrow A_i = \pi$ with composite phases $\theta_i \rightarrow (\varphi_i - \pi/2)/2$, the broadband half-wave plate is designed. **XN** sequences are equivalent to the results in the article, as the absolute trace fidelity in both cases have equal broadness range. Despite this, **X5** and **X11** are broader than the five and the eleven sequences in the transition probability (equivalent to the conversion efficiency in **PO**), but **X13** is slightly narrower than the thirteen sequence in Table 1 in [119]. Note that, hereby, we design up to 17 **CPs** for half-wave plates, up to 15 **CPs** for quarter-wave plates and the symmetric sequences (the best ones) for arbitrary-wave plates. The same scheme can be used for the quarter- and arbitrary-wave plates, viz., $\varphi_i \rightarrow A_i$ with composite phases $\theta_i \rightarrow (\varphi_i - \pi/2)/2$.

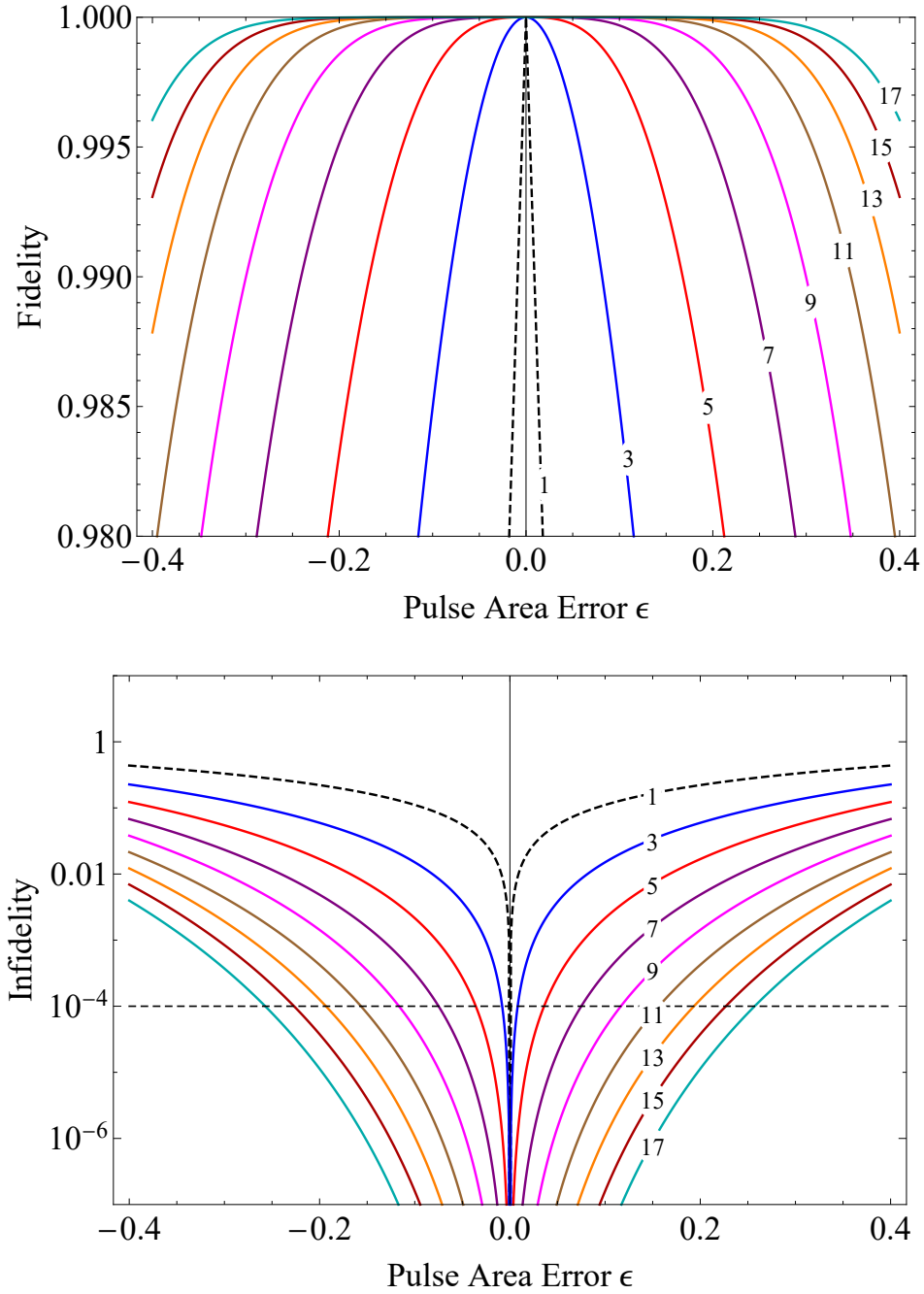


Figure 2.2: Frobenius distance fidelity F (top) and infidelity (bottom) of composite X gates. The infidelity is in logarithmic scale in order to better visualize the high-fidelity (low-infidelity) range. The numbers N on the curves refer to composite sequences XN listed in Table 2.1.

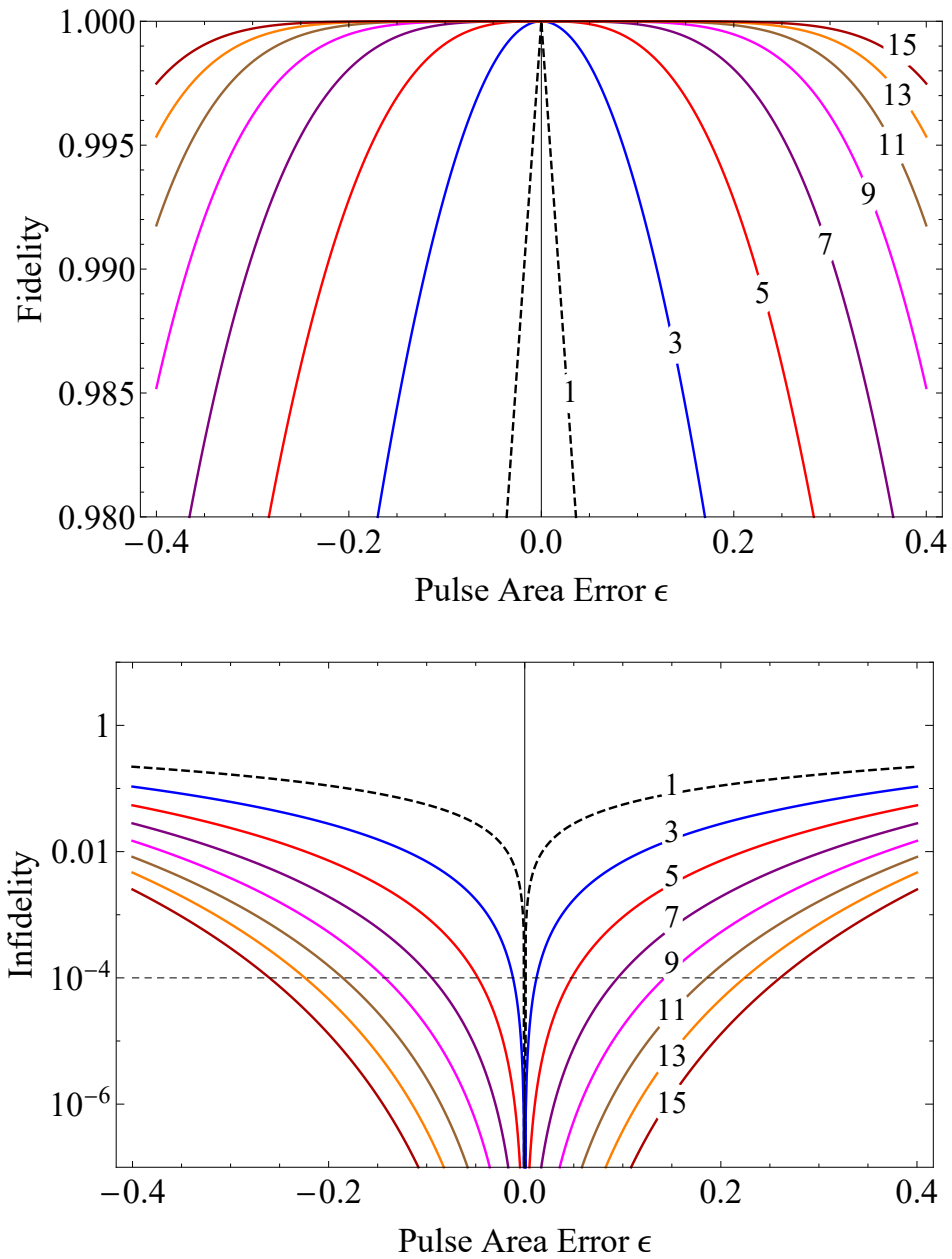


Figure 2.3: Frobenius distance fidelity (top) and infidelity (bottom) of composite Hadamard gates produced by using the symmetric composite sequences HNs from Table 2.2.

Table 2.1: Phases of symmetric composite sequences of $N = 2n + 1$ nominal π pulses, which produce the X gate with a pulse area error compensation up to order $O(\epsilon^n)$. The last column gives the high-fidelity range $[\pi(1 - \epsilon_0), \pi(1 + \epsilon_0)]$ of pulse area error compensation wherein the Frobenius distance fidelity is above the value 0.9999, i.e. the fidelity error is below 10^{-4} .

Name	Pulses	$O(\epsilon^n)$	Phases $\phi_1, \phi_2, \dots, \phi_n$ (in units π) (according to (2.23))	High-fidelity error correction range
single	1	$O(\epsilon^0)$	$\frac{1}{2}$	$[0.99991\pi, 1.00009\pi]$
X3	3	$O(\epsilon)$	$\frac{1}{6}, \frac{5}{6}$	$[0.992\pi, 1.008\pi]$
X5	5	$O(\epsilon^2)$	0.0672, 0.3854, 1.1364	$[0.964\pi, 1.036\pi]$
X7	7	$O(\epsilon^3)$	0.2560, 1.6839, 0.5932, 0.8306	$[0.925\pi, 1.075\pi]$
X9	9	$O(\epsilon^4)$	0.3951, 1.2211, 0.7805, 1.9335, 0.4580	$[0.883\pi, 1.117\pi]$
X11	11	$O(\epsilon^5)$	0.2984, 1.8782, 1.1547, 0.0982, 0.6883, 0.8300	$[0.843\pi, 1.157\pi]$
X13	13	$O(\epsilon^6)$	0.8800, 0.6048, 1.4357, 0.9817, 0.0781, 0.5025, 1.8904	$[0.807\pi, 1.193\pi]$
X15	15	$O(\epsilon^7)$	0.5672, 1.4322, 0.9040, 0.2397, 0.9118, 0.5426, 1.6518, 0.1406	$[0.773\pi, 1.227\pi]$
X17	17	$O(\epsilon^8)$	0.3604, 1.1000, 0.7753, 1.6298, 1.2338, 0.2969, 0.6148, 1.9298, 0.4443	$[0.743\pi, 1.257\pi]$

Table 2.2: Phases of symmetric composite sequences of $N = 2n + 1$ nominal π pulses, which produce the X gate with a pulse area error compensation up to order $O(\epsilon^n)$. The last column gives the high-fidelity range $[\pi(1 - \epsilon_0), \pi(1 + \epsilon_0)]$ of pulse area error compensation wherein the Frobenius distance fidelity is above the value 0.9999, i.e. the fidelity error is below 10^{-4} .

Symmetric sequences $\alpha_{\phi_1} \pi_{\phi_2} \cdots \pi_{\phi_n} \pi_{\phi_{n+1}} \pi_{\phi_n} \cdots \pi_{\phi_2} \alpha_{\phi_1}$						
notation	N	$O(\epsilon^n)$	α	$\phi_1, \phi_2, \dots, \phi_n$ (in units π) (according to (5.33))	\mathcal{A}_{tot}	Range
H3s	3	$O(\epsilon)$	0.6399	0.8442, 0.0587	2.28π	$[0.988, 1.012]\pi$
H5s	5	$O(\epsilon^2)$	0.45	1.9494, 0.5106, 1.3179	3.90π	$[0.952, 1.048]\pi$
H7s	7	$O(\epsilon^3)$	0.2769	1.6803, 0.2724, 0.8255, 1.6624	5.55π	$[0.905, 1.095]\pi$
H9s	9	$O(\epsilon^4)$	0.2947	1.2711, 0.1069, 0.5283, 1.1283, 1.9884	7.59π	$[0.857, 1.143]\pi$
H11s	11	$O(\epsilon^5)$	0.2985	1.7377, 0.1651, 0.9147, 0.1510, 0.9331, 1.6415	9.60π	$[0.814, 1.186]\pi$
H13s	13	$O(\epsilon^6)$	0.5065	0.0065, 1.7755, 0.7155, 0.5188, 0.2662, 1.2251, 1.3189	12.01π	$[0.776, 1.224]\pi$
H15s	15	$O(\epsilon^7)$	0.3213	1.2316, 0.9204, 0.2043, 1.9199, 0.8910, 0.7381, 1.9612, 1.3649	13.64π	$[0.740, 1.260]\pi$
Asymmetric sequences $(\pi/2)_{\phi_1} \pi_{\phi_2} \pi_{\phi_3} \cdots \pi_{\phi_{N-1}} \pi_{\phi_N}$						
notation	N	$O(\epsilon^n)$	α, β	$\phi_1, \phi_2, \dots, \phi_N$ (in units π) (according to (2.10))	\mathcal{A}_{tot}	Range
H5w	5	$O(\epsilon^2)$	0.5, 1.0	0.5, 1.0399, 0.1197, 0.1197, 1.0399	4.50π	$[0.952, 1.048]\pi$
H7w	7	$O(\epsilon^3)$	0.5, 1.0	0.5, 1.4581, 0.7153, 0.1495, 1.3738, 0.2568, 0.7752	6.50π	$[0.905, 1.095]\pi$
H9w	9	$O(\epsilon^4)$	0.5, 1.0	0.5, 0.9681, 1.4004, 0.4203, 0.0927, 0.0927, 0.4203, 1.4004, 0.9681	8.50π	$[0.857, 1.143]\pi$
H11w	11	$O(\epsilon^5)$	0.5, 1.0	0.5, 0.7807, 0.1769, 1.4678, 0.1085, 1.0174, 0.2988, 0.8883,	10.50π	$[0.814, 1.186]\pi$
			0.5, 1.0	1.2697, 0.3773, 1.6775		
H13w	13	$O(\epsilon^6)$	0.5, 1.0	0.5, 0.6106, 1.5228, 0.9960, 0.2743, 1.4857, 0.3020, 0.3020,		

1.4857, 0.2743, 0.9960, 1.5228, 0.6106							12.50 π	[0.776, 1.224] π
Asymmetric sequences $\alpha_{\phi_1} \pi_{\phi_2} \pi_{\phi_3} \cdots \pi_{\phi_{N-1}} \beta_{\phi_N}$								
notation	N	$O(\epsilon^n)$	α, β	$\phi_1, \phi_2, \dots, \phi_N$ (in units π) (according to (2.11))			\mathcal{A}_{tot}	Range
H4a	4	$O(\epsilon^2)$	0.7821, 1.3914	1.8226, 0.6492, 1.2131, 0.3071			4.17 π	[0.952, 1.048] π
H6a	6	$O(\epsilon^3)$	0.5917, 1.1305	1.5943, 0.2860, 0.8435, 1.6553, 0.7962, 0.2523			5.72 π	[0.905, 1.095] π
H8a	8	$O(\epsilon^4)$	0.4954, 0.9028	1.5971, 0.7674, 0.5721, 1.8487, 1.0592, 1.9512, 0.3824, 0.9846			7.40 π	[0.857, 1.143] π
H10a	10	$O(\epsilon^5)$	0.6041, 1.1819	1.3480, 0.9259, 0.0292, 0.7288, 0.0996, 1.3909, 0.0183, 0.9322, 0.2169, 0.7975			9.79 π	[0.814, 1.186] π
H12a	12	$O(\epsilon^6)$	0.4168, 0.8841	1.5817, 1.1160, 0.3751, 0.9583, 0.1333, 1.9445, 1.0381, 1.6293, 0.4845, 0.0046, 0.8278, 0.7416			11.30 π	[0.776, 1.224] π

Table 2.3: Pulse area α and phases of composite pulse sequences which produce rotation gates of angle θ (according to (5.33)). The area α and all phases are given in units π . The case of $\theta = \frac{1}{2}\pi$ repeats the symmetric Hadamard gate already presented in Sec. 2.4; they are given here for the sake of comparison and completeness.

	3 pulses, $O(\epsilon)$	5 pulses, $O(\epsilon^2)$	7 pulses, $O(\epsilon^3)$	9 pulses, $O(\epsilon^4)$
	$\alpha_{\phi_1} \pi_{\phi_2} \alpha_{\phi_1}$	$\alpha_{\phi_1} \pi_{\phi_2} \pi_{\phi_3} \pi_{\phi_2} \alpha_{\phi_1}$	$\alpha_{\phi_1} \pi_{\phi_2} \pi_{\phi_3} \pi_{\phi_4} \pi_{\phi_3} \pi_{\phi_2} \alpha_{\phi_1}$	$\alpha_{\phi_1} \pi_{\phi_2} \pi_{\phi_3} \pi_{\phi_4} \pi_{\phi_5} \pi_{\phi_4} \pi_{\phi_3} \pi_{\phi_2} \alpha_{\phi_1}$
θ	$\alpha; \phi_1, \phi_2$	$\alpha; \phi_1, \phi_2, \phi_3$	$\alpha; \phi_1, \phi_2, \phi_3, \phi_4$	$\alpha; \phi_1, \phi_2, \phi_3, \phi_4, \phi_5$
$\frac{1}{10}$	0.5061; 0.5389, 1.4892	0.4548; 0.1416, 1.0230, 1.9258	0.4625; 0.2317, 1.3366, 0.5783, 1.6821	0.5125; 1.4200, 0.3412, 1.0473, 1.7812, 0.6816
$\frac{1}{8}$	0.5096; 0.5483, 1.4865	0.4453; 0.1626, 1.0245, 1.9168	0.4500; 0.2069, 1.3222, 0.5860, 1.6970	0.5101; 1.4490, 0.3687, 1.0489, 1.7665, 0.6618
$\frac{1}{6}$	0.5169; 0.5636, 1.4819	0.4315; 0.1964, 1.0259, 1.9032	0.4277; 0.1691, 1.3020, 0.5976, 1.7183	0.5022; 1.4918, 0.4092, 1.0502, 1.7455, 0.6340
$\frac{1}{5}$	0.5242; 0.5754, 1.4782	0.4225; 0.2231, 1.0263, 1.8934	0.4090; 0.1404, 1.2886, 0.6061, 1.7334	0.4926; 1.5229, 0.4382, 1.0502, 1.7308, 0.6148
$\frac{1}{4}$	0.5375; 0.5921, 1.4726	0.4129; 0.2630, 1.0259, 1.8796	0.3803; 0.0977, 1.2717, 0.6181, 1.7536	0.4729; 1.5661, 0.4770, 1.0491, 1.7110, 0.5894
$\frac{1}{3}$	0.5653; 0.6173, 1.4628	0.4087; 0.3293, 1.0231, 1.8583	0.3336; 0.0212, 1.2505, 0.6370, 1.7836	0.4269; 1.6326, 0.5314, 1.0448, 1.6815, 0.5525
$\frac{1}{2}$	0.6399; 0.6558, 1.4413	0.4500; 0.4494, 1.0106, 1.8179	0.2769; 1.8197, 1.2275, 0.6745, 1.8376	0.2947; 1.7711, 0.6069, 1.0283, 1.6283, 0.4884
$\frac{2}{3}$	0.7365; 0.6779, 1.4155	0.5563; 0.5329, 0.9886, 1.7746	0.3410; 1.6020, 1.2252, 0.7168, 1.8923	0.1700; 0.0700, 0.6449, 1.0009, 1.5735, 0.4254
$\frac{3}{4}$	0.7925; 0.6827, 1.4000	0.6322; 0.5585, 0.9728, 1.7498	0.4269; 1.5309, 1.2317, 0.7421, 1.9230	0.2045; 0.3134, 0.6515, 0.9816, 1.5423, 0.3905
$\frac{4}{5}$	0.8288; 0.6834, 1.3895	0.6857; 0.5688, 0.9613, 1.7332	0.4947; 1.5017, 1.2386, 0.7595, 1.9436	0.2726; 0.4091, 0.6514, 0.9674, 1.5212, 0.3672
$\frac{5}{6}$	0.8542; 0.6829, 1.3819	0.7251; 0.5735, 0.9526, 1.7210	0.5474; 1.4872, 1.2446, 0.7725, 1.9586	0.3336; 0.4507, 0.6495, 0.9564, 1.5055, 0.3501
$\frac{7}{8}$	0.8874; 0.6812, 1.3717	0.7795; 0.5770, 0.9401, 1.7044	0.6234; 1.4741, 1.2542, 0.7907, 1.9795	0.4275; 0.4853, 0.6446, 0.9404, 1.4837, 0.3264
$\frac{9}{10}$	0.9083; 0.6795, 1.3650	0.8154; 0.5777, 0.9316, 1.6934	0.6759; 1.46887, 1.2613, 0.8030, 1.9935	0.4952; 0.4992, 0.6402, 0.9291, 1.4688, 0.3103

COMPOSITE PULSES FOR ROBUST ULTRAHIGH-FIDELITY PHASE GATES

A number of CP sequences for four basic quantum phase gates — the Z, S, T and general phase gates — are presented. The CP sequences contain up to 18 pulses and can compensate up to eight orders of experimental errors in the pulse amplitude and duration. The short CP sequences (up to 8 pulses) are calculated analytically and the longer ones numerically. The results presented in this article demonstrate the remarkable flexibility of CPs accompanied by extreme accuracy and robustness to errors — three features that cannot be simultaneously achieved by any other coherent control technique. These CP sequences, in particular the Z, S and T gates, can be very useful quantum control tools in quantum information applications, because they provide a variety of options to find the optimal balance between ultrahigh fidelity, error range and speed, which may be different in different physical systems.

3.1 INTRODUCTION

Phase coherence is of paramount importance in modern quantum information technologies and it is one of the most significant differences between classical and quantum computing [1, 2, 63, 64]. Phase coherence is created and controlled by quantum phase gates, such as the Z, S and T gates, which are key elements in any quantum circuit. Because of the vast number of such gates involved even in moderate quantum circuits their fidelity is of crucial significance for the success of any quantum algorithm.

Among the existing quantum control techniques capable of efficient manipulation of quantum systems, composite pulse (CP) sequences [44, 45] stand out as a very powerful tool which offers a unique combination of accuracy of operations, robustness to experimental errors, flexibility and versatility as it can be adopted and applied to essentially any qubit control task — a set of features that can only be found in composite pulses. A composite pulse is actually a train of pulses with

well defined relative phases which are used as control parameters in order to shape the excitation profile, and generally, the propagator, in a desired manner.

The vast majority of composite pulses are designed to produce complete and partial rotations on the Bloch sphere [3, 44, 45, 47, 48, 89, 90, 99]. Among these, a clear distinction exists between the so-called variable and constant rotations. Variable rotations start on one of the poles of the Bloch sphere and move the Bloch vector at a particular latitude, i.e. on a particular parallel, without controlling the longitude. Constant rotations do not require a specific initial condition and produce the desired rotation starting at any point on the Bloch sphere. In quantum control language, the variable rotations are characterized by well-defined absolute values (i.e. populations) of the propagator elements but not well-defined phases. Constant rotations (or phase-distortionless rotations) are characterized by both well-defined populations and phases of the propagator, i.e. the quantum gate. Obviously, constant rotations are much more demanding to generate, but they are exactly what is required for reliable and scalable quantum computing circuits. Over the year, variable and constant composite rotations have been demonstrated on multiple occasions in NMR [3, 44, 45, 85–90], trapped ions [15, 16, 18–22, 74], neutral atoms [23, 34–37], quantum dots [27–32], doped solids [24–26, 93], superconducting qubits [120, 121], etc., featuring remarkable accuracy and robustness. A variation of the composite idea, with the detuning rather than the phase of each constituent pulse in the composite sequence used as the control parameter, has also been proposed and experimentally demonstrated [122].

Very few proposals exist for composite phase gates [109]. In the present chapter, we make a step toward filling this gap: we supplement the library of composite pulses with composite pulses which produce arbitrary quantum phase gates, with a focus at the most important ones for quantum information processing: the S, T and Z gates.

An arbitrary phase shift at an angle ϕ , being rotation around z axis, can be implemented by two resonant π pulses up to an undetectable global phase. However, resonant driving is prone to errors in the experimental parameters, e.g. the pulse amplitude, duration, and detuning. Here the phase gates are implemented as the sequences of π rotations with specific phases. Hence, the various quantum control techniques and proposals that make rotation gates error-resilient, are applicable in this context. Application of composite pulses to produce well-defined phase shifts of the two states of a qubit is presented in [109]. Here, we use analytic approaches and brute-force numerics to derive composite sequences for Z, S, T and general phase gates, which achieve error compensation of up to 8th order. Compared to Ref. [109], we go a step further: by compensating all elements in a general phase-gate matrix, we also ensure that these composite pulses are phase-distortionless.

This chapter is organized as follows. In Sec. 3.2 we explain the derivation method. Design and performance of phase gates are presented in Sec. 3.3. Finally, Sec. 3.4 presents the conclusions.

3.2 SU(2) APPROACH

Our objective in this chapter is to construct the qubit phase-shift gate $\hat{F}(\phi) = e^{-i(\phi/2)\hat{\sigma}_z}$ (1.12). Under the assumption of a single systematic pulse area error ϵ , we can expand the composite propagator (2.3) in a Taylor series versus ϵ . Because of the SU(2) symmetry of the overall propagator, it suffices to expand only two of its elements, say $\mathcal{U}_{11}(\epsilon)$ and $\mathcal{U}_{12}(\epsilon)$. We set their zero-error values to the target values,

$$\mathcal{U}_{11}(0) = e^{-i\phi/2}, \quad \mathcal{U}_{12}(0) = 0, \quad (3.1)$$

and we set as many of their derivatives with respect to ϵ , in the increasing order, as possible,

$$\mathcal{U}_{11}^{(m)}(0) = 0, \quad \mathcal{U}_{12}^{(m)}(0) = 0, \quad (m = 1, 2, \dots, n), \quad (3.2)$$

where $\mathcal{U}_{jl}^{(m)} = \partial_\epsilon^m \mathcal{U}_{jl}$ denotes the m th derivative of \mathcal{U}_{jl} with respect to ϵ . The largest derivative order n satisfying Eqs. (3.2) gives the order of the error compensation $O(\epsilon^n)$.

Equations (3.1) and (3.2) generate a system of $2(n+1)$ algebraic equations for the nominal pulse areas A_k and the composite phases ϕ_k ($k = 1, 2, \dots, N$). The equations are complex-valued and generally we have to solve $4(n+1)$ equations with the $2N$ free parameters (nominal pulse areas and phases). Only the equation (3.1) can be satisfied at least by two π pulses (see (1.13)). Taking into account this fact, and because of the normalization condition $|\mathcal{U}_{11}|^2 + |\mathcal{U}_{12}|^2 = 1$, an error compensation of order n requires a CP sequence of $N = 2n + 2$ pieces of π pulses.

As stated above, the derivation of the CP sequences requires the solution of Eqs. (3.1) and (3.2). For a small number of pulses (up to about eight π pulses), the set of equations can be solved analytically. For longer sequences, Eqs. (3.1) and the first, second and third two equations ($n = 3$) of Eqs. (3.2) can be solved analytically, but the higher orders in Eqs. (3.2) they are solved numerically. We do this by using standard routines in MATHEMATICA[®].

3.3 BROADBAND COMPOSITE PHASE GATES

3.3.1 Design for composite phase gates

Based on numerical evidence, we consider symmetric type (in pulse areas) of CP sequences, designed by π pulses.

Each symmetric sequence consists of a sequence of $2n + 2$ nominal π pulses, with asymmetrically ordered phases,

$$\pi_\nu \pi_{\nu+\phi_1} \pi_{\nu+\phi_2} \cdots \pi_{\nu+\phi_n} \cdot \pi_{\nu+\pi-\frac{1}{2}\phi} \pi_{\nu+\phi_1+\pi-\frac{1}{2}\phi} \pi_{\nu+\phi_2+\pi-\frac{1}{2}\phi} \cdots \pi_{\nu+\phi_n+\pi-\frac{1}{2}\phi}, \quad (3.3)$$

equivalent to

$$\pi_{\nu+\pi+\frac{1}{2}\phi} \pi_{\nu+\phi_1+\pi+\frac{1}{2}\phi} \pi_{\nu+\phi_2+\pi+\frac{1}{2}\phi} \cdots \pi_{\nu+\phi_n+\pi+\frac{1}{2}\phi} \cdot \pi_\nu \pi_{\nu+\phi_1} \pi_{\nu+\phi_2} \cdots \pi_{\nu+\phi_n}. \quad (3.4)$$

These sequences generalize the initial two-pulse sequence (see (1.13)) and have similar design. Due to this specific structure of composite phases, the equations (3.1) are satisfied, all odd-order derivatives $\mathcal{U}_{11}^{(2k+1)}(0)$ of the major-diagonal elements in Eq. (3.2) vanish, and so do all even-order derivatives $\mathcal{U}_{12}^{(2k)}(0)$ of the minor-diagonal elements. Despite this fact, we call the compensation order n the maximum number m for which all major-diagonal and minor-diagonal elements are optimized simultaneously from 1 to n . This can be obtained with the precise choice of the available composite phases in (3.3).

From an infinite number of solutions, we choose solutions of the type (3.3) and with a free parameter $\nu = 0$, as the choice of relative phases $\phi_1, \phi_2, \dots, \phi_n$ is of importance. Henceforth, we target and use a form

$$\pi_0 \pi_{\phi_1} \pi_{\phi_2} \cdots \pi_{\phi_n} \cdot \pi_{\pi-\frac{1}{2}\phi} \pi_{\phi_1+\pi-\frac{1}{2}\phi} \pi_{\phi_2+\pi-\frac{1}{2}\phi} \cdots \pi_{\phi_n+\pi-\frac{1}{2}\phi}, \quad (3.5)$$

and other possible solutions can be obtained by choosing an arbitrary parameter ν in (3.3) or/and by passing to the type (3.4).

3.3.2 General Phase-shift gate

As it is well known, such a gate can be produced by two resonant pulses of total temporal area 2π (see (1.13) with $\nu = 0$). The propagator of two pulses reads

$$\mathbf{U} = \begin{bmatrix} e^{-i\phi/2} \cos^2(\pi\epsilon/2) + \sin^2(\pi\epsilon/2) & \frac{1}{2}i(1 - e^{-i\phi/2}) \sin(\pi\epsilon) \\ \frac{1}{2}i(1 - e^{i\phi/2}) \sin(\pi\epsilon) & e^{i\phi/2} \cos^2(\pi\epsilon/2) + \sin^2(\pi\epsilon/2) \end{bmatrix}, \quad (3.6)$$

where ϵ is the pulse area error. The Frobenius distance fidelity (2.7) reads for phase-shift gate $\mathbf{F}(\phi) = \mathcal{U}(0)$

$$\mathcal{F} = 1 - \sqrt{2} \left| \sin \frac{\pi\epsilon}{2} \right| \left| \sin \frac{\phi}{4} \right|. \quad (3.7)$$

For comparison, the trace fidelity is

$$\mathcal{F}_T = 1 - 2 \sin^2 \frac{\pi\epsilon}{2} \sin^2 \frac{\phi}{4}. \quad (3.8)$$

Obviously the error stemming from the Frobenius distance fidelity (3.7), which is of order $O(\epsilon)$, is far greater than the value of the error stemming from the trace fidelity (3.8), which is of order $O(\epsilon^2)$ (as for the rotation gate).

Longer pulses have a higher order of compensation, which is noticeable in fidelity frames. Below we consider these sequences, in the increasing order of error compensation.

3.3.2.1 First-order error compensation

The careful analysis of Eqs. (3.1) and (3.2) shows that the shortest possible CP which can compensate first-order errors (both in major and minor diagonal elements) consists of four pulses, each with a pulse area of π , and asymmetric phases, with the structure similar to the two pulses,

$$\pi_0 \pi_{\phi_1} \pi_{\pi - \frac{1}{2}\phi} \pi_{\phi_1 + \pi - \frac{1}{2}\phi}. \quad (3.9)$$

Solving Eq. (3.1) along with Eq. (3.2) for the first derivatives gives two solutions for the phases,

$$\pi_0 \pi_{-\frac{1}{4}\phi} \pi_{\pi - \frac{1}{2}\phi} \pi_{\frac{3}{4}\pi - \frac{1}{2}\phi'} \quad (3.10a)$$

$$\pi_0 \pi_{\frac{3}{4}\phi} \pi_{\pi - \frac{1}{2}\phi} \pi_{\frac{7}{4}\pi - \frac{1}{2}\phi}. \quad (3.10b)$$

These two sequences generate the same propagator and hence the same fidelity.

The Frobenius distance and trace distance fidelities read

$$\mathcal{F} = 1 - \sqrt{2} \left| \sin^2 \frac{\pi\epsilon}{2} \right| \left| \sin \frac{\phi}{4} \right|, \quad (3.11a)$$

$$\mathcal{F}_T = 1 - 2 \sin^4 \frac{\pi\epsilon}{2} \sin^2 \frac{\phi}{4}. \quad (3.11b)$$

Obviously, the Frobenius distance infidelity for four sequences is of order $O(\epsilon^2)$ and it is much larger than the trace distance infidelity, which is of order $O(\epsilon^4)$. The

trace distance fidelity is much higher than the Frobenius distance fidelity, similar to rotation gates. With respect to the quantum computation benchmark fidelity value of $1 - 10^{-4}$, the Frobenius distance fidelity (3.11a) for the four-pulse composite Z4 gates of Eqs. (3.10) remains above this value in the pulse area interval $(0.9936\pi, 1.0064\pi)$, i.e. for relative errors up to $|\epsilon| < 0.0064$ to be more precise. For comparison, the trace distance fidelity (3.11b) remains above this value in the pulse area interval $(0.936\pi, 1.064\pi)$, i.e. for relative errors up to $|\epsilon| < 0.064$, a factor of 10 larger. Again we notice that the Frobenius distance fidelity is a much more stringent measure of quality.

For four-pulse composite S4 gate, the Frobenius interval is $(0.9913\pi, 1.0087\pi)$ with the relative errors up to $|\epsilon| < 0.0087$, and the trace interval is $(0.913\pi, 1.087\pi)$ with the relative errors up to $|\epsilon| < 0.087$, a factor of 10 larger. For four-pulse composite T4 gate, the Frobenius interval is $(0.9879\pi, 1.0121\pi)$ with the relative errors up to $|\epsilon| < 0.0121$, and the trace interval is $(0.878\pi, 1.122\pi)$ with the relative errors up to $|\epsilon| < 0.122$, a factor of 10 larger.

Both the Frobenius and the trace distance fidelities depend on the phase flip angle ϕ . The pulse area intervals for the four-pulse composite S4 gates are larger than for the four-pulse composite Z4 gates and smaller than for the four-pulse composite T4 gates. This monotonic pattern persists for longer sequences as well.

3.3.2.2 Second-order error compensation

For sequences of six- π pulses, it becomes possible to annul also the second-order derivatives in Eq. (3.2). Design of this asymmetric sequence make it possible to derive analytic solutions

$$\pi_{\phi_0} \pi_{\phi_1} \pi_{\phi_2} \pi_{\phi_0 + \pi - \frac{1}{2}\phi} \pi_{\phi_1 + \pi - \frac{1}{2}\phi} \pi_{\phi_2 + \pi - \frac{1}{2}\phi} \quad (3.12)$$

The careful analysis of these type of sequences shows that they can be written in a compact form as

$$\pi_{\chi} (2\pi)_0 \pi_{\chi + \pi - \frac{1}{2}\phi} (2\pi)_{\pi - \frac{1}{2}\phi'} \quad (3.13a)$$

$$\pi_{\pi + \frac{1}{2}\phi - \chi} (2\pi)_0 \pi_{-\chi} (2\pi)_{\pi - \frac{1}{2}\phi'} \quad (3.13b)$$

$$(2\pi)_0 \pi_{\pi - \frac{1}{2}\phi + \chi} (2\pi)_{\pi - \frac{1}{2}\phi} \pi_{-\phi + \chi'} \quad (3.13c)$$

$$(2\pi)_0 \pi_{-\chi} (2\pi)_{\pi - \frac{1}{2}\phi} \pi_{-\chi + \pi - \frac{1}{2}\phi'} \quad (3.13d)$$

where $\chi = \frac{1}{4}\phi + \arcsin\left(\frac{1}{2}\sin\left(\frac{1}{4}\phi\right)\right)$.

The Frobenius distance and trace distance fidelities for these second-order sequences read

$$\mathcal{F} = 1 - \sqrt{2} \left| \sin^3 \frac{\pi\epsilon}{2} \right| \left| \sin \frac{\phi}{4} \right|, \quad (3.14a)$$

$$\mathcal{F}_T = 1 - 2 \sin^6 \frac{\pi\epsilon}{2} \sin^2 \frac{\phi}{4}. \quad (3.14b)$$

3.3.2.3 Third-order error compensation

Nullification of the third-order derivatives in Eq. (3.2) as well, requires eight- π pulses. Here, in contrast to the rotation gates, the composite phase gates with eight pulses

$$\pi_{\phi_0} \pi_{\phi_1} \pi_{\phi_2} \pi_{\phi_3} \pi_{\phi_0+\pi-\frac{1}{2}\phi} \pi_{\phi_1+\pi-\frac{1}{2}\phi} \pi_{\phi_2+\pi-\frac{1}{2}\phi} \pi_{\phi_3+\pi-\frac{1}{2}\phi}, \quad (3.15)$$

can be simplified giving analytic solutions. Careful analysis of these type of sequences shows that they can be written in a compact form as

$$\pi_{\chi} (2\pi)_0 \pi_{\chi+\pi-\frac{1}{4}\phi} \pi_{\chi+\pi-\frac{1}{2}\phi} (2\pi)_{\pi-\frac{1}{2}\phi} \pi_{\chi-\frac{3}{4}\phi}, \quad (3.16a)$$

$$\pi_{-\chi+\pi+\frac{1}{4}\phi} (2\pi)_0 \pi_{-\chi} \pi_{-\chi-\frac{1}{4}\phi} (2\pi)_{\pi-\frac{1}{2}\phi} \pi_{-\chi+\pi-\frac{1}{2}\phi}, \quad (3.16b)$$

$$(2\pi)_0 \pi_{\chi+\pi-\frac{1}{4}\phi} \pi_{\chi+\pi-\frac{1}{2}\phi} (2\pi)_{\pi-\frac{1}{2}\phi} \pi_{\chi-\frac{3}{4}\phi} \pi_{\chi-\phi}, \quad (3.16c)$$

$$(2\pi)_0 \pi_{-\chi} \pi_{-\chi-\frac{1}{4}\phi} (2\pi)_{\pi-\frac{1}{2}\phi} \pi_{-\chi+\pi-\frac{1}{2}\phi} \pi_{-\chi+\pi-\frac{3}{4}\phi}, \quad (3.16d)$$

$$\pi_{\chi+\frac{1}{4}\phi} \pi_{\chi} (2\pi)_0 \pi_{\chi+\pi-\frac{1}{4}\phi} \pi_{\chi+\pi-\frac{1}{2}\phi} (2\pi)_{\pi-\frac{1}{2}\phi}, \quad (3.16e)$$

$$\pi_{-\chi+\pi+\frac{1}{2}\phi} \pi_{-\chi+\pi+\frac{1}{4}\phi} (2\pi)_0 \pi_{-\chi} \pi_{-\chi-\frac{1}{4}\phi} (2\pi)_{\pi-\frac{1}{2}\phi}, \quad (3.16f)$$

where $\chi = \frac{1}{8}\phi + \arcsin\left(\frac{1}{2} \sin\left(\frac{1}{8}\phi\right)\right)$. The Frobenius distance and trace distance fidelities for these third-order sequences read

$$\mathcal{F} = 1 - \sqrt{2} \left| \sin^4 \frac{\pi\epsilon}{2} \right| \left| \sin \frac{\phi}{4} \right|, \quad (3.17a)$$

$$\mathcal{F}_T = 1 - 2 \sin^8 \frac{\pi\epsilon}{2} \sin^2 \frac{\phi}{4}. \quad (3.17b)$$

3.3.2.4 Higher-order error compensation

For CP sequences of more than eight- π pulses, the equations for the composite phases quickly get very bulky and unattainable to guess analytically. General form for these sequences is (3.5). Despite this, they can be written in a concise form. They reiterate the pattern of the sequences of four, six and eight pulses above: the

CP sequences of $2n + 2$ pulses have a total pulse area of $(2n + 2)\pi$, with all pulses in the sequence being nominal π pulses. Sequences of $2n + 2$ pulses produce error compensation of the order $O(\epsilon^n)$ and fidelity profiles

$$\mathcal{F} \cong 1 - \sqrt{2} \left| \sin^{n+1} \frac{\pi\epsilon}{2} \right| \left| \sin \frac{\phi}{4} \right|, \quad (3.18a)$$

$$\mathcal{F}_T \cong 1 - 2 \sin^{2n+2} \frac{\pi\epsilon}{2} \sin^2 \frac{\phi}{4}, \quad (3.18b)$$

where fidelities are sensitive to the choice of the composite phases and are approximately equal to their precise values. This type of composite phase gates, the precision of which deviates from the theoretically optimal accuracy (3.18), which is too significant for sequences with twelve- π and fourteen- π , but has the most concise form and shows a structural form for arbitrary phase shift angles. Design of this sequences is shown in the next indent.

We have derived numerically the composite phases for higher order phase gates. The fourth-order compensating ten- π sequences can be written in a compact form

$$(3\pi)_0 \pi_{\phi_3} \pi_{\phi_4} (3\pi)_{\pi - \frac{1}{2}\phi} \pi_{\phi_3 + \pi - \frac{1}{2}\phi} \pi_{\phi_4 + \pi - \frac{1}{2}\phi}. \quad (3.19)$$

For brevity, we release other configurations with arrangements between 3π pulse and π pulses, because all these designs have equal total pulse area, i.e. operation run-time. The reader can obtain such solutions by interchanging pulses in the sequence similar to (3.10), (3.13) and (3.16). The fifth-order compensating twelve- π sequences can be written in a compact form

$$(3\pi)_0 \pi_{\phi_3} \pi_{\phi_4} \pi_{\phi_4 - \phi_3 - \frac{1}{4}\phi} (3\pi)_{\pi - \frac{1}{2}\phi} \pi_{\phi_3 + \pi - \frac{1}{2}\phi} \pi_{\phi_4 + \pi - \frac{1}{2}\phi} \pi_{\phi_4 - \phi_3 + \pi - \frac{3}{4}\phi} \quad (3.20)$$

and the sixth-order compensating fourteen- π sequences can be written in a compact form

$$(4\pi)_0 \pi_{\phi_4} \pi_{\phi_5} \pi_{\phi_6} (4\pi)_{\pi - \frac{1}{2}\phi} \pi_{\phi_3 + \pi - \frac{1}{2}\phi} \pi_{\phi_4 + \pi - \frac{1}{2}\phi} \pi_{\phi_5 + \pi - \frac{3}{4}\phi}. \quad (3.21)$$

The composite phases for this type of composite phase gates for arbitrary phase flip angles are presented in Table 3.4. The structure of these sequences corresponds to (3.3) with $\nu = 0$ and zero first phases for long sequences, i.e. with accordance to (3.10a), (3.13d), (3.16d), (3.19), (3.20) and (3.21). Note that the 3π and 4π pulses in the CP sequence are poor candidates for designing longer phase gates with higher order of compensation.

We have derived numerically another type of sequences consisting of only π and 2π pulses. Their precision exactly matches the theoretically optimal accuracy (3.18). The fourth-order compensating ten- π sequences can be written in a form

$$\pi_0(2\pi)_{\phi_1}\pi_{\phi_3}\pi_{\phi_4}\pi_{\pi-\frac{1}{2}\phi}(2\pi)_{\phi_1+\pi-\frac{1}{2}\phi}\pi_{\phi_3+\pi-\frac{1}{2}\phi}\pi_{\phi_4+\pi-\frac{1}{2}\phi}. \quad (3.22)$$

For brevity, we release other configurations with arrangements between 2π pulse and π pulses, because all these designs have equal total pulse area, i.e. operation run-time. The reader can obtain such solutions by interchanging pulses in the sequence similar to (3.10), (3.13) and (3.16).

The fifth-order compensating twelve- π sequences can be written in a form

$$(2\pi)_0(2\pi)_{\phi_2}\pi_{\phi_4}\pi_{\phi_4-\frac{1}{4}\phi}(2\pi)_{\pi-\frac{1}{2}\phi}(2\pi)_{\phi_2+\pi-\frac{1}{2}\phi}\pi_{\phi_4+\pi-\frac{1}{2}\phi}\pi_{\phi_4+\pi-\frac{3}{4}\phi}, \quad (3.23)$$

and the sixth-order compensating fourteen- π sequences can be written in a form

$$\pi_0(2\pi)_{\phi_1}(2\pi)_{\phi_3}\pi_{\phi_5}\pi_{\phi_6}\pi_{\pi-\frac{1}{2}\phi}(2\pi)_{\phi_1+\pi-\frac{1}{2}\phi}(2\pi)_{\phi_3+\pi-\frac{1}{2}\phi}\pi_{\phi_5+\pi-\frac{1}{2}\phi}\pi_{\phi_6+\pi-\frac{1}{2}\phi}. \quad (3.24)$$

Similarly, the seventh-order compensating sixteen- π sequences can be written in a form

$$(2\pi)_0(2\pi)_{\phi_2}(2\pi)_{\phi_4}\pi_{\phi_6}\pi_{\phi_6-\frac{1}{4}\phi}(2\pi)_{\pi-\frac{1}{2}\phi}(2\pi)_{\phi_2+\pi-\frac{1}{2}\phi}(2\pi)_{\phi_4+\pi-\frac{1}{2}\phi}\pi_{\phi_6+\pi-\frac{1}{2}\phi}\pi_{\phi_6+\pi-\frac{3}{4}\phi}, \quad (3.25)$$

and the eighth-order compensating eighteen- π sequences can be written in a form

$$\begin{aligned} &\pi_0(2\pi)_{\phi_1}(2\pi)_{\phi_3}(2\pi)_{\phi_5}\pi_{\phi_7}\pi_{\phi_8}\pi_{\pi-\frac{1}{2}\phi} \\ &\cdot (2\pi)_{\phi_1+\pi-\frac{1}{2}\phi}(2\pi)_{\phi_3+\pi-\frac{1}{2}\phi}(2\pi)_{\phi_5+\pi-\frac{1}{2}\phi}\pi_{\phi_7+\pi-\frac{1}{2}\phi}\pi_{\phi_8+\pi-\frac{1}{2}\phi}. \end{aligned} \quad (3.26)$$

We have derived numerically the composite phases of this type of sequences of an even number of pulses. They are presented in Tables 3.1, 3.2 and 3.3 for Z, S and T gates correspondingly. The fidelities of these composite Z, S and T gates are plotted in Figures 3.1, 3.2, 3.3 respectively.

It can be seen from the tables and figures that two pulses have very little room for error, since high-fidelity Z, S and T gates allow pulse area errors of less than 0.01%, about 0.01%, about 0.02%, respectively. The four-pulse composite phase gate offers some leeway, with the admissible error of 0.6%, 0.9% and 1.2% for Z, S and T cases. The significant pulse area error correction effect is achieved with the CP sequences of 6 to 10 pulses, for which the high-fidelity range of admissible errors increases from 3% to 10.1% for Z, from 3.6% to 11.5% for S, and from 4.5% to 13.1% for T.

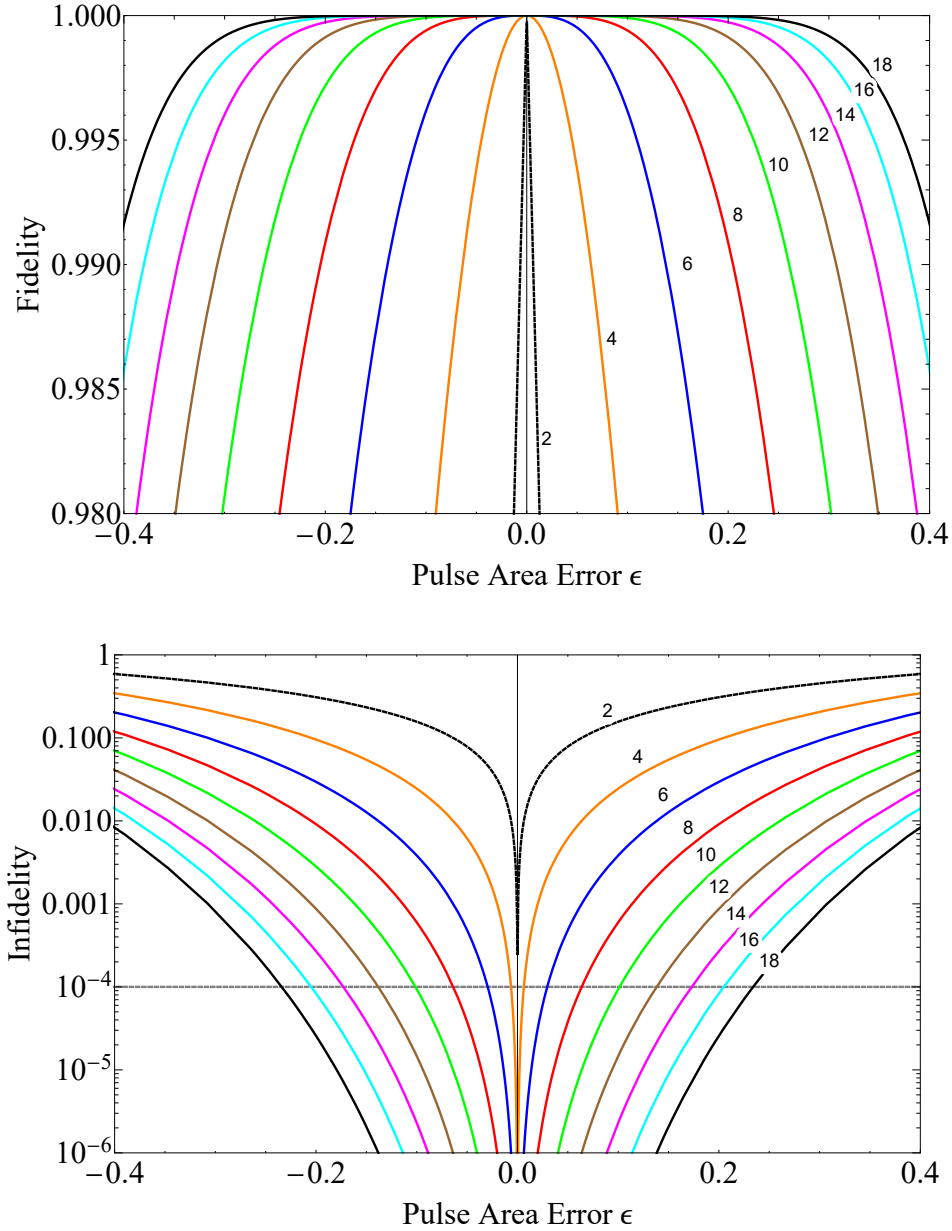


Figure 3.1: Frobenius distance fidelity F (top) and infidelity (bottom) of composite Z gates. The infidelity is in logarithmic scale in order to better visualize the high-fidelity (low-infidelity) range. The numbers N on the curves refer to CP sequences ZN listed in the Table 3.1.

Quite notably, errors of up to 23.4%, 25.1% and 27.1% can be eliminated for Z, S and T, and ultrahigh fidelity maintained, with the 18-pulse composite phase gate. Note that these error ranges are calculated by using the rather tough Frobenius distance fidelity (2.7). Again, had we used the much more relaxed trace distance fidelity (2.8), these ranges would be much broader. Table 3.4 presents composite pulse parameters of general phase gates for different phase angles.

Hereby, very long sequences are barely practical because the gate is much slower. The quantum computer is not required to operate with a pulse area error of 23%

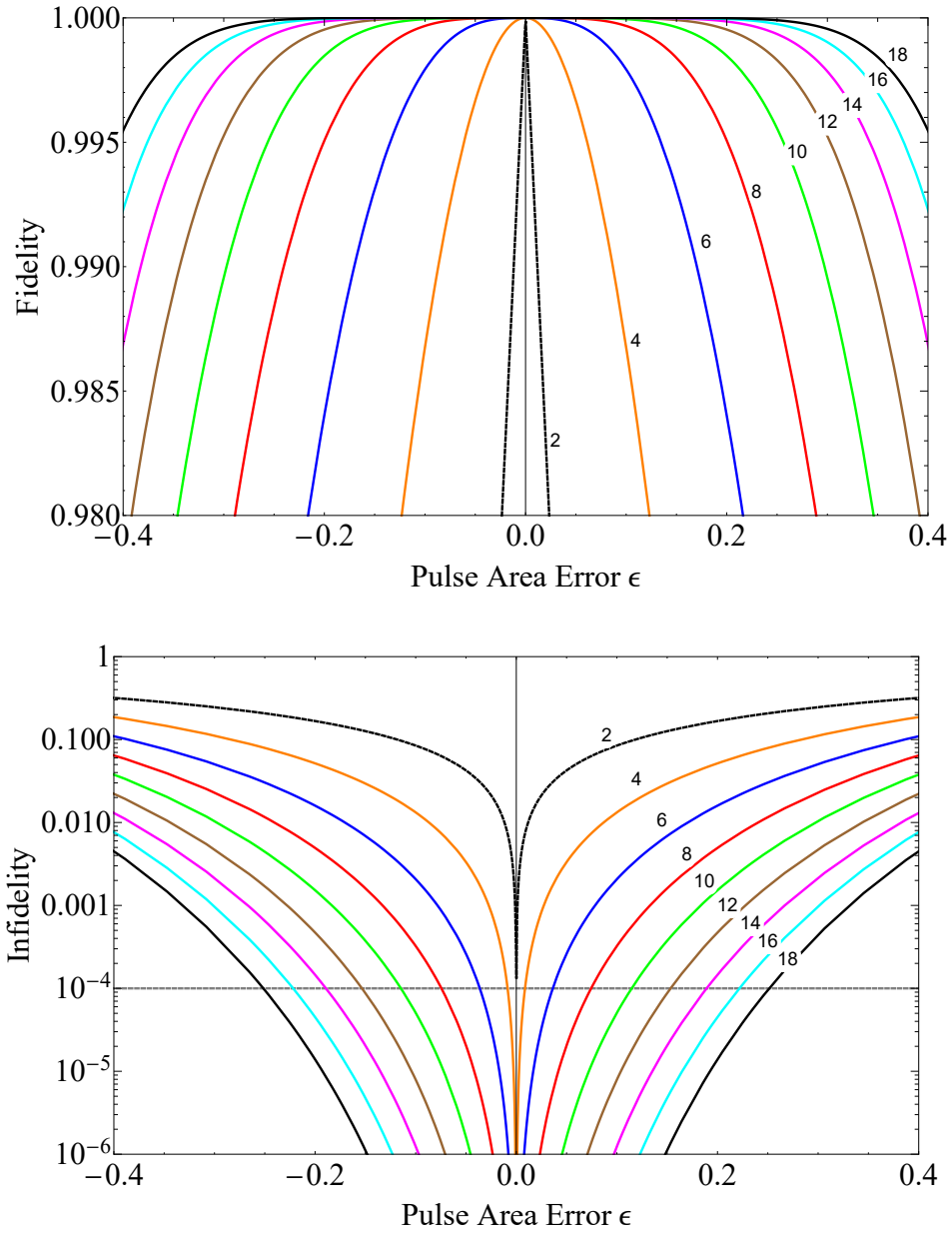


Figure 3.2: Frobenius distance fidelity F (top) and infidelity (bottom) of composite S gates. The infidelity is in logarithmic scale in order to better visualize the high-fidelity (low-infidelity) range. The numbers N on the curves refer to CP sequences SN listed in the Table 3.2.

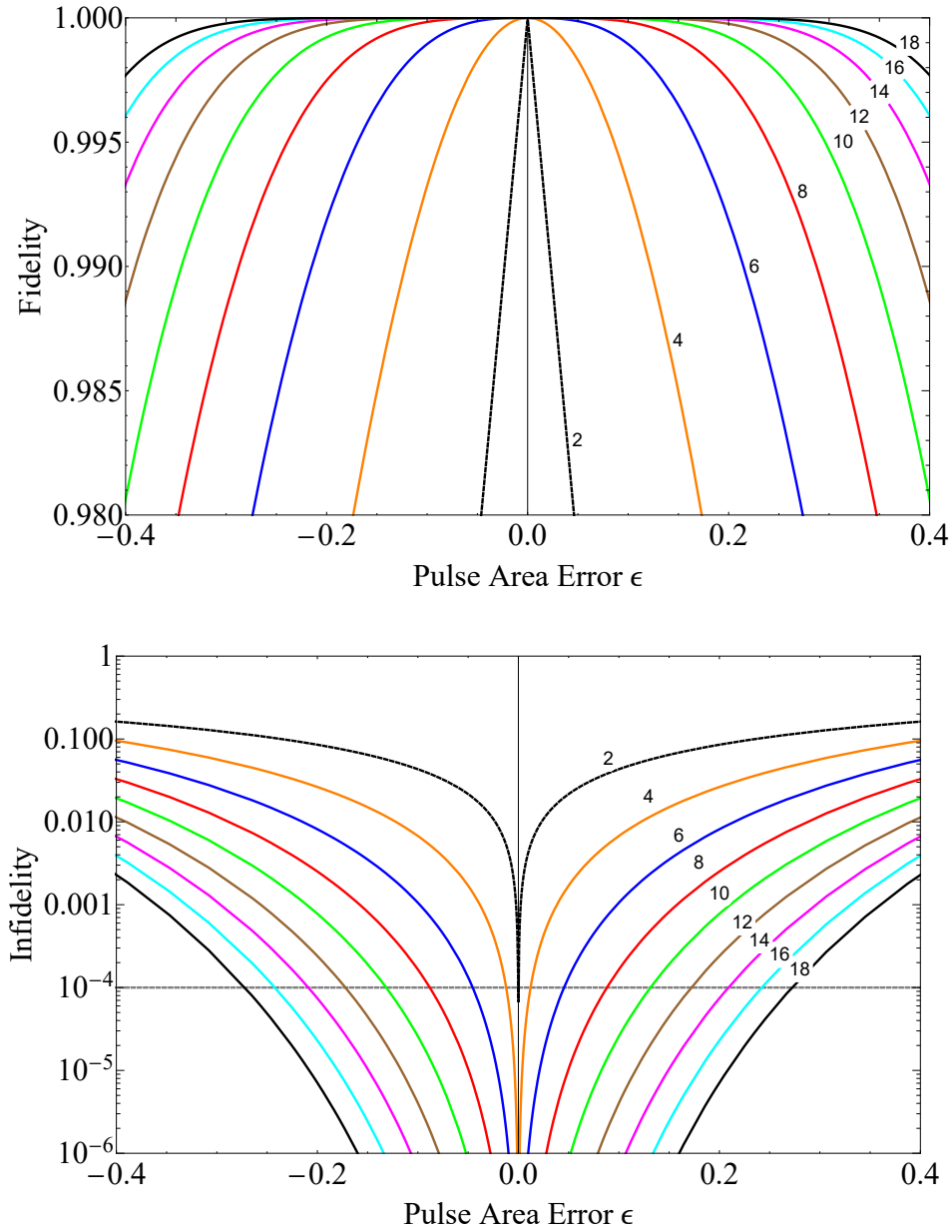


Figure 3.3: Frobenius distance fidelity F (top) and infidelity (bottom) of composite T gates. The infidelity is in logarithmic scale in order to better visualize the high-fidelity (low-infidelity) range. The numbers N on the curves refer to CP sequences TN listed in the Table 3.3.

Table 3.1: Phases of asymmetric composite sequences of $N = 2n + 2$ nominal π pulses, which produce the Z gate with a pulse area error compensation up to order $O(\epsilon^n)$. The last column gives the high-fidelity range $[\pi(1 - \epsilon_0), \pi(1 + \epsilon_0)]$ of pulse area error compensation wherein the Frobenius distance fidelity is above the value 0.9999, i.e. the fidelity error is below 10^{-4} .

Name	Pulses	$O(\epsilon^n)$	Phases $\phi_0, \phi_1, \phi_2, \dots, \phi_n, \phi_{n+1}, \dots, \phi_{2n+1}$ (in units π) (according to (3.3))	High-fidelity error correction range
two	2	$O(\epsilon^0)$	$0, \frac{1}{2}$	$[0.99994\pi, 1.00006\pi]$
Z4	4	$O(\epsilon)$	$0, \frac{7}{4}, \frac{1}{2}, \frac{1}{4}$	$[0.994\pi, 1.006\pi]$
Z6	6	$O(\epsilon^2)$	$0, 0, 1.6350, \frac{1}{2}, \frac{1}{2}, 0.1350$	$[0.970\pi, 1.030\pi]$
Z8	8	$O(\epsilon^3)$	$0, 0, 1.8137, 1.5637, \frac{1}{2}, \frac{1}{2}, 0.3137, 0.0637$	$[0.936\pi, 1.064\pi]$
Z10	10	$O(\epsilon^4)$	$0, 1.0992, 1.0992, 1.8315, 0.0203, \frac{1}{2}, 1.5992, 1.5992, 0.3315, 0.5203$	$[0.899\pi, 1.101\pi]$
Z12	12	$O(\epsilon^5)$	$0, 0, 0.4492, 0.4492, 1.4099, 1.1599, \frac{1}{2}, \frac{1}{2}, 0.9492, 0.9492, 1.9099, 1.6599$	$[0.862\pi, 1.138\pi]$
Z14	14	$O(\epsilon^6)$	$0, 0.7815, 0.7815, 1.9963, 1.9963, 0.8915, 0.3245, \frac{1}{2}, 1.2815, 1.2815, 0.4963,$ $0.4963, 1.3915, 0.8245$	$[0.823\pi, 1.177\pi]$
Z16	16	$O(\epsilon^7)$	$0, 0, 1.8969, 1.8969, 1.0586, 1.0586, 0.0214, 1.7714, \frac{1}{2}, \frac{1}{2}, 0.3969, 0.3969, 1.5586,$ $1.5586, 0.5214, 0.2714$	$[0.795\pi, 1.205\pi]$
Z18	18	$O(\epsilon^8)$	$0, 0.1421, 0.1421, 1.0834, 1.0834, 0.5572, 0.5572, 1.4991, 1.0352, \frac{1}{2}, 0.6421, 0.6421,$ $1.5834, 1.5834, 1.0572, 1.0572, 1.9991, 1.5352$	$[0.766\pi, 1.234\pi]$

Table 3.2: Phases of asymmetric composite sequences of $N = 2n + 2$ nominal π pulses, which produce the S gate with a pulse area error compensation up to order $O(\epsilon^n)$. The last column gives the high-fidelity range $[\pi(1 - \epsilon_0), \pi(1 + \epsilon_0)]$ of pulse area error compensation wherein the Frobenius distance fidelity is above the value 0.9999, i.e. the fidelity error is below 10^{-4} .

Name	Pulses	$O(\epsilon^n)$	Phases $\phi_0, \phi_1, \phi_2, \dots, \phi_n, \phi_{n+1}, \dots, \phi_{2n+1}$ (in units π) (according to (3.3))	High-fidelity error correction range
two	2	$O(\epsilon^0)$	$0, \frac{3}{4}$	$[0.99988\pi, 1.00012\pi]$
S4	4	$O(\epsilon)$	$0, \frac{15}{8}, \frac{3}{4}, \frac{5}{8}$	$[0.991\pi, 1.009\pi]$
S6	6	$O(\epsilon^2)$	$0, 0, 1.8137, \frac{3}{4}, \frac{3}{4}, 0.5637$	$[0.964\pi, 1.036\pi]$
S8	8	$O(\epsilon^3)$	$0, 0, 1.9064, 1.7814, \frac{3}{4}, \frac{3}{4}, 0.6564, 0.5314$	$[0.926\pi, 1.074\pi]$
S10	10	$O(\epsilon^4)$	$0, 0.8226, 0.8226, 1.9152, 0.4416, \frac{3}{4}, 1.5726, 1.5726, 0.6652, 1.1916$	$[0.885\pi, 1.115\pi]$
S12	12	$O(\epsilon^5)$	$0, 0, 1.3587, 1.3587, 0.3367, 0.2117, \frac{3}{4}, \frac{3}{4}, 0.1087, 0.1087, 1.0867, 0.9617$	$[0.847\pi, 1.153\pi]$
S14	14	$O(\epsilon^6)$	$0, 0.8197, 0.8197, 1.6756, 1.6756, 0.7586, 1.1000, \frac{3}{4}, 1.5697, 1.5697, 0.4255,$ $0.4255, 1.5086, 1.8500$	$[0.811\pi, 1.189\pi]$
S16	16	$O(\epsilon^7)$	$0, 0, 1.9466, 1.9466, 1.1420, 1.1420, 0.1251, 0.0001, \frac{3}{4}, \frac{3}{4}, 0.6966, 0.6966, 1.8920,$ $1.8920, 0.8751, 0.7501$	$[0.778\pi, 1.222\pi]$
S18	18	$O(\epsilon^8)$	$0, 0.3453, 0.3453, 1.4636, 1.4636, 0.2616, 0.2616, 1.3543, 0.0643, \frac{3}{4}, 1.0953, 1.0953,$ $0.2136, 0.2136, 1.0116, 1.0116, 0.1043, 0.8143$	$[0.749\pi, 1.251\pi]$

Table 3.3: Phases of asymmetric composite sequences of $N = 2n + 2$ nominal π pulses, which produce the T gate with a pulse area error compensation up to order $O(\epsilon^n)$. The last column gives the high-fidelity range $[\pi(1 - \epsilon_0), \pi(1 + \epsilon_0)]$ of pulse area error compensation wherein the Frobenius distance fidelity is above the value 0.9999, i.e. the fidelity error is below 10^{-4} .

Name	Pulses	$O(\epsilon^n)$	Phases $\phi_0, \phi_1, \phi_2, \dots, \phi_n, \phi_{n+1}, \dots, \phi_{2n+1}$ (in units π) (according to (3.3))	High-fidelity error correction range
two	2	$O(\epsilon^0)$	$0, \frac{7}{8}$	$[0.99977\pi, 1.00023\pi]$
T4	4	$O(\epsilon)$	$0, \frac{31}{16}, \frac{7}{8}, \frac{13}{16}$	$[0.988\pi, 1.012\pi]$
T6	6	$O(\epsilon^2)$	$0, 0, 1.9064, \frac{7}{8}, \frac{7}{8}, 0.7814$	$[0.955\pi, 1.045\pi]$
T8	8	$O(\epsilon^3)$	$0, 0, 1.9531, 1.8906, \frac{7}{8}, \frac{7}{8}, 0.8281, 0.7656$	$[0.912\pi, 1.088\pi]$
T10	10	$O(\epsilon^4)$	$0, 1.1086, 1.1086, 0.0218, 0.2593, \frac{7}{8}, 1.9836, 1.9836, 0.8968, 1.1343$	$[0.869\pi, 1.131\pi]$
T12	12	$O(\epsilon^5)$	$0, 0, 0.5488, 0.5488, 1.5386, 1.4761, \frac{7}{8}, \frac{7}{8}, 1.4238, 1.4238, 0.4136, 0.3511$	$[0.828\pi, 1.172\pi]$
T14	14	$O(\epsilon^6)$	$0, 0.9406, 0.9406, 0.2214, 0.2214, 1.1532, 1.3379, \frac{7}{8}, 1.8156, 1.8156, 1.0964,$ $1.0964, 0.0282, 0.2129$	$[0.791\pi, 1.209\pi]$
T16	16	$O(\epsilon^7)$	$0, 0, 1.9724, 1.9724, 0.7247, 0.7247, 1.7171, 1.6546, \frac{7}{8}, \frac{7}{8}, 0.8474, 0.8474, 1.5997,$ $1.5997, 0.5921, 0.5296$	$[0.758\pi, 1.242\pi]$
T18	18	$O(\epsilon^8)$	$0, 0.9424, 0.9424, 0.5711, 0.5711, 1.3429, 1.3429, 0.3645, 0.6381, \frac{7}{8}, 1.8174, 1.8174,$ $1.4461, 1.4461, 0.2179, 0.2179, 1.2395, 1.5131$	$[0.728\pi, 1.272\pi]$

Table 3.4: Phases of composite pulse sequences which produce phase gates of angle ϕ (according to (3.3)). The all phases are given in units π . The cases of $\phi = \pi$, $\phi = \frac{1}{2}\pi$ and $\phi = \frac{1}{4}\pi$ repeat the asymmetric Z, S and T gates respectively, already presented in Subsec. 3.3.2; they are given here for the sake of comparison and completeness.

	4 pulses, $O(\epsilon)$	6 pulses, $O(\epsilon^2)$	8 pulses, $O(\epsilon^3)$	10 pulses, $O(\epsilon^4)$	12 pulses, $O(\epsilon^5)$	14 pulses, $O(\epsilon^6)$
ϕ	ϕ_1 (see (3.10a))	ϕ_2 (see (3.13d))	ϕ_2, ϕ_3 (see (3.16d))	ϕ_3, ϕ_4 (see (3.19))	ϕ_3, ϕ_4, ϕ_5 (see (3.20))	ϕ_4, ϕ_5, ϕ_6 (see (3.21))
$\frac{1}{16}$	$\frac{127}{64} = 1.984375$	1.9766	1.9883, 1.9727	0.9980, 0.9883	1.0316, 1.7227, 0.6755	0.9995, 0.9960, 0.9857
$\frac{1}{12}$	$\frac{95}{48} = 1.9791(6)$	1.9688	1.9844, 1.9635	0.9974, 0.9844	1.0342, 1.6996, 0.6446	0.9993, 0.9947, 0.9809
$\frac{1}{8}$	$\frac{63}{32} = 1.96875$	1.9531	1.9766, 1.9453	0.9961, 0.9765	1.0379, 1.6646, 0.5955	0.9990, 0.9922, 0.9716
$\frac{1}{6}$	$\frac{47}{24} = 1.958(3)$	1.9375	1.9688, 1.9271	0.9948, 0.9687	1.0405, 1.6378, 0.5556	0.9987, 0.9895, 0.9620
$\frac{1}{4}$	$\frac{31}{16} = 1.9375$	1.9064	1.9531, 1.8906	0.9922, 0.9530	1.0439, 1.5966, 0.4901	0.9980, 0.9843, 0.9431
$\frac{1}{3}$	$\frac{23}{12} = 1.91(6)$	1.8754	1.9375, 1.8542	0.9895, 0.9371	1.0459, 1.5642, 0.4349	0.9974, 0.9790, 0.9240
$\frac{1}{2}$	$\frac{15}{8} = 1.875$	1.8137	1.9064, 1.7814	0.9842, 0.9050	1.0477, 1.5126, 0.3399	0.9961, 0.9684, 0.8855
$\frac{2}{3}$	$\frac{11}{6} = 1.8(3)$	1.7529	1.8754, 1.7087	0.9787, 0.8721	1.0479, 1.4703, 0.2558	0.9947, 0.9575, 0.8460
$\frac{3}{4}$	$\frac{29}{16} = 1.8125$	1.7229	1.8599, 1.6724	0.9759, 0.8552	1.0475, 1.4512, 0.2162	0.9941, 0.9520, 0.8259
$\frac{5}{6}$	$\frac{43}{24} = 1.791(6)$	1.6932	1.8444, 1.6361	0.9731, 0.8381	1.0470, 1.4332, 0.1779	0.9934, 0.9464, 0.8056
$\frac{7}{8}$	$\frac{57}{32} = 1.78125$	1.6785	1.8368, 1.6180	0.9717, 0.8294	1.0467, 1.4245, 0.1591	0.9930, 0.9436, 0.7953
$\frac{11}{12}$	$\frac{85}{48} = 1.7708(3)$	1.6639	1.8291, 1.5999	0.9702, 0.8206	1.0463, 1.4161, 0.1405	0.9927, 0.9407, 0.7849
$\frac{15}{16}$	$\frac{113}{64} = 1.765625$	1.6566	1.8252, 1.5908	0.9695, 0.8161	1.0462, 1.4119, 0.1314	0.9925, 0.9393, 0.7797
1	$\frac{7}{4} = 1.75$	1.6350	1.8137, 1.5637	0.9673, 0.8027	1.0456, 1.4000, 0.1041	0.9920, 0.9350, 0.7638

or more. Thereby, the CP sequences of 6, 8 and 10 pulses seems to offer the best fidelity-to-speed ratio.

3.4 COMMENTS AND CONCLUSIONS

In this chapter we presented a number of CP sequences for four basic quantum gates — the Z gate, the S gate, the T gate and general phase gates. The CP sequences contain up to 18 pulses and can compensate up to eight orders of experimental errors in the pulse amplitude and duration. The short CP sequences (up to 8 pulses) are calculated analytically and the longer ones numerically.

Only one class of asymmetric CP sequences, consisting of nominal π pulses with asymmetric phases (cf. (3.3) and (3.4)), has the role to provide composite phase gates. Although longer composite phase gates can be derived numerically, their fidelity profiles have analytic dependence on the pulse area error, correspond to (3.18) and (3.18a), and show trigonometric relationship with phase-shift angles. Similar class of asymmetric CP sequences for phase gates is derived in [109], where they are build from the θ rotation gates, having twice of total pulse area of them (similar to nesting approach). For this reason, four, eight, twelve, and sixteen CPs are missing, but six, ten, fourteen, and eighteen CPs are given by the simple analytic formula (are more convenient to apply) and have performance equal to the composite gates shown in this chapter. This does not apply to composite phase gates constructed by the universal CPs [93] in [109]¹.

For the general phase gates, we have presented another type of the asymmetric sequences in Table 3.4 for the sake of brevity.

The results presented in this chapter demonstrate the remarkable flexibility of CPs accompanied by extreme accuracy and robustness to errors — three features that cannot be achieved together by any other coherent control technique. We expect these CP sequences, in particular the Z, the S and the T gates, to be very useful quantum control tools in QI applications, because they provide a variety of options to find the optimal balance between ultrahigh fidelity, error range and speed, which may be different in different physical systems.

Besides all, the results presented in this chapter can be applied into PO to obtain broadband polarization rotators using stacked single polarization half-wave plates with the optical axes rotated by precisely chosen rotation angles (composite phases). It is able to be done due to quantum-classical analogy of composite rota-

¹ The target matrix differs from our (1.12) by changing the phase $\phi \rightarrow -\phi$, hence, to compare the results from [109] with ours, it is necessary to change the sign of all phases, viz., the parameters $\phi_k \rightarrow -\phi_k$ and $\chi \rightarrow \chi = -\phi_k + \pi - \phi/2$ in the article. Hereby, we design twice-even number of CP sequences for composite phase gates, in addition to twice-odd number of pulses (already existing).

tions on the Bloch and the Poincaré spheres (cf. 6.2). Hereby, we demonstrate the possibility to design the broadband polarization rotators with $\pi/2$, $\pi/4$, $\pi/8$ and arbitrary phase shift angles, by up to 18 CP sequences².

2 Composite phases in the rotation gate matrix and in the Jones matrix are related. Let's compare the results in the Table 3.1 and in the article [119]. Using asymmetric ZN sequences $\varphi_i \rightarrow A_i = \pi$ with composite phases $\theta_i \rightarrow \phi_i/2$, the broadband $\alpha = \pi/2$ (as the target rotation angle is assigned in the article) rotator is designed. Z6 sequence is equivalent to the six sequence in the article in the Table 2 of [119], as the absolute trace fidelity in both cases have equal broadness range. Z10 outperform the ten sequence in the ultrahigh precision and even in the 99.9% trace fidelity, but since high-precision (90%) is necessary in PO, the ten sequence is comparable with our Z14 sequence. Fourteen sequence is slightly worse than Z12. Eighteen and fourteen sequences have equal performance (may be due to over-approximation of composite phases). Despite this, to obtain the results for $\alpha = \pi/4$ (S gate), $\alpha = \pi/8$ (T gate) and arbitrary polarization rotators, it is necessary to apply the structure $(\theta_1, \theta_2, \dots, \theta_{n+1}, \theta_1 + \alpha/2, \theta_2 + \alpha/2, \dots, \theta_{n+1} + \alpha/2)$ of the composite phases (where the first few rotation angles can be taken as zero and n is the broadness order) and to compute the phases. Note that, hereby, we demonstrate the possibility to design broadband arbitrary rotators by up to 18 CP sequences.

NARROWBAND AND PASSBAND COMPOSITE PULSES: APPLICATION TO QUANTUM SENSING

4.1 INTRODUCTION

Quantum rotation gates [1, 2], are the key elements in experimental QC. Interestingly, a Rabi rotation gate, being SU(2), is in the heart of various QC devices, especially AMO (atomic, molecular, optical), while suggested theoretical quantum gates are U(2). Furthermore, a quantum circuit designed by multiple quantum gates represents a composite rotation on a Bloch sphere. X (NOT) and Hadamard rotation gates are two special cases of a single θ pulse or rotation, when $\theta = \pi$ and $\theta = \pi/2$, respectively. On contrary, phase gates require at least two rotations. A method that reveals the benefits of composite rotation gates is CPs.

Although CPs, first, have been used in PO [5, 6], the name, classification and development of the technique belongs to the area of NMR [3, 44, 45, 85, 86, 89, 123, 124]. Being efficient and versatile control technique, CPs may easily adapt to various requirements. This feature manifests in the wide range of applications in both quantum and classical physics — qubit control in trapped ions [15–19, 21, 22], neutral atoms [23], doped solids [24, 25], NV centers in diamond [33, 125], and quantum dots [27–30], high-accuracy optical clocks [34], cold-atom interferometry [35–37], optically dense atomic ensembles [38], magnetometry [39], optomechanics [40], Josephson junctions [126], magnetic resonance imaging (MRI) [127], NMR quantum computation [128], entanglement generation [125], teleportation [15, 129, 130], molecular spectroscopy [131] etc. The possibility of applying a deep neural network for design of CPs is distinguished by its modernity [132].

A CP sequence is a finite train of pulses with specified pulse areas (θ -s) and relative phases (ϕ -s), and in a specific order. Since the initial target in NMR was a composite π pulse with the structure known beforehand (requires a sequence of π pulses), composite phases were in the foreground. Considering various engineering perspectives, it is common to divide CPs into the three main branches —

broadband (BB), narrowband (NB) and passband (PB) classes, given by Wimperis [3, 89].

From the point of view of mathematics, the CPs can be represented as composite rotations on the Bloch-Poincaré sphere. This leads to the second kind of classification of CPs — *variable* (class B) and *constant* (phase-distortionless, fully-compensating or class A) *rotations*, given by Levitt [44–46].

Constant rotation CPs are independent of the initial state and not permit distortions of the phase of the overall propagator in the rotation axis over a wide error band, if not over the entire error range. Combining in one word, they are “universal” over the entire Bloch sphere, which, for instance, makes them applicable to quantum computation [48]. In NMR and magnetic resonance imaging (MRI), constant rotations are often used in advanced, phase-sensitive (require phase cycling) two-dimensional NMR experiments, like COSY [59] and TOCSY, providing a powerful tool for the determination of the chemical structure of molecules.

BB CPs act as TARGET operator in a broad range of errors around 0 value (flat-top fidelity), and as IDENTITY operator only at ± 1 , which expands the fidelity profile, when NB CPs act as TARGET only at 0, and as IDENTITY at the ranges left to 1 and right to -1 (flat-bottom fidelity), which squeezes the fidelity profile. PB CPs merge these two properties, i.e., they are expanded at the center and squeezed at the edges. Longer sequences can enhance the property: designing broader or/and narrower fidelity profiles.

Also it is possible to enhance the property more, using (NB2, BB2, PB2)-like CPs, which we call *ultra-sequences* (ultra-BB, ultra-NB, ultra-PB). These CPs improve with a loss in precision that now fluctuates within a certain range and is no longer flat. Ultra-sequences are applicable in areas where ultrahigh-precision is optional [61].

In a recent chapter, we present narrowband and passband CPs for constant rotations, namely rotation gates. Constant rotations are obviously more demanding than variable ones [99] and require longer sequences for the same order of compensation, as they require propagator-optimization (or so-called full-compensation). Previously, this was theoretically done using the theory of the average Hamiltonian, the Magnus expansion, or the theory of quaternions. Using theoretical way, Wimperis found NB1 and PB1 constant rotations [3], which have second order of optimization. We propose SU(2) random search method to numerically generate constant rotations in a structured way: searching for all candidates in accordance with the compensation order.

This chapter is organized as follows. In Sec. 4.2 we explain the derivation methods. Composite X gates are presented in Sec. 4.3, while composite Hadamard gates in Sec. 4.4. Sec. 4.5 is devoted to the general rotation gates. The last-mentioned

three sections are divided into two subsections, presenting narrowband and pass-band rotations. Finally, Sec. 4.6 presents the conclusions.

4.2 DERIVATION

We derive constant rotations similar to the previous work [48]. We are dealing with the propagator (1.2) with SU(2) symmetry, where a and b are the complex-valued Cayley-Klein parameters satisfying $|a|^2 + |b|^2 = 1$, where $a = \cos(A/2)$ and $b = -i \sin(A/2)e^{i\phi}$. A represents the temporal pulse area $A = \int_{t_i}^{t_f} \Omega(t) dt$ in quantum optics, the pulse width or amplitude θ in NMR, and the phase shift $\varphi = 2\pi L(n_f - n_s)/\lambda$ [119] in PO. Without loss of generality of the problem, we will use the terminology of QC.

A rotation gate (1.2) can be represented by Pauli matrices

$$\mathbf{U}_\phi = e^{-iA(\sigma_x \cos \phi - \sigma_y \sin \phi)}. \quad (4.1)$$

CPs require chronological action of evolutions of the (4.1) type. A train of N pulses (2.2), each with area A_k and phase ϕ_k (applied from left to right), produces the propagator (2.3) (acting, as usual, from right to left).

Under the assumption of a single systematic error of pulse area ϵ (all the pulse areas are errant $A_k \rightarrow A_k(1 + \epsilon)$), we can expand the composite propagator (2.3) in a Taylor series versus ϵ . Because of the SU(2) symmetry of the overall propagator, it suffices to expand only two of its elements, say $\mathcal{U}_{11}(\epsilon)$ and $\mathcal{U}_{12}(\epsilon)$. Since our TARGET operator is the so-called θ pulse (with phase $\phi = \pi/2$) or θ rotation gate, i.e.

$$\text{TARGET} \triangleq \mathbf{R}(\theta) = e^{i\theta\sigma_y/2}, \quad (4.2)$$

again we set their zero-error values to the target values (see (2.4)).

Constant rotations require propagator-optimization, hence, we will optimize both major $\mathcal{U}_{11}(\epsilon)$ and minor $\mathcal{U}_{12}(\epsilon)$ diagonal elements.

4.2.1 Narrowband composite pulses

4.2.1.1 SU(2) approach

Here, we set as many of their derivatives with respect to ϵ at ± 1 , in the increasing order, as possible,

$$\mathcal{U}_{11}^{(m)}(\pm) = 0, \quad \mathcal{U}_{12}^{(m)}(\pm) = 0, \quad (m = 1, 2, \dots, n_s), \quad (4.3)$$

where $\mathcal{U}_{jl}^{(m)} = \partial_\epsilon^m \mathcal{U}_{jl}$ denotes the m th derivative of \mathcal{U}_{jl} with respect to ϵ . The largest derivative order n_s satisfying Eqs. (4.3) gives the order of sensitivity $O(\epsilon^{n_s})$.

Derivation of the NB CPs requires the solution of Eqs. (2.4) and (4.3). We do this numerically by using standard routines in MATHEMATICA: we minimize the following loss or error function of optimization

$$\mathcal{E} = \mathcal{E}_0 + \sum_{k=1}^{n_s} \left[|\mathcal{U}_{11}^{(k)}(-)|^2 + |\mathcal{U}_{11}^{(k)}(+)|^2 + |\mathcal{U}_{12}^{(k)}(-)|^2 + |\mathcal{U}_{12}^{(k)}(+)|^2 \right], \quad (4.4)$$

where the initial condition (targeted gate) is captured by $\mathcal{E}_0 = |\mathcal{U}_{11}(0) - \cos \theta/2|^2 + |\mathcal{U}_{12}(0) - \sin \theta/2|^2$, and n_s is the narrowness or sensitivity order. This minimization method is similar to the least squares, since the sum of the absolute squares of the components of error function are taken. Random search of the minimum of this form provides fast results. For example, the well-known NB1 CP can be derived by using SU(2) approach.

4.2.1.2 Modified-SU(2) approach

We have noticed that sometimes it is better to use the modified version of SU(2) approach. Major and minor diagonal elements of SU(2) matrix are related $|\mathcal{U}_{11}(\epsilon)|^2 + |\mathcal{U}_{21}(\epsilon)|^2 = 1$, being Cayley-Klein parameters. Due to this dependence, optimization of one will directly narrower the other one. To ensure the stability of the phase of constant rotation, we optimize the minor diagonal element. So, the loss function is the following

$$\mathcal{E} = \mathcal{E}_0 + \sum_{k=1}^{2n_s} \left[|\mathcal{U}_{12}^{(k)}(-)|^2 + |\mathcal{U}_{12}^{(k)}(+)|^2 \right]. \quad (4.5)$$

Modified SU(2) approach works for X gate or π rotations, and give better results than by using SU(2). The number of derivatives optimized by both methods is equal, but by this method the minor element (of the actual gate matrix) $\mathcal{U}_{21}(\epsilon)$ is optimized by the order of $2n_s$, two times the sensitivity order. The major element vs error $\mathcal{U}_{11}(\epsilon)$ dependence is already sharp-narrow and symmetric, but minor element vs error $\mathcal{U}_{21}(\epsilon)$ is bell-shaped.

Unfortunately, this method does not work for Hadamard gate or $\pi/2$ rotations. The reason is an asymmetry in both major and minor element dependences $\mathcal{U}_{11}(\epsilon)$ and $\mathcal{U}_{21}(\epsilon)$, which can not be modified to be symmetric. One side is easier to optimize than the other side. The optimization of $\mathcal{U}_{11}(\epsilon)$ at negative side $\epsilon = -1$ is easier than at positive side $\epsilon = 1$, and vice versa for $\mathcal{U}_{12}(\epsilon)$. Maybe there is a method which can do asymmetric optimization which will give better results

for Hadamard gate in fidelity representation, but we limit ourselves to the SU(2) approach, since for rotation gate both sides are important.

4.2.2 Passband composite pulses

4.2.2.1 SU(2) approach

As already mentioned, PB CPs have the properties of both BB and NB CPs. In addition to the narrowband property (4.3), we add broadband property

$$\mathcal{U}_{11}^{(k)}(0) = 0, \quad \mathcal{U}_{12}^{(k)}(0) = 0, \quad (k = 1, 2, \dots, n_r), \quad (4.6a)$$

$$\mathcal{U}_{11}^{(m)}(\pm) = 0, \quad \mathcal{U}_{12}^{(m)}(\pm) = 0, \quad (m = 1, 2, \dots, n_s). \quad (4.6b)$$

Now, in addition to sensitivity order n_s in Eq. (4.6b), we also have n_r which is the largest derivative order satisfying Eq. (4.6a) and gives the order of robustness $O(\epsilon^{n_r})$. Pulse sequence with any combination of n_s and n_r both greater than one is passband. Therefore, we examine two types of passband CPs, namely

- *pari passu* passband CPs, for which robustness and sensitivity orders are equal and define the passband order $n_p = n_r = n_s$,
- *diversis passuum* passband CPs, for which one of the above properties is superior to the other $n_r \neq n_s$.

Derivation of the PB CPs requires the solution of Eqs. (2.4), and (4.6). We do this numerically by using standard routines in MATHEMATICA: we minimize the following loss function of optimization

$$\begin{aligned} \mathcal{E} = \mathcal{E}_0 + \sum_{k=1}^{n_r} \left[|\mathcal{U}_{11}^{(k)}(0)|^2 + |\mathcal{U}_{12}^{(k)}(0)|^2 \right] + \\ + \sum_{k=1}^{n_s} \left[|\mathcal{U}_{11}^{(k)}(-)|^2 + |\mathcal{U}_{11}^{(k)}(+)|^2 + |\mathcal{U}_{12}^{(k)}(-)|^2 + |\mathcal{U}_{12}^{(k)}(+)|^2 \right]. \end{aligned} \quad (4.7)$$

For example, the well-known SK1 ($n_p = 1$) (Solovay-Kitaev method [49]) and PB1 ($n_p = 2$) (Wimperis [3]) and CPs can be derived by using SU(2) approach, which, of course, are *pari passu*. But for $n_p \geq 3$, this straightforward cancellation of required derivatives in both major and minor elements result in the alternating or wiggled CPs. In our opinion, the CP can't take on such a precise optimization — due to this inflexible method, the CP tends to be more square than possible, and these wiggles occur. For this reason, we use more flexible method of the propagator-optimization,

called the method of regularization. Despite this, this method is useful for obtaining diversis passuum CPs (not longer ones since the wiggles occur in the same sense).

4.2.2.2 Regularization approach

Results obtained by the SU(2) method of derivation besides SK1 and PB1, had wiggles on the edges, arising negative fidelity. The optimization method, alternative to SU(2), is more flexible and gives better results is a regularization method

$$\begin{aligned} \mathcal{E} = \mathcal{E}_0 + \sum_{k=1}^{2n_p} & \left[|\mathcal{F}_T^{(k)}(0)|^2 + |\mathcal{F}_T^{(k)}(-)|^2 + |\mathcal{F}_T^{(k)}(+)|^2 \right] + \\ & + \lambda \left[|\mathcal{U}'_{11}(0)|^2 + |\mathcal{U}'_{12}(0)|^2 + |\mathcal{U}'_{11}(+)|^2 + \right. \\ & \left. + |\mathcal{U}'_{11}(-)|^2 + |\mathcal{U}'_{12}(+) + |\mathcal{U}'_{12}(-)|^2 \right], \end{aligned} \quad (4.8)$$

where $2n_p$ orders of narrowness/broadness of trace fidelity of SU(2) matrix are optimized, which is equivalent to the optimization of SU(2) matrix elements by the order of n_p (two times lower). A regularizer $\lambda \neq 0$ constrains the result to be constant rotation and without unnecessary wiggles. In our optimization, it is taken $\lambda = 1$. As you may notice, we constrain ourselves to deriving the pari passu CPs using the regularization method, although it can also be used to derive the diversis passuum CPs. The aim of our work is to show the diversity of the CPs and how to derive them.

4.2.3 Performance measures

As in our previous work [48], here we also use the Frobenius distance fidelity (2.7), as the measure of performance of rotation gates. Alternatively, since this is a common practice in the NMR QC community, the trace fidelity can be used (2.8).

Since we consider constant rotations, the fidelities can not be negative, while it can be the case for CPs alternating at the bottom, i.e. like NB2 and PB2. This problem of negative fidelities could be solved by taking absolute value as was done for the trace fidelity, but we suggest not to take since it has meaning which can be neglected in the opposite case. Negative fidelity means that actual and target matrices are so far from each other, that the infidelity or the norm $\|\mathcal{U}(\epsilon) - \mathbf{R}(\theta)\| = \sqrt{\frac{1}{4} \sum_{j,k=1}^2 |\mathcal{U}_{jk} - R_{jk}|^2}$, the square root of the sum of the squares of absolute values of closeness of matrix elements, is greater than 1. In the worst case, when actual and target matrices have opposite signs, the possible minimum values of fidelities are -1 and $1 - \sqrt{2}$ for trace and distance fidelities, respectively. Opposite sign

represents inessential global phase for quantum gates, and taking absolute value of the fidelity is associated with this consideration. Anyway, this is not our case, since we do not have alternations or wiggles of the fidelity and the minimum of fidelity is at it's boundaries $\epsilon = \pm 1$. As we notice, maximum or top fidelity is equal 100% and represents pure correspondence of actual and target gates $[\mathcal{F}(\theta)]_{max} = [\mathcal{F}(\theta)]_{\epsilon=0} = 1$. Despite this, the minimum or bottom fidelity depends on the θ parameter

$$[\mathcal{F}_T(\theta)]_{min} = [\mathcal{F}_T(\theta)]_{\epsilon=\pm 1} = \cos \frac{\theta}{2}, \quad (4.9a)$$

$$[\mathcal{F}(\theta)]_{min} = [\mathcal{F}(\theta)]_{\epsilon=\pm 1} = 1 - \sqrt{1 - \cos \frac{\theta}{2}}. \quad (4.9b)$$

For the X gate both fidelity measures are zero at the bottom $[\mathcal{F}(\pi)]_{min} = [\mathcal{F}_T(\pi)]_{min} = 0$, when for the Hadamard gate $[\mathcal{F}(\pi/2)]_{min} = 1 - \sqrt{1 - \frac{1}{\sqrt{2}}}$, $[\mathcal{F}_T(\pi/2)]_{min} = \frac{1}{\sqrt{2}}$ they are greater than zero and differ from each other. Moving from $\pi + \pi k$ rotations to the $\pi/2 + \pi k$ ($\forall k \in \mathbb{Z}$), the bottom fidelity increases. Hence, the performances of different rotation gates can not be compared perfectly. This is a drawback of the fidelity measures. Especially, for sensitivity (narrowness of fidelity) measures, the presence of a bottom fidelity can not be neglected. We calculate full width at half-maximum (FWHM) for narrowband composite rotation gates at $\mathcal{F}_{HM} = \frac{[\mathcal{F}]_{max} + [\mathcal{F}(\theta)]_{min}}{2} = \frac{1 + [\mathcal{F}(\theta)]_{min}}{2}$, where $[\mathcal{F}(\theta)]_{min}$ is a bottom fidelity. Likewise, UL-fidelity (ultralow) is computed by adding the value of 10^{-4} to the bottom fidelity $[\mathcal{F}(\theta)]_{min}$, when UH-fidelity (ultrahigh) were computed by substituting this value from the top fidelity 1.

We propose to use the measure $\Delta(\alpha_0) = |\epsilon(\mathcal{F} = \alpha_0)| - |\epsilon(\mathcal{F} = 1 - \alpha_0)|$ of the rectangularity of passband CPs. In our case for rotation gates, we choose α_0 equal to 10^{-4} , which corresponds to the quantum computation benchmark, and rectangularity measure $\Delta \stackrel{\Delta}{=} \Delta(10^{-4})$ is the difference between absolute errors at UL- (ultralow) and UH-fidelities (ultrahigh). Since the slope coefficient (is approximated by a straight line $\tan \beta_0 \simeq \frac{\Delta \mathcal{F}}{\Delta(\alpha_0)} = \frac{1 - 2\alpha_0}{\Delta(\alpha_0)}$) is inversely proportional to Δ , hence, smaller Δ , higher the rectangularity of the fidelity line.

4.3 X GATE

4.3.1 Narrowband

Derivation of the narrowband (hence passband) CPs, contrary to broadband ones, reveals that they must have asymmetric design of phases, which puts up a barrier for derivation of longer sequences due to heavy numerical calculations. As it was

mentioned narrowband pulses are prone to superfluous wiggles when derived by SU(2) method. Nevertheless, we derive composite X gates by this method. To accomplish that, we set two appropriate designs of CPs — antisymmetric AN and Wimperis-kind WN, both are the sequences of π pulses.

If we target pure π composite rotations ($\phi = 0$), AN has the following structure or design

$$\pi_{\phi_1} \pi_{\phi_2} \cdots \pi_{\phi_{n_s}} \pi_{\phi_{n_s+1}} \pi_{-\phi_{n_s}} \cdots \pi_{-\phi_2} \pi_{-\phi_1}, \quad (4.10)$$

and consists of the odd number of π pulses, which besides the middle one, have phases with equal absolute value but with opposite signs when tracking from the left to right and from the right to left. Since we target X gate ($\phi = \pi/2$), $\pi/2$ is added to all phases with both minus and plus signs $\pm\phi_k \rightarrow \pm\phi_k + \pi/2$.

Again, for π composite rotations ($\phi = 0$), WN design looks more interpretable

$$\pi_{\phi_1} \pi_{\phi_2} \pi_{\phi_3} \cdots \pi_{\phi_{n_s+1}} \pi_{\phi_{n_s+1}} \cdots \pi_{\phi_3} \pi_{\phi_2}, \quad (4.11)$$

and consists of the odd number of π pulses, where, besides the first pulse, the second half of the structure is a mirror image of the first half, i.e. in the second half, phases are written in the opposite direction. Again, since we target X gate ($\phi = \pi/2$), $\pi/2$ is added to all phases $\phi_k \rightarrow \phi_k + \pi/2$.

Interestingly, one gets wiggles in the case of AN with 5, 9, 13 pulses, but the gap was filled with WN, which are useful for 5, 9, 13, Lowest member of WN is the well-known NB1 pulse of Wimperis (W5), hence the name of the design. AN and WN CPs for X gate derived by SU(2) approach are listed in Table 4.1. We choose FWHM as the performance measure of sensitivity (narrowness) of narrowband composite X gates.

Curiously, for X gate or π rotation, the modified-SU(2) approach improves the results obtained by the SU(2) method. We derived up to 13 CPs by this method, called AN-m, which have the same antisymmetric design of AN. For example, A3 is derived by both methods. Table 4.2 shows that the AN-m CPs for X gate derived by the modified version of SU(2) outperform the same members N obtained by conventional one. This shows the privilege of antisymmetric pulses over Wimperis-kind ones.

4.3.2 Passband

4.3.2.1 *Pari passu*

Difficulty of derivation of the passband rotation gates is manifested in the appearance of alternation in fidelity (deriving by SU(2)), not established by the derivation

method, exhibiting their tenderness. This problem can be solved by using a regularization method, instead of the strict SU(2) method. Despite that it was possible to derive SK1 and PB1 as the first and second order pari passu passband pulses, respectively (wiggles arise for longer sequences). In both methods, the design of pari passu passband pulses is the same

$$\pi_{\phi_1}(2\pi)_{\phi_2}(2\pi)_{\phi_3} \cdots (2\pi)_{\phi_N}, \quad (4.12)$$

the sequence of nominal 2π pulses, preceded (or succeeded) by a pulse of area π , and the number of pulses N is odd. Sequences obtained by regularization method PN for X gate are listed in Table 4.4. The first member P3 is SK1 ($n_p = 1$), and the second member P5 outperforms PB1 (both $n_p = 2$) by means of error sensitivity range and rectangularity. Increasing the number of pulses, performance measures, namely, sensitivity, robustness and rectangularity, improve regularly. This is not the case for SU(2) method, when using ultrahigh-precision measures — the UL-fidelity range of PB1 remains equal to the same of SK1.

Intersection of fidelities of P3 and P5 is at $\epsilon_{35} = 0.454371$ and $\mathcal{F}(\epsilon_{35}) = 0.461157$, accordingly for P5 and P7: $\epsilon_{57} = 0.471023$ and $\mathcal{F}(\epsilon_{57}) = 0.423852$, and for P7 and P9: $\epsilon_{79} = 0.478761$ and $\mathcal{F}(\epsilon_{79}) = 0.403605$. It seems that intersection $\epsilon_{N-2,N}$ converges to $\epsilon_p = 0.5$ when $N \gg 1$, and one may get square fidelity for sufficiently large $N \geq N_p$. To obtain N_p seems to be done by supercomputer (or maybe quantum computer), neural networks, or their combination, depending on the complexity of the optimization algorithm.

In our opinion, the value $\epsilon_p = 0.5$ is suggested by the method we use, since the fidelity both at the bottom and at the top is optimized with equal force and with equal step (pari passu).

4.3.2.2 *Diversis passuum*

Heterogeneous optimization of broadband and narrowband properties generates another type of passband pulses, called *diversis passuum*, which can be derived using SU(2) method, denoted as DN

$$\pi_{\phi_1}\pi_{\phi_2} \cdots \pi_{\phi_N}, \quad (4.13)$$

which don't have special design in general, although for the lowest members D7a and D7b phases have a simple structure (see Table 4.6).

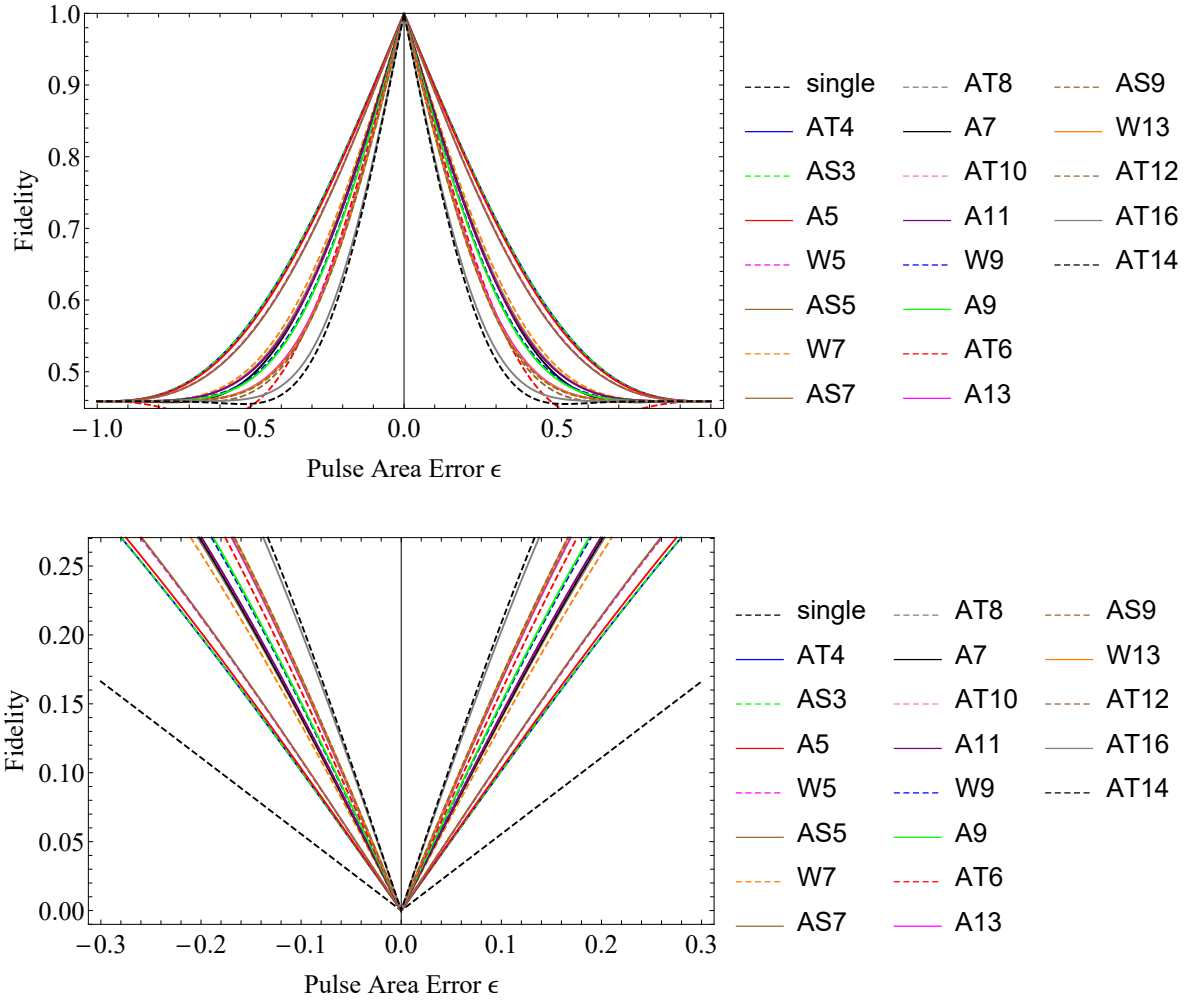


Figure 4.1: Frobenius distance fidelity (top) and infidelity (bottom) of composite narrowband Hadamard gates produced by the four families of composite sequences from the Table 4.3.

4.4 HADAMARD GATE

4.4.1 *Narrowband*

In the case of non- π rotations, both major and minor element dependences $\mathcal{U}_{11}(\epsilon)$ and $\mathcal{U}_{21}(\epsilon)$ are asymmetric and can not be modified to be symmetric. Considering also the fact that the useful CPs are asymmetric for narrowband rotations, the hard numerical calculations are necessary for obtaining the results.

For optimization of non- π rotations, the SU(2) method is used. Four designs or structures can be used to derive narrowband Hadamard gate — antisymmetric 1st type and 2nd type, Wimperis-kind and asymmetric, general structure of which liberally presented in Sec. 4.5.1. Corresponding members of these four families are displayed in Table 4.3 and Fig. 4.1.

Two facts must be acknowledged for rotations other than π :

- The error sensitivity range of the resulting narrowband CPs depends on the design (the structure of the pulse areas) used rather than the order of optimization. For a particular structure, increasing the optimization order for longer pulses makes the pulses narrower, but different structures differ in error sensitivity ranges for the same optimization order. The reason is that different structures already optimize the overall gate error at different levels. For example, the structure AN without optimization already nullifies the odd derivatives $1, 3, 5, 7, \dots$ of $\mathcal{U}_{11}(\epsilon)$ at $\epsilon = -1$ and the even derivatives $2, 4, 6, 8, \dots$ of $\mathcal{U}_{21}(\epsilon)$ at $\epsilon = -1$.
- The case of X gate is special: the number of pulses of AN is lower by two — A5 of Hadamard gate (and non- π general rotation gate) is equivalent to A3 of X gate, A7 to A5, and so forth.

4.4.2 Passband

Pari passu passband PN CPs for Hadamard gate have the structure presented in Sec. 4.5.2 and are displayed in Table 4.5.

Intersection of fidelities of P3 and P5 is at $\epsilon_{35} = 0.44608$ and $\mathcal{F}(\epsilon_{35}) = 0.726128$, accordingly for P5 and P7: $\epsilon_{57} = 0.465489$ and $\mathcal{F}(\epsilon_{57}) = 0.702619$, and for P7 and P9: $\epsilon_{79} = 0.474985$ and $\mathcal{F}(\epsilon_{79}) = 0.689117$. As for X gate, here also we see tendency $\epsilon_{N-2,N} \rightarrow \epsilon_p$ when $N \gg 1$.

Diversis passuum passband DN CPs for Hadamard gate have the structure presented in Sec. 4.5.2 and are displayed in Table 4.7.

4.5 GENERAL ROTATION GATE

General rotation gates, narrowband and passband, being non- π rotations, can be obtained in the same fashion as Hadamard gate ($\theta = \pi/2$).

4.5.1 Narrowband

Generalization of AN CPs, i.e. antisymmetric sequence of 1st type, have the following structure in general presented by θ parameter

$$\left(\frac{\pi - \theta}{2}\right)_{\phi_0} \pi_{\phi_1} \cdots \pi_{\phi_{n_s}} \pi_{\phi_{n_s+1}} \pi_{-\phi_{n_s}} \cdots \pi_{-\phi_1} \left(\frac{\pi - \theta}{2}\right)_{-\phi_0}. \quad (4.14)$$

When targeting general rotation gates ($\phi = \pi/2$), as usual, this $\pi/2$ phase change must be done for all the components in the structure. For non- π rotations the number of pulses is $N = 2n_s + 3$, where n_s is the sensitivity order. In the case of π rotations ($\theta = \pi$) we transition to the Eq. (4.10), where one gets rid of the first and the last pulses (being zero rotations), hence ϕ_0 , and the number of constituent pulses becomes $N = 2n_s + 1$. General formula for the number of pulses and total operation time can be presented using a step function σ ,

$$N(\theta) = 2n_s + 1 + 2\sigma(\theta), \quad (4.15a)$$

$$\mathcal{A}_{tot}(\theta) = N(\theta)\pi - 2\theta, \quad (4.15b)$$

$$\sigma(\theta) = \begin{cases} 1 & \text{if } \theta \in (0, \pi), \\ 0 & \text{if } \theta = \pi. \end{cases} \quad (4.15c)$$

In the case of the 1st type, we pre-set the structure (4.14) and optimization is done afterwards. As was mentioned, the performance of the resulting narrowband CPs depends on the used design rather than the order of optimization. Already, choosing the design one may get many derivatives zero beforehand. This is a case for the 1st type. Although some lose on speed of operation, AN is much robust and has systematic design compared to the rest, providing systematic pattern in performance measures. For the same n_s it gives the best performance. For π rotations AN-m are the best ones having the same AN design.

Alternatively, one may use 2nd type of antisymmetric design ATN

$$\alpha_{\phi_1} \pi_{\phi_2} \cdots \pi_{\phi_{n_s+1}} \pi_{-\phi_{n_s+1}} \cdots \pi_{-\phi_2} \alpha_{-\phi_1}, \quad (4.16)$$

where the all phase structure is added by $\pi/2$ to obtain a general rotation gate. When $\theta = \pi$, α is equal to $\pi/2$ and one gets the alternative to (4.10) structure which have the same performance (in \mathcal{A}_{tot} and sensitivity). Results of 2nd type with number $N + 1$ derived by SU(2) method will not differ in either speed or sensitivity from the 1st type with number N in Table 4.1. So separation of antisymmetric sequences to two types becomes important in the case of non- π rotation gates.

Two asymmetric sequences are also useful for general rotation gates, Wimperis-kind and just asymmetric. Wimperis-kind WN design, written for $\phi = 0$, is

$$\theta_{\phi_1} \pi_{\phi_2} \cdots \pi_{\phi_{2n_s+1}}, \quad (4.17)$$

phases of which have simpler structure in the case of $N = 5, 9, 13, \dots$:

$$\theta_{\phi_1} \pi_{\phi_2} \cdots \pi_{\phi_{n_s+1}} \pi_{\phi_{n_s+1}} \pi_{\phi_{n_s}} \cdots \pi_{\phi_2}. \quad (4.18)$$

Unfortunately, *WN* didn't have 1st order member. The lowest member is the 2nd order pulse known as *NB1* with the simplified structure (again for $\phi = 0$)

$$\theta_0 \pi_\chi \pi_{-\chi} \pi_{-\chi} \pi_{-\chi}, \quad (4.19)$$

where $\chi = \arccos\left(-\frac{\theta}{4\pi}\right)$. To obtain rotation gates from these sequences, one must add $\pi/2$ to the phase structures in (4.17), (4.18) and (4.19). For X gate $\chi \approx 0.580431\pi$ and for Hadamard $\chi \approx 0.539893\pi$.

Since the sequence of π pulses in the CP carry the optimization process and seeds a stable design, the most fictitious asymmetric pulse may have the following design

$$\alpha \phi_1 \pi_{\phi_2} \pi_{\phi_3} \cdots \pi_{\phi_{2n_s-1}} \pi_{\phi_{2n_s}} \beta \phi_{2n_s+1}, \quad (4.20)$$

denoted as *ASN*. Sometimes, it is possible to find the best trade-off in speed and accuracy by these sequences. Good example is *AS9* in Table 4.3.

Both Wimperis-kind and asymmetric designs converge to the sequence of π pulses in the case of π rotations (X gate), and in that case the most neat structure is antisymmetric, i.e. *AN*.

4.5.2 Passband

Pari passu passband rotation gates *PN* are subjected to the following design ($\phi = \pi/2$ must be added to all the phases)

$$\theta_{\phi_1} (2\pi)_{\phi_2} (2\pi)_{\phi_3} \cdots (2\pi)_{\phi_{2n_p+1}}, \quad (4.21)$$

which can be considered as the generalization of the *SK1*:

$$\theta_0 (2\pi)_\chi (2\pi)_{-\chi}, \quad (4.22)$$

where $\chi = \arccos\left(-\frac{\theta}{4\pi}\right)$, and the *PB1*:

$$\theta_0 (2\pi)_\chi (2\pi)_{-\chi} (2\pi)_{-\chi} (2\pi)_\chi, \quad (4.23)$$

where $\chi = \arccos\left(-\frac{\theta}{8\pi}\right)$.

Both *SK1* and *PB1* can be derived using *SU(2)* method, but, unfortunately, this optimization is strict to use for longer sequences. Longer ones can be obtained using another propagator-optimization method, where the fidelity is optimized instead of matrix elements. It also ensures constant rotations due to regularizer

used, hence, we call it a regularization method. Both methods can be used to derive any θ rotation gate.

Diversis passuum passband rotation gates DN have the design similar to (4.17)

$$\theta_{\phi_1} \pi_{\phi_2} \cdots \pi_{\phi_{2(n_r+n_s)+1}}, \quad (4.24)$$

but here the number of pulses is equal to $N = 2(n_r + n_s) + 1$. It was possible to find the simpler structure of phases for the lowest members: more sensitive D7a with $(n_s, n_r) = (2, 1)$ and more robust D7b with $(n_s, n_r) = (1, 2)$

$$\theta_{\phi_1} \pi_{\phi_2} \pi_{\phi_3} \pi_{\phi_4} \pi_{-\phi_3} \pi_{-\phi_4} \pi_{\phi_2} \pi_{-\phi_1}. \quad (4.25)$$

Although we use only SU(2) method to derive DN-s, the regularization method can be applied as an alternative.

4.6 CONCLUSIONS

We presented CPs which produce narrowband and passband rotational single-qubit gates, namely — X, Hadamard and general rotation gates. Narrowband and passband CPs tend to alternate (wiggle) in fidelity, which is an unintended result of derivation method. Furthermore, having the same order of optimization, these CPs differ in performance depending on the structure of the pulse area (design) and the method of derivation used.

Three types of optimization methods were used — SU(2), modified-SU(2), and regularization. Narrowband X gates derived by the modified-SU(2) approach are superior to corresponding gates obtained using the SU(2) approach by means of sensitivity, for the same sensitivity order. For example, the antisymmetric A5-m pulse outperforms well-known NB1 — FWHM of A5-m is about 42.8%, which is narrower than FWHM of NB1 49.4% of whole error bandwidth. Since we have not found an alternative to the SU(2) method for narrowband Hadamard or general rotation gates, we apply this old method to two antisymmetric and two asymmetric pulse designs.

We propose two types of passband CPs — *pari passu* PN, with passband order, and *diversis passuum* DN, with different sensitivity and robustness orders. PN sequences are derived by the regularization method, and show systematic improvement in all the performance characteristics — sensitivity, robustness and rectangularity. DN sequences are derived by the SU(2) method, although regularization method can also be used.

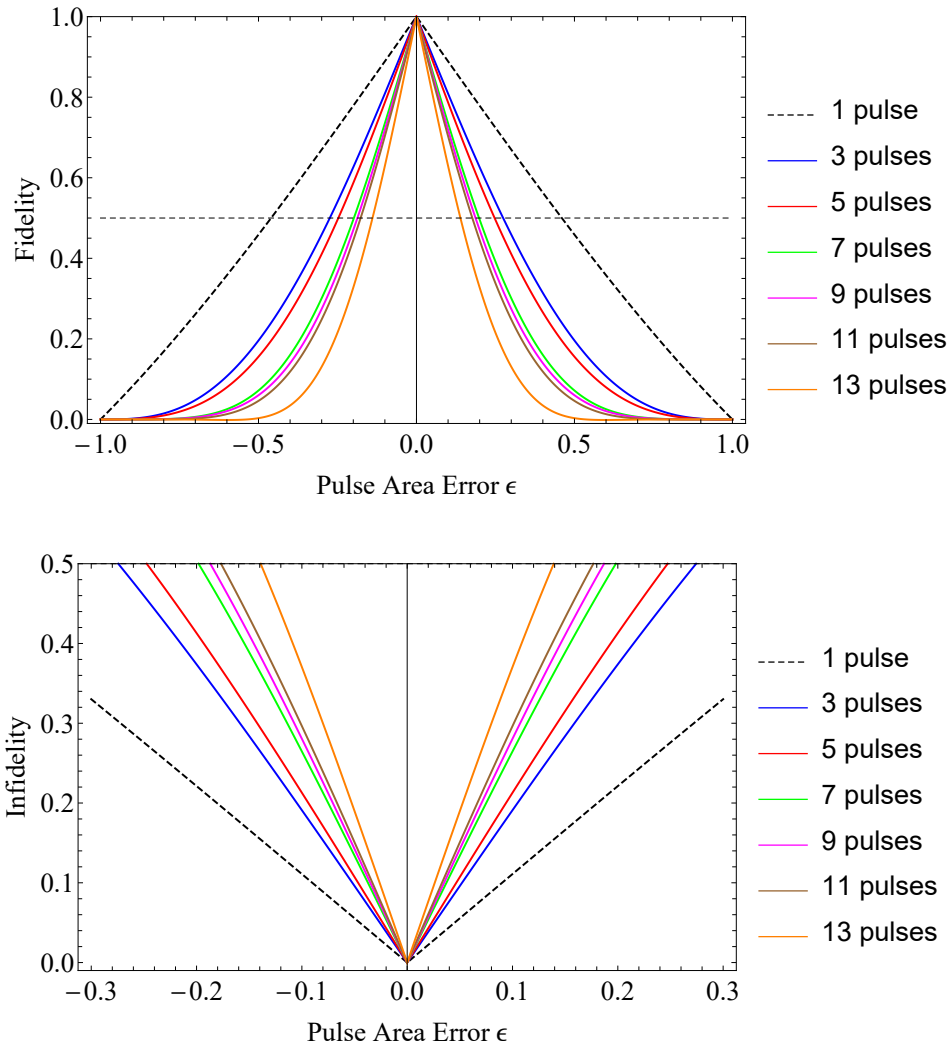


Figure 4.2: Frobenius distance fidelity (top) and infidelity (bottom) of composite narrow-band X gates produced by the antisymmetric composite sequences ANs (3,7,11 pulses) and WNs (5,9,13 pulses) from the Table 4.1.

The results in this chapter can be useful in applications such as spatial localization in *in vivo* NMR spectroscopy, selective and local spatial addressing of trapped ions or atoms in optical lattices by tightly focused laser beams in QS, narrowband polarization filters and passband polarization retarders in PO.

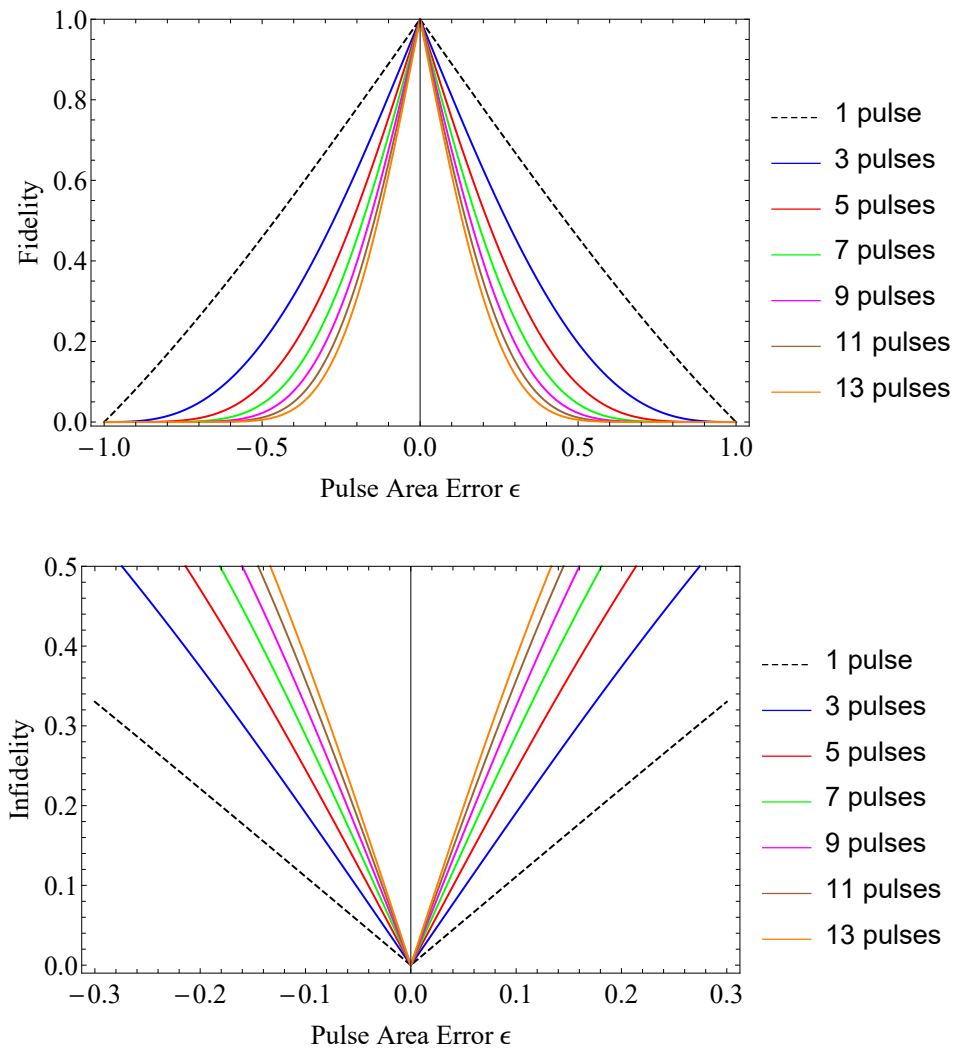


Figure 4.3: Frobenius distance fidelity (top) and infidelity (bottom) of composite X gates produced by the antisymmetric composite sequences AN - m designed by the regularization method from the Table 4.2.

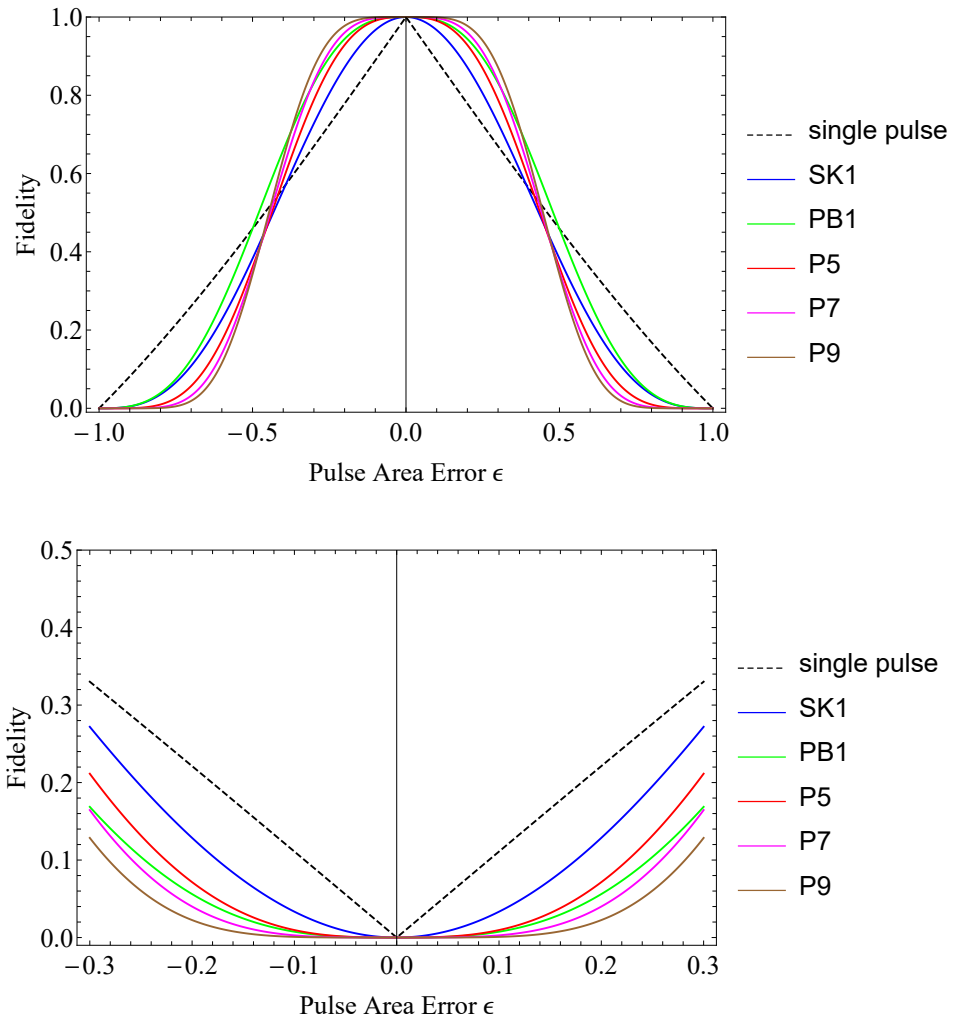


Figure 4.4: Frobenius distance fidelity (top) and infidelity (bottom) of composite passband X gates produced by PN (pari passu) sequences from the Table 4.4.

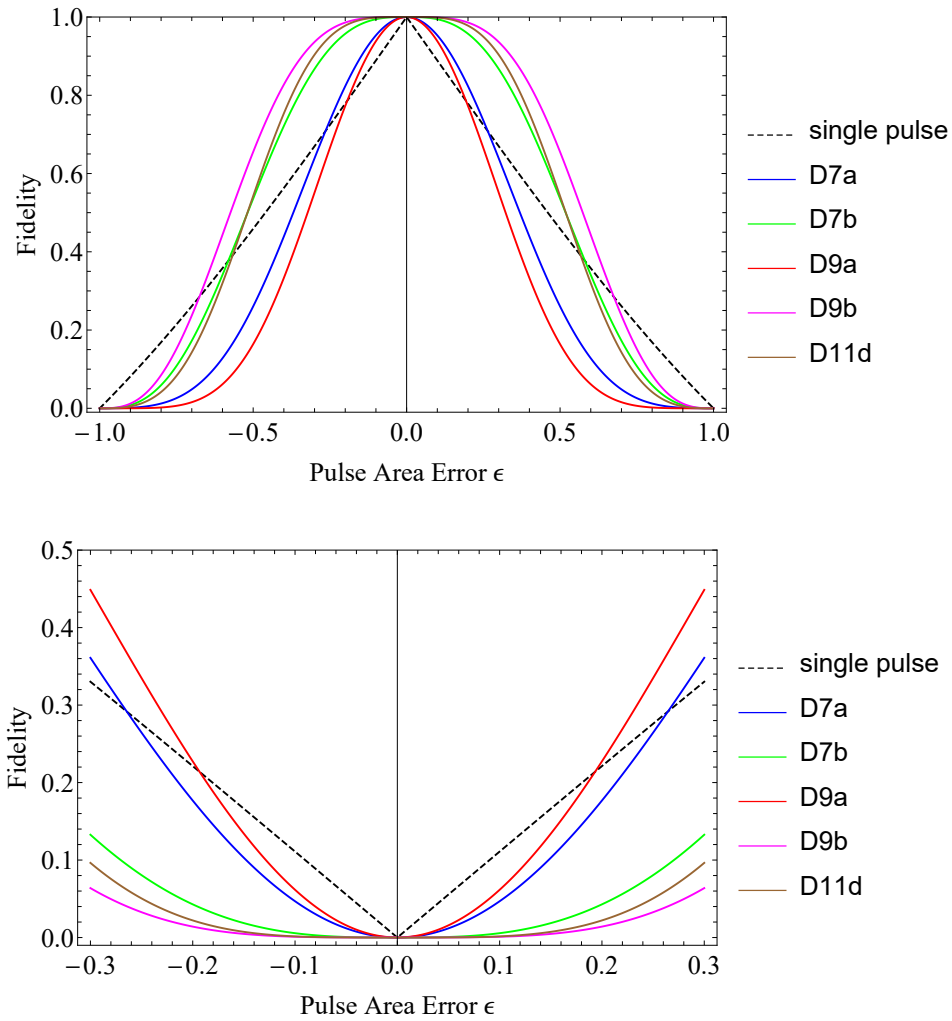


Figure 4.5: Frobenius distance fidelity (top) and infidelity (bottom) of composite passband X gates produced by DN (diversis passuum) sequences from the Table 4.6.

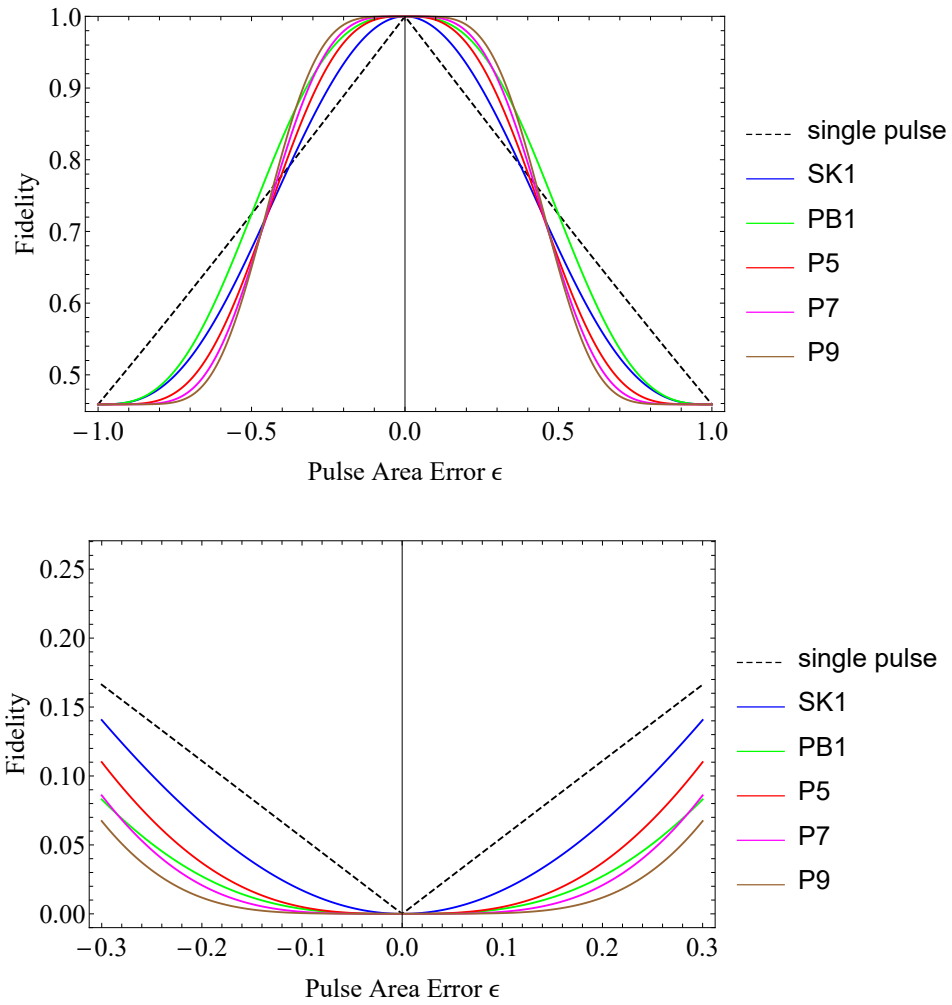


Figure 4.6: Frobenius distance fidelity (top) and infidelity (bottom) of composite passband Hadamard gates produced by PN (pari passu) sequences from the Table 4.5.

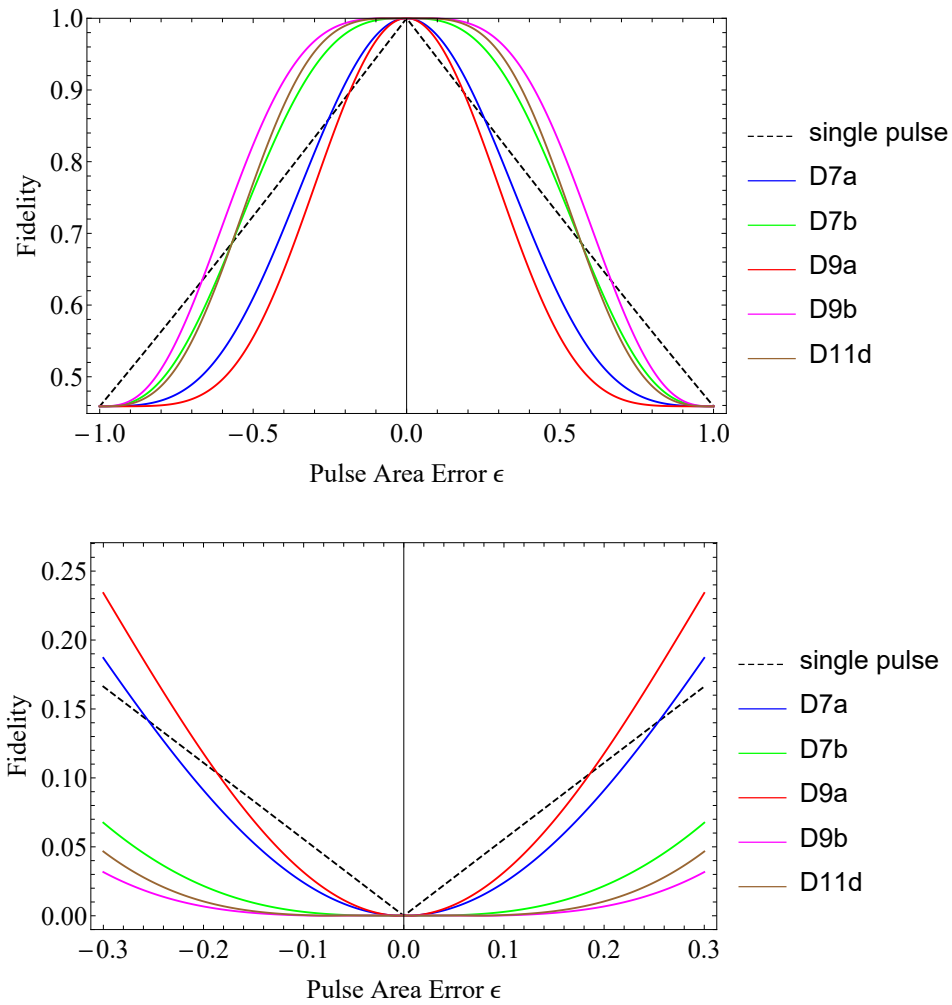


Figure 4.7: Frobenius distance fidelity (top) and infidelity (bottom) of composite pass-band Hadamard gates produced by DN (diversis passuum) sequences from the Table 4.7.

Table 4.1: Phases of antisymmetric composite sequences of $N = 2n_s + 1$ nominal π pulses, which produce the π rotation with a pulse area error sensitivity up to order $O(\epsilon^{n_s})$. The last column gives the half-fidelity range or, so called, FWHM (full width at half maximum) $[\pi(1 - \epsilon_0), \pi(1 + \epsilon_0)]$ of pulse area error sensitivity wherein the Frobenius distance fidelity is above the value 0.5, i.e. the infidelity is below $\text{HM} = \frac{\text{MAX} + \text{MIN}}{2} = \frac{1 + 0}{2} = 0.5$.

Name	Pulses	$O(\epsilon^{n_s})$	Phases (in units π)	FWHM (error sensitivity range)
Antisymmetric sequences				
$\{\phi_1, \phi_2, \dots, \phi_{n_s}, \phi_{n_s+1}, -\phi_{n_s}, \dots, -\phi_2, -\phi_1\} + 1/2$				
single	1	$O(\epsilon^0)$	0	$[0.53989\pi, 1.46011\pi]$
A3	3	$O(\epsilon)$	$\frac{1}{3}, 1$	$[0.726\pi, 1.274\pi]$
A7	7	$O(\epsilon^3)$	0.244, 1.6719, 0.7626, 1	$[0.802\pi, 1.198\pi]$
A11	11	$O(\epsilon^5)$	0.3468, 1.0836, 0.6708, 0.8186, 0.2655, 1	$[0.823\pi, 1.177\pi]$
Wimperis-kind sequences				
$\{\phi_1, \phi_2, \dots, \phi_{n_s-1}, \phi_{n_s+1}, \phi_{n_s+1}, \phi_{n_s-1}, \dots, \phi_2\} + 1/2$				
W5 \triangleq NB1	5	$O(\epsilon^2)$	0, 0.5804, 1.4196	$[0.753\pi, 1.247\pi]$
W9	9	$O(\epsilon^4)$	0, 0.4417, 1.8105, 0.8737, 1.3	$[0.813\pi, 0.187\pi]$
W13	13	$O(\epsilon^6)$	0, 1.2863, 0.7778, 1.4773, 0.3446, 0.5632, 1.7414	$[0.861\pi, 1.139\pi]$

Table 4.2: Phases of antisymmetric composite sequences of $N = 2n_s + 1$ nominal π pulses, which produce the π rotation with a pulse area error sensitivity up to order $O(\epsilon^{n_s})$. The last column gives the half-fidelity range or, so called, FWHM (full width at half maximum) $[\pi(1 - \epsilon_0), \pi(1 + \epsilon_0)]$ of pulse area error sensitivity wherein the Frobenius distance fidelity is above the value 0.5, i.e. the infidelity is below $\text{HM} = \frac{\text{MAX} + \text{MIN}}{2} = \frac{1+0}{2} = 0.5$.

Name	Pulses	$O(\epsilon^{n_s})$	Phases (in units π)	FWHM (error sensitivity range)
Antisymmetric sequences				
$\{\phi_1, \phi_2, \dots, \phi_{n_s}, \phi_{n_s+1}, -\phi_{n_s}, \dots, -\phi_2, -\phi_1\} + 1/2$				
single	1	$O(\epsilon^0)$	0	$[0.53989\pi, 1.46011\pi]$
A3	3	$O(\epsilon)$	$\frac{1}{3}, 1$	$[0.726\pi, 1.274\pi]$
A5-m	5	$O(\epsilon^2)$	$\frac{4}{5}, \frac{8}{5}, 0$ $\frac{6}{5}, \frac{2}{5}, 0$	$[0.786\pi, 1.214\pi]$
A7-m	7	$O(\epsilon^3)$	$\frac{5}{7}, \frac{13}{7}, \frac{11}{7}, 1$ $\frac{9}{7}, \frac{1}{7}, \frac{3}{7}, 1$	$[0.819\pi, 1.181\pi]$
A9-m	9	$O(\epsilon^4)$	$\frac{2}{9}, \frac{12}{9}, \frac{10}{9}, \frac{4}{9}, 0$ $\frac{14}{9}, \frac{12}{9}, \frac{16}{9}, \frac{10}{9}, 0$	$[0.840\pi, 1.160\pi]$
A11-m	11	$O(\epsilon^5)$	$\frac{7}{11}, \frac{1}{11}, \frac{13}{11}, \frac{17}{11}, \frac{19}{11}, 1$ $\frac{9}{11}, \frac{17}{11}, \frac{1}{11}, \frac{3}{11}, \frac{15}{11}, 1$	$[0.855\pi, 1.145\pi]$
A13-m	13	$O(\epsilon^6)$	$\frac{20}{13}, \frac{18}{13}, \frac{22}{13}, \frac{16}{13}, \frac{24}{13}, \frac{14}{13}, 0$	$[0.867\pi, 1.133\pi]$

Table 4.3: Phases of AN: antisymmetric composite sequences of $N - 2$ nominal π pulses, sandwiched by two pulses of areas $\pi/4$, and WN: asymmetric Wimperis-kind composite sequences of $N - 1$ nominal π pulses, preceded (or succeeded) by a pulse of area $\theta = \pi/2$; which produce the $\theta = \pi/2$ rotation with a pulse area error sensitivity up to order $O(\epsilon^{n_s})$. The last column gives FWHM (full width at half maximum) $[\pi(1 - \epsilon_0), \pi(1 + \epsilon_0)]$ of pulse area error sensitivity wherein the Frobenius distance fidelity is above the value $\frac{1+(1-\sqrt{1-1/\sqrt{2}})}{2}$, i.e. the infidelity is below $\text{HM} = \frac{\text{MAX} + \text{MIN}}{2} = \frac{1+(1-\sqrt{1-1/\sqrt{2}})}{2} \approx 0.7294$, where the minimum (at $\epsilon = \pm 1$) Frobenius distance fidelity for $\pi/2$ rotations is $\text{MIN} = 1 - \sqrt{1 - 1/\sqrt{2}} \approx 0.4588$.

Name	Pulses	$O(\epsilon^{n_s})$	Phases (in units π)	\mathcal{A}_{tot}	FWHM (error sensitivity range)
Antisymmetric sequences (1st type)					
$\{\phi_0, \phi_1, \phi_2, \dots, \phi_{n_s}, \phi_{n_s+1}, -\phi_{n_s}, \dots, -\phi_2, -\phi_1, -\phi_0\} + 1/2$					
single	1	$O(\epsilon^0)$	0	$\pi/2$	$[0.50973\pi, 1.49027\pi]$
A5	5	$O(\epsilon)$	1, 0.2301, 1	3.5π	$[0.725\pi, 1.275\pi]$
A7	7	$O(\epsilon^2)$	1, 0.2954, 0.8230, 0	5.5π	$[0.7987\pi, 1.2013\pi]$
A9	9	$O(\epsilon^3)$	1, 0.3082, 0.7709, 0.1152, 1	7.5π	$[0.8123\pi, 1.1877\pi]$
A11	11	$O(\epsilon^4)$	1, 1.9962, 0.8077, 1.4886, 0.6279, 0	9.5π	$[0.8006\pi, 1.1994\pi]$
A13	13	$O(\epsilon^5)$	1, 0.2291, 1.9036, 1.5659, 0.5577, 0.9389, 1	11.5π	$[0.8306\pi, 1.1694\pi]$
Asymmetric sequences (Wimperis-kind)					
$\{\phi_1, \phi_2, \dots, \phi_{2n_s+1}\} + 1/2$					
$\text{W5} \triangleq \text{NB1}$	5	$O(\epsilon^2)$	0, 0.539893, -0.539893, -0.539893, 0.539893	4.5π	$[0.7396\pi, 0.2604\pi]$
W7	7	$O(\epsilon^3)$	0, 0.958038, 1.70099, 1.13518, 1.91065, 0.793721, 0.27538	6.5π	$[0.7897\pi, 1.2103\pi]$

W9	9	$O(\epsilon^4)$	0, 1.26578, 0.415523, 0.152784, 1.2404, 1.2404, 0.152784, 0.415523, 1.26578	8.5π	$[0.8105\pi, 1.1895\pi]$
W13	13	$O(\epsilon^6)$	0, 1.88926, 0.801439, 1.32824, 0.606488, 1.39505, 0.211373, 0.211373, 1.39505, 0.606488, 1.32824, 0.801439, 1.88926	12.5π	$[0.8332\pi, 1.1668\pi]$

Asymmetric sequences

$$\alpha_{\phi_1} \pi_{\phi_2} \cdots \pi_{\phi_{N-1}} \beta_{\phi_N}$$

$$\alpha, \beta; \phi_1, \phi_2, \dots, \phi_N$$

AS3	3	$O(\epsilon)$	0.486, 1.2463; 0.2540, 1.8598, 0.9799	2.7323π	$[0.7204\pi, 1.2796\pi]$
AS5	5	$O(\epsilon^2)$	0.6298, 0.8426; 0.4083, 1.6092, 0.7888, 1.4389, 0.3147	4.4723π	$[0.7407\pi, 1.2593\pi]$
AS5a	5	$O(\epsilon^2)$	0.778276, 0.69444; 1.8521, 0.997442, 0.280465, 1.05988, 1.88585	4.4727π	$[0.741\pi, 0.259\pi]$
AS7	7	$O(\epsilon^3)$	0.38093, 1.2554; 1.7684, 1.9270, 0.8589, 1.3447, 0.6742, 1.4987, 0.3302	6.6363π	$[0.797\pi, 1.203\pi]$
AS7a	7	$O(\epsilon^3)$	0.320885, 1.31241; 0.27189, 0.17642, 1.26598, 0.642382, 1.33723, 0.600511, 1.72175	6.6333π	$[0.797\pi, 1.203\pi]$
AS9	9	$O(\epsilon^4)$	0.33322, 0.21161; 1.13696, 1.70097, 1.57736, 0.33491, 1.46716, 0.61094, 0.87834, 0.32587, 1.19906	7.5448π	$[0.8314\pi, 1.1686\pi]$

Antisymmetric sequences (2nd type)

$$\alpha; \{\phi_1, \phi_2, \dots, \phi_{n_s+1}, -\phi_{n_s+1}, \dots, -\phi_2, -\phi_1\} + 1/2$$

AT4	4	$O(\epsilon)$	0.344509; 0.32165, 0.55861	2.689π	$[0.7202\pi, 1.2798\pi]$
-----	---	---------------	----------------------------	------------	--------------------------

AT6 ¹	6	$O(\epsilon^2)$	0.415106; 0.411914, 0.561681, 0.474778	4.83π	$[0.8243\pi, 1.1757\pi]$
AT8	8	$O(\epsilon^3)$	0.317054; 0.275735, 0.230584, 1.33439, 0.651125	6.634π	$[0.7971\pi, 1.2029\pi]$
AT10	10	$O(\epsilon^4)$	0.255798; 0.0853904, 1.66734, 0.759385, 1.0321, 1.92737	8.512π	$[0.8004\pi, 1.1996\pi]$
AT12	12	$O(\epsilon^5)$	0.307743; 0.2576, 0.157112, 1.53557, 0.46763, 1.25254, 0.70666	10.615π	$[0.8335\pi, 1.1665\pi]$
AT14 ²	14	$O(\epsilon^6)$	0.370181; 0.357786, 0.457094, 0.992936, 1.887852, 1.39542, 0.54164, 0.4294	12.74π	$[0.8668\pi, 1.1332\pi]$
AT16	16	$O(\epsilon^7)$	0.320743; 1.7175, 0.17708, 1.09267, 1.11819, 0.345712, 1.70626, 0.28594, 1.17393	14.641π	$[0.8622\pi, 1.1378\pi]$

1 AT6 is not flat bottom.

2 AT14 is not perfectly flat bottom.

Table 4.4: Phases of pari passu passband pulses for X gate. PB1-like pulse structure is used (2π pulses with single π).

Name	Pulses	n_p	Phases (in units π) $\{\phi_1, \phi_2, \dots, \phi_N\} + 1/2$	UL-fidelity (error sensitivity range)	UH-fidelity (error robustness range)	Δ (rectangularity)
single	1	0	0	$[0.00013\pi, 1.99987\pi]$	$[0.99991\pi, 1.00009\pi]$	0.99978π
P3 \triangleq SK1	3	1	0, 0.58043, 1.41957	$[0.027\pi, 1.973\pi]$	$[0.995\pi, 1.005\pi]$	0.967π
P5	5	2	0, 1.78506, 0.48331, 1.34363, 0.83030	$[0.077\pi, 1.923\pi]$	$[0.978\pi, 1.022\pi]$	0.901π
P7	7	3	0, 1.07359, 0.772099, 1.32971, 0.436728, 1.69584, 0.0868198	$[0.120\pi, 1.880\pi]$	$[0.957\pi, 1.043\pi]$	0.837π
P9	9	4	0, 1.97287, 0.139635, 1.67993, 0.430437, 1.33878, 0.762866, 1.11383, 0.97606	$[0.154\pi, 1.846\pi]$	$[0.936\pi, 1.064\pi]$	0.782π
PB1	5	2	0, 0.539893, 1.46011, 1.46011, 0.539893	$[0.027\pi, 1.973\pi]$	$[0.976\pi, 1.024\pi]$	0.949π

Table 4.5: Phases of pari passu passband pulses for Hadamard gate. PB1-like pulse structure is used (2π pulses with single $\pi/2$).

Name	Pulses	n_p	Phases (in units π) $\{\phi_1, \phi_2, \dots, \phi_N\} + 1/2$	UL-fidelity (error sensitivity range)	UH-fidelity (error robustness range)	Δ (rectangularity)
single	1	0	0	$[0.00019\pi, 1.99981\pi]$	$[0.99982\pi, 1.00018\pi]$	0.99963π
P3 \triangleq SK1	3	1	0, 0.539893, 1.46011	$[0.031\pi, 1.969\pi]$	$[0.992\pi, 1.008\pi]$	0.961π
P5	5	2	0, 0.816729, 1.37808, 0.447255, 1.79388	$[0.084\pi, 1.916\pi]$	$[0.973\pi, 1.027\pi]$	0.889π
P7	7	3	0, 1.07705, 0.752636, 1.35704, 0.410338, 1.71464, 0.0836752	$[0.128\pi, 1.872\pi]$	$[0.949\pi, 1.051\pi]$	0.821π
P9	9	4	0, 0.85519, 0.665578, 1.75921, 1.44318, 0.526885, 0.761473, 1.67661, 1.84619	$[0.145\pi, 1.855\pi]$	$[0.947\pi, 1.053\pi]$	0.803π
PB1	5	2	0, 0.519907, 1.48009, 1.48009, 0.519907	$[0.031\pi, 1.969\pi]$	$[0.970\pi, 1.030\pi]$	0.939π

Table 4.6: Phases of diversis passuum passband pulses for X gate.

Name	Pulses	n_s, n_r	Phases (in units π) $\{\phi_1, \phi_2, \dots, \phi_N\} + 1/2$	UL-fidelity (error sensitivity range)	UH-fidelity (error robustness range)	Δ (rectangularity)
			$\phi_1, \phi_2, \phi_3, \phi_4, -\phi_3, -\phi_4, \phi_2 - 1$			
D7a	7	2, 1	0, 1.24005, 0.851488, 0.371396	$[0.043\pi, 1.957\pi]$	$[0.995\pi, 1.005\pi]$	0.952 π
	7	2, 1	0, 1.75995, 0.371396, 0.851488			
D7b	7	1, 2	0, 1.24005, 1.6286, 1.14851	$[0.023\pi, 1.977\pi]$	$[0.974\pi, 1.026\pi]$	0.951 π
	7	1, 2	0, 0.759954, 0.371396, 0.851488			
D9a	9	3, 1	0, 1.1196, 0.735454, 0.733506, 1.38161, 0.680734, 1.93256, 1.56754, 0.0517938	$[0.109\pi, 1.891\pi]$	$[0.998\pi, 1.002\pi]$	0.889 π
D9b	9	1, 3	0, 1.1196, 1.50375, 1.50181, 0.853711, 0.152812, 0.900982, 0.535975, 0.0517144	$[0.020\pi, 1.980\pi]$	$[0.967\pi, 1.033\pi]$	0.947 π
D11d ³	11	2, 3	0, 0.6661, 1.1385, 1.0056, 1.8812, 1.5879, 0.9755, 0.6004, 0.2092, 1.4173, 0.0729	$[0.028\pi, 1.972\pi]$	$[0.936\pi, 1.064\pi]$	0.908 π

³ Possible R11a, R11b and R11c, respectively, for $(n_s, n_r) = (4, 1), (1, 4)$ and $(3, 2)$, derived with our method, are alternating pulses with wiggles, not relevant to rotation gates.

Table 4.7: Phases of diversis passuum passband pulses for Hadamard gate.

Name	Pulses	n_s, n_r	Phases (in units π) $\{\phi_1, \phi_2, \dots, \phi_N\} + 1/2$ $\phi_1, \phi_2, \phi_3, \phi_4, -\phi_3, -\phi_4, \phi_2 - 1$	UL-fidelity (error sensitivity range)	UH-fidelity (error robustness range)	Δ (rectangularity)
D7a	7	2, 1	0, 1.24751, 0.803639, 0.308613	$[0.0491\pi, 1.9509\pi]$	$[0.9936\pi, 1.0064\pi]$	0.9445π
	7	2, 1	0, 0.752487, 1.19636, 1.69139			
D7b	7	1, 2	0.247513, 0.803639, 0.308613	$[0.0260\pi, 1.9740\pi]$	$[0.9674\pi, 1.0326\pi]$	0.9414π
	7	1, 2	0, 0.752487, 0.308613, 0.803639			
D9a	9	3, 1	0, 1.1113, 0.6905, 0.7503, 1.4422, 0.5945, 1.8509, 1.6036, 0.0760	$[0.1205\pi, 1.8795\pi]$	$[0.9901\pi, 1.0099\pi]$	0.8696π
D9b	9	1, 3	0, 0.8886, 0.4679, 0.4081, 1.1000, 1.9477, 1.2041, 1.4515, 1.9238	$[0.0227\pi, 1.9773\pi]$	$[0.9342\pi, 1.0658\pi]$	0.9116π
D11d ⁴	11	2, 3	0, 1.9174, 0.9827, 1.2348, 0.7041, 0.1794, 0.6527, 1.5332, 1.0226, 1.6844, 0.1870	$[0.0307\pi, 1.9693\pi]$	$[0.9329\pi, 1.0671\pi]$	0.9021π

⁴ Possible R11a, R11b and R11c, respectively, for $(n_s, n_r) = (4, 1), (1, 4)$ and $(3, 2)$, derived with our method, are alternating pulses with wiggles, not relevant to rotation gates.

DETERMINISTIC GENERATION OF ARBITRARY ULTRASMALL EXCITATION OF QUANTUM SYSTEMS BY COMPOSITE PULSE SEQUENCES

In some applications of quantum control, it is necessary to produce very weak excitation of a quantum system. Such an example is presented by the concept of single-photon generation in cold atomic ensembles or doped solids, e.g. by the DLCZ protocol, for which a single excitation is shared among thousands and millions atoms or ions. Another example is the possibility to create huge Dicke state of N qubits sharing a single or a few excitations. Other examples are using tiny rotations to tune high-fidelity quantum gates or using these tiny rotations for testing high-fidelity quantum process tomography protocols. Ultrasmall excitation of a quantum transition can be generated by either a very weak or far-detuned driving field. However, these two approaches are sensitive to variations in the experimental parameters, e.g. the transition probability varies with the square of the pulse area. Here we propose a different method for generating a well-defined pre-selected very small transition probability — of the order of 10^{-2} to 10^{-8} — by using composite pulse sequences. The method features high fidelity and robustness to variations in the pulse area and the pulse duration.

5.1 INTRODUCTION

In almost all applications of quantum control, the focus is either on complete population inversion (known as X gate in quantum information) or half excitation (known as Hadamard or \sqrt{X} gate in quantum information). These are produced most often by resonant excitation by π and $\pi/2$ pulses, but adiabatic and composite methods have also been used. These methods have different advantages and shortcomings. For instance, resonant excitation is the fastest method and is very accurate if the parameter values are very precise [133, 134], but it is sensitive to

parameter variations. Adiabatic methods [65, 75] are robust to experimental errors but are slow and it is difficult to reach high accuracy with them. (A cure is offered by the “shortcuts-to-adiabaticity” approach [135], but it comes with the necessity of accurate pulse shaping or additional fields.) Composite pulses — trains of pulses with well-defined relative phases used as control parameters [44, 45] — sit somewhere in the “sweet spot” as they feature extreme accuracy and robustness, while being significantly faster than adiabatic methods (but slower than resonant excitation by a factor of 2-3 or more).

However, quantum control offers the opportunity for partial excitation with any transition probability, rather than just 1 and $\frac{1}{2}$. For instance, there are applications in which a very small transition probability is required. One prominent example is the DLCZ protocol for single-photon generation in an ensemble of ultracold atoms or in a doped solid and its variations and extensions [136–142]. Single photons are the physical platform for such advanced technologies as quantum communications [143–147] and photonic quantum computing [148–151]. In this protocol, a three-level Raman system $|g_1\rangle \leftrightarrow |e\rangle \leftrightarrow |g_2\rangle$ is used. In the *writing* process, the atomic transition $|g_1\rangle \leftrightarrow |e\rangle$ is excited with a very low probability by an off-resonant laser pulse with a wave vector \vec{k}_w , such that a single (or a few) atomic excitation is stored in the ensemble as a shared excitation by all atoms. Then collective spontaneous emission on the transition $|e\rangle \rightarrow |g_2\rangle$ occurs at a random time, in which a (Stokes) photon is emitted in a random direction. However, a single-photon detector is placed along a particular spatial direction and any click in it is considered as a “heralded” photon, with a well-defined wave vector \vec{k}_s . In the *reading* process, a resonant laser pulse with a wave vector \vec{k}_r is applied on the atomic transition $|g_2\rangle \leftrightarrow |e\rangle$, which stimulates the emission of a (anti-Stokes) photon on the pump transition $|e\rangle \rightarrow |g_1\rangle$, in a well-defined spatial direction \vec{k}_a , determined by the phase-matching condition $\vec{k}_a = \vec{k}_s + \vec{k}_w - \vec{k}_r$. In this protocol, one of the crucial conditions is to be able to produce only one shared excitation among a large number of atoms N , i.e. a driving field which generates a transition probability of $1/N$ is needed.

Another example is the possibility to create huge entangled Dicke states [152]. These very special states share a fixed number of excitations n evenly among N qubits, a special case of which (for $n = 1$) is the W state. A prominent feature of the Dicke states is that they are immune against collective dephasing, which is ubiquitous in various systems. Therefore, the Dicke sub-space, which is $N!/n!(N - n)!$ -dimensional, can be used as a decoherence-free computational subspace [153–155]. Dicke states possess genuine multi-partite entanglement [156, 157], which is, moreover, very robust against particle loss [158–160]: the loss of a qubit reduces the N -dimensional Dicke state to a $N - 1$ -dimensional one. Dicke states have been

proposed and demonstrated in various physical systems, including ensembles of neutral atoms [161, 162], trapped ions [163–166], quantum dots [167], and using linear optics [162, 168]. Many of these proposals and demonstrations have various restrictions, as they cannot create arbitrary but only particular Dicke states, individual qubit addressing is required, the number of the necessary physical interactions scales very fast with N , a special initial (Fock) state is required, insufficient efficiency, very long interaction times, etc. Composite pulses of ultrasmall probability offer a direct path toward the creation of large Dicke states as they can produce a specific number of shared excitations among large- N ensembles of qubits.

A third example when a well-defined small transition probability is needed arises when fine tuning quantum gates: in order to reach ultrahigh gate fidelity a rotation gate at a well-defined tiny angle can be very useful. Moreover, such small rotations alone can be used to test the accuracy of various quantum process tomography protocols.

In this paper, we address this specific problem by designing composite pulse sequences, which seem to be the only quantum control technique capable to generate a tiny transition probability that is robust to variations of the experimental parameters. The dominant majority of composite pulses in the literature are designed to produce specific rotations on the Bloch sphere, typically at angles π (generating complete population transfer), $\pi/2$ (half population transfer), $\pi/4$ and $3\pi/4$, as reviewed in Refs. [44, 45]. There exist just a few composite sequences which produce general rotations at arbitrary angles [3, 47, 48, 89, 90, 99]. Some of them can be used for the present task of ultrasmall probability and they are listed below, along with many newly derived composite sequences.

Composite rotations are broadly divided into two large groups called variable and constant rotations. The variable rotations [44, 47, 99] feature well-defined transition probability but not well-defined phases of the propagator. Constant (or phase-distortionless rotations) feature both well-defined populations and well-defined phases of the propagator [3, 89, 90]. There are large markets for either of these, with only constant rotations being suitable for quantum gates. However, they are much more demanding to generate and much longer than variable rotations, for the same order of error compensation. This will be clearly seen below as we consider one type of constant rotations and two types of variable rotations.

After a description of the derivation method we present specific composite sequences of 2, 3 and 4 pulses, many of which have analytic expressions for the composite parameters, and then proceed to longer sequences.

5.2 THE METHOD

We wish to construct composite pulses, which produce a very low probability of transition between two states $|1\rangle \rightarrow |2\rangle$, in an efficient and robust manner. Such composite pulses are known as θ -pulses, as they produce a transition probability $p = \sin^2(\theta/2)$. In the NMR literature one can find a number of θ pulses for $\theta = \pi/4$ (called 45° pulses), $\theta = \pi/2$ (called 90° pulses), and $\theta = 3\pi/4$ (called 135° pulses). Very few general formulae for an arbitrary value of θ exist in the literature. In our case we need composite pulses, which produce transition probability $p = 1/N \ll 1$, which implies $\theta \ll 1$. Such composite pulses are designed here.

Each pulse in a composite sequence is considered resonant and hence it generates the propagator

$$\mathbf{U}(A, \phi) = \begin{bmatrix} \cos(A/2) & -ie^{i\phi} \sin(A/2) \\ -ie^{-i\phi} \sin(A/2) & \cos(A/2) \end{bmatrix}, \quad (5.1)$$

where ϕ is the phase of the coupling. The overall propagator for a sequence of n pulses,

$$(A_1)_{\phi_1} (A_2)_{\phi_2} \cdots (A_n)_{\phi_n}, \quad (5.2)$$

each with a pulse area A_k and phase ϕ_k , reads

$$\mathbf{U}_n = \mathbf{U}(A_n, \phi_n) \mathbf{U}(A_{n-1}, \phi_{n-1}) \cdots \mathbf{U}(A_2, \phi_2) \mathbf{U}(A_1, \phi_1), \quad (5.3)$$

which, by convention, acts from right to left. One of the phases is always irrelevant for the physically observed quantities (it is related to the global phase of the wavefunction), and can be set to zero. As such, we always choose the first phase: $\phi_1 = 0$. In other words, all other phases are relative phases of the respective pulse to the phase of the first pulse.

The pulse areas A_k and the phases ϕ_k are the control parameters, which are selected from the conditions that the transition probability,

$$P = |\mathbf{U}_{12}|^2, \quad (5.4)$$

has a specific target value p and it is robust to variations ϵ in the pulse area $A_k(1 + \epsilon)$. The error-free values of the pulse areas A_k are called *nominal* values. The relative error ϵ is assumed to be the same for all pulses in the composite sequence. This is reasonable if they are derived from the same source, which is usually the case.

The multiplication of the two-dimensional matrices in Eq. (5.3) leads to rapidly growing expressions. Still, these are far more manageable than the ones coming

from the three-dimensional matrices in the usual Bloch-vector derivation of composite sequences.

One can proceed in two directions.

- One possibility is to expand the transition probability of Eq. (5.4) in a Taylor-Maclaurin series vs ϵ . The coefficients in this series are functions of all A_k and ϕ_k ($k = 1, 2, \dots, n$). We nullify as many of the first few such coefficients (i.e. derivatives vs ϵ) as possible, which generate a set of equations for A_k and ϕ_k . The result is a transition probability with a Taylor-Maclaurin series expansion

$$P(\epsilon) = p + O(\epsilon^m), \quad (5.5)$$

where p is the target value. We say that the respective composite sequence is accurate up to order $O(\epsilon^m)$. We shall first present such composite sequences, which are known as *variable rotations* in NMR and allow to easily reach error compensation of very high order.

- Alternatively, one can take the propagator elements $U_{11} = U_{22}^*$ and $U_{12} = -U_{21}^*$, expand them in Taylor-Maclaurin series vs ϵ , and carry out elimination of as many lowest-order terms as possible. The result is a Taylor-Maclaurin expansion of the propagator,

$$\mathbf{U}_n(\epsilon) = \mathbf{U}_n + O(\epsilon^l). \quad (5.6)$$

Obviously, with the same number of free parameters, one can cancel of factor of 2 fewer terms now, than in the expansion of the probability P . However, the resulting composite sequences will be stabilized with respect to both the amplitudes and the phases of the overall propagator, rather than with respect to the amplitudes only, as with Eq. (5.5). Such composite sequences create constant rotations in NMR language, or, in quantum information terms, *quantum rotation gates*.

We begin with the first approach, which delivers expressions as in Eq. (5.5), and then proceed with the second approach, which delivers expressions of the type (5.6).

5.3 SMALL-PROBABILITY COMPOSITE SEQUENCES

5.3.1 Two-pulse composite sequences

We have derived two types of two-pulse composite sequences.

5.3.1.1 Symmetric sequence of pulses

In the first type, the two pulse areas are equal to $\pi/2$,

$$S2 : \quad \left(\frac{1}{2}\pi\right)_0\left(\frac{1}{2}\pi\right)_{\pi-\theta}. \quad (5.7)$$

The transition probability is

$$P = \cos^2 \frac{\pi\epsilon}{2} \sin^2 \frac{\theta}{2}. \quad (5.8)$$

For

$$\theta = \arccos(1 - 2p) = 2 \arcsin(\sqrt{p}), \quad (5.9)$$

we find

$$P = p[1 - \sin^2(\frac{1}{2}\pi\epsilon)] = p[1 + O(\epsilon^2)]. \quad (5.10)$$

This simplest composite sequence is accurate up to the second order $O(\epsilon^2)$. For example, for probabilities $p = 10^{-2}$, 10^{-3} , 10^{-4} and 10^{-5} we find $\phi = 0.0638\pi$, 0.0201π , 0.0064π , and 0.0020π . These values correspond to 11.48° , 3.62° , 1.15° , and 0.36° .

The advantage of these sequences is their extreme simplicity and the analytic formula for the phase, which make it possible to immediately write down the sequence for any target transition probability. The disadvantage is the availability of a single control parameter only, which limits the error compensation to the first order only. This is still superior over a single resonant pulse, which is accurate to zeroth order only.

5.3.1.2 Asymmetric sequence of pulses

In the second two-pulse sequence, the pulse areas are different,

$$A2 : \quad (A_1)_0(A_2)_{\phi_2}. \quad (5.11)$$

Here we have three control parameters — two pulse areas and a phase — which allow us to compensate higher orders of errors. Now closed analytic expressions for the parameters are not possible to derive. However, due to the fact that $p \ll 1$, we can use perturbation theory, which gives us the approximations

$$A_1 = x - y, \quad A_2 = x + y, \quad \phi_2 = \pi - \phi, \quad (5.12)$$

p	A_1	A_2	ϕ
10^{-2}	0.689806	0.741105	0.048767
10^{-3}	0.707103	0.723255	0.015417
10^{-4}	0.712599	0.717704	0.004875
10^{-5}	0.714341	0.715956	0.001542
10^{-6}	0.714894	0.715404	4.88×10^{-4}
10^{-7}	0.715068	0.715229	1.54×10^{-4}
10^{-8}	0.715123	0.715174	4.88×10^{-5}

Table 5.1: Pulse areas and phases (in units of π) for the composite sequence (5.11) (in units of π) for a few values of the transition probability. All composite sequences have the error order $O(\epsilon^3)$.

with $x \approx 0.7151\pi$, $y \approx 0.2553\pi\sqrt{p}$, and $\phi \approx 0.4875\pi\sqrt{p}$. All these are valid for $p \ll 1$. The pulse areas and the phases for a few values of the transition probability are given in Table 5.1.

The advantage of the composite sequence (5.11) over the symmetric one (5.7) is that it is accurate to the third order in ϵ ,

$$P = p[1 + O(\epsilon^3)]. \quad (5.13)$$

The disadvantage is that it requires a larger total pulse area, about 1.43π compared to just π for the symmetric sequence (5.7).

The performance of the two sequences is compared in Fig. 5.1. Both sequences (5.7) and (5.11) outperform significantly the conventional single-pulse excitation probability, which is very sensitive to pulse area errors. The asymmetric sequence A2 of Eq. (5.11), with its three control parameters and error order $O(\epsilon^3)$, outperforms the symmetric sequence S2 of Eq. (5.7), which has only one control parameter and error order $O(\epsilon^2)$.

5.3.2 Three-pulse composite sequences

We have derived three three-pulse composite sequences, two symmetric and one asymmetric.

5.3.2.1 Symmetric sequence of pulses

The symmetric sequence of pulses reads

$$S3: \quad \left(\frac{1}{2}\pi\right)_0 \pi_{\alpha+\beta} \left(\frac{1}{2}\pi\right)_{2\beta}, \quad (5.14)$$

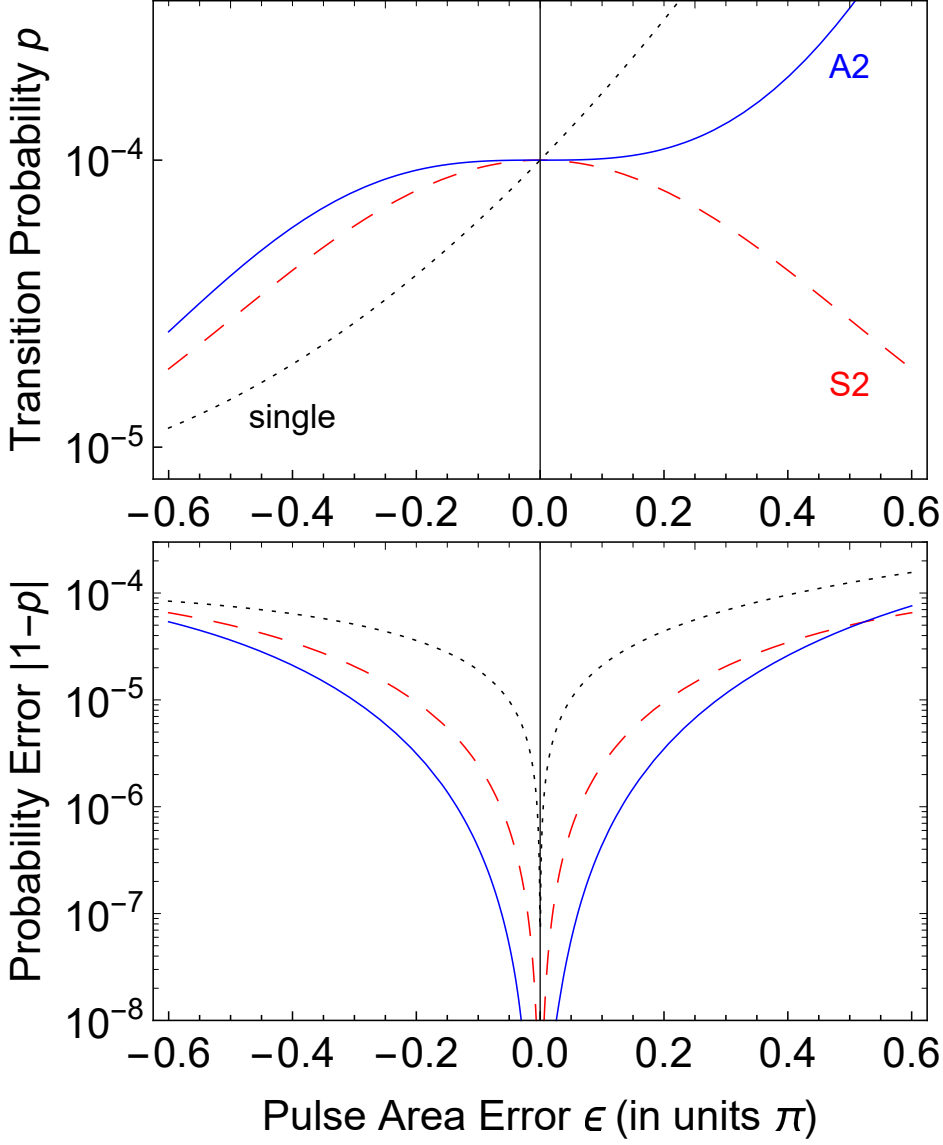


Figure 5.1: Performance of the two-pulse composite sequences (5.7) (red dashed) and (5.11) (blue solid) for the transition probability $p = 10^{-4}$. The dotted curves show the single pulse excitation probability for comparison.

where

$$\alpha = \theta/2, \quad (5.15a)$$

$$\beta = \arccos(\sin \alpha - \cos \alpha), \quad (5.15b)$$

$$\theta = \arccos(1 - 2p) = 2 \arcsin(\sqrt{p}). \quad (5.15c)$$

The transition probability reads

$$P = [1 - \sin^4(\epsilon/2)] \sin^2(\theta/2). \quad (5.16)$$

It is obviously accurate up to order $O(\epsilon^4)$.

p	A_1	A_2	A_3	ϕ_2	ϕ_3
10^{-2}	0.5682	1.2436	0.6292	1.1533	0.2546
10^{-3}	0.5904	1.2276	0.6232	1.0785	0.1405
10^{-4}	0.6001	1.2229	0.6184	1.0419	0.0785
10^{-5}	0.6049	1.2214	0.6151	1.0229	0.0441
10^{-6}	0.6074	1.2209	0.6131	1.0126	0.0248
10^{-7}	0.6087	1.2208	0.6119	1.0070	0.0139
10^{-8}	0.6094	1.2207	0.6113	1.0039	0.0078

Table 5.2: Pulse areas and phases (in units of π) for the composite sequences of 3 pulses (5.22) for a few values of the transition probability p . All composite sequences have the error order $O(\epsilon^5)$.

The sequence (5.14) is derived as follows. First, we calculate the overall propagator of Eq. (5.3) for $N = 3$ pulses. Numerical evidence suggests that the pulse areas could be taken as in Eq. (5.14), i.e. a π pulse in the middle sandwiched by two half- π pulses. We take the first phase to be 0, and we are left with two phases to be determined. The overall three-pulse transition probability for zero error ($\epsilon = 0$) is readily calculated to be

$$P = |U_{21}|^2 = \sin^2(\phi_2 - \phi_3/2). \quad (5.17)$$

If we set $P = \sin^2(\theta/2)$ (as for a resonant θ pulse), we find $\phi_3 = 2\phi_2 - \theta$. Next we calculate the first few derivatives of U_{21} with respect to the error ϵ and find

$$U'_{21}(\epsilon = 0) = 0, \quad (5.18)$$

$$U''_{21}(\epsilon = 0) = [1 + 2 \cos(\theta) + 2 \cos(\phi_2) + 2 \cos(\theta - \phi_2) + \cos(\theta - 2\phi_2)]/8, \quad (5.19)$$

$$U'''_{21}(\epsilon = 0) = 0. \quad (5.20)$$

The vanishing of the odd-order derivatives follows from the choice of symmetric pulse areas in Eq. (5.14). By setting $\phi_2 = \theta/2 + \beta$ the equation for $U''_{21}(\epsilon = 0)$ reduces to

$$2 \cos \beta \cos(\theta/2) + \cos^2 \beta + \cos \theta = 0. \quad (5.21)$$

has 4 solutions, two complex and two real, of which one positive and one negative. The real positive solution is given by the expression listed in Eq. (5.14). The first nonzero derivative is $U_{21}^{(4)}(\epsilon = 0)$. The availability of analytic formulae for the phases allows us to find their values for any value of the transition probability.

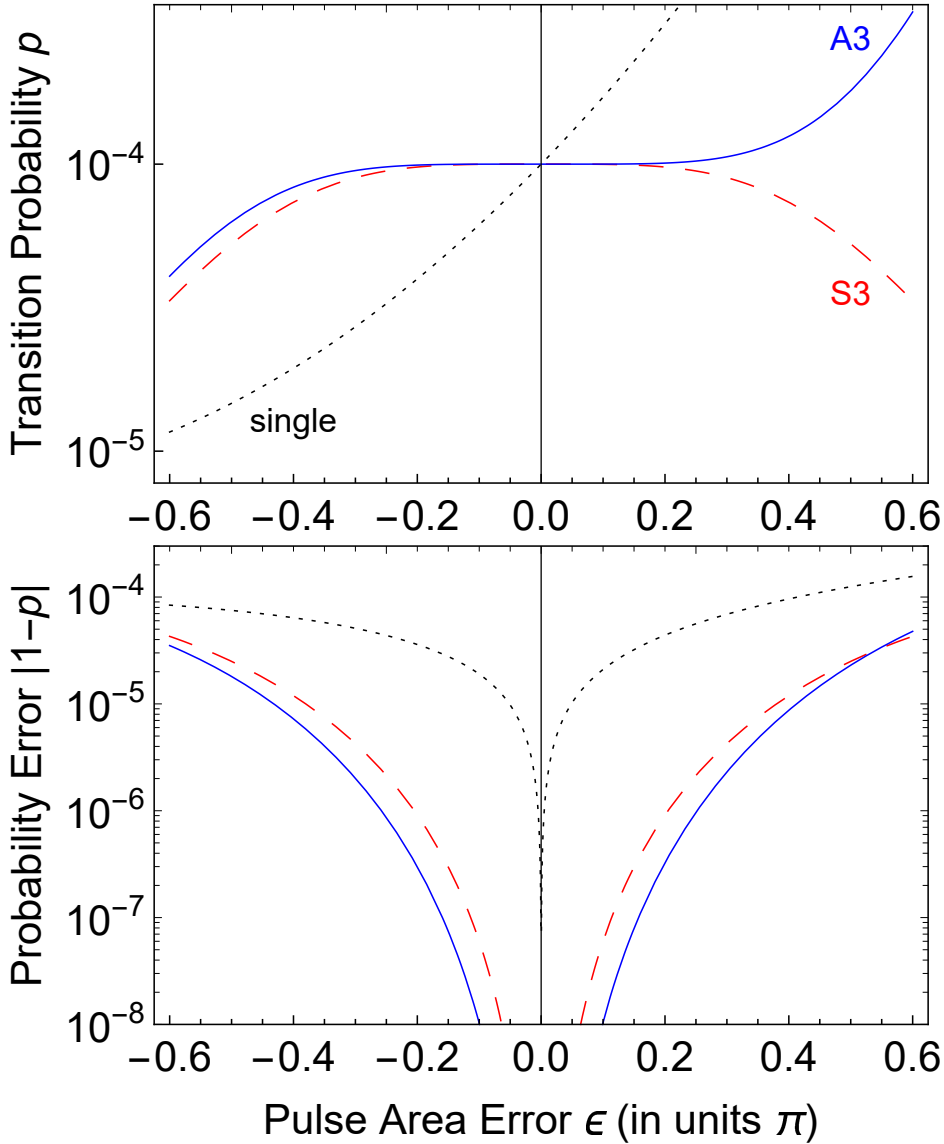


Figure 5.2: Performance of the three-pulse composite sequences (5.14) (red dashed) and (5.22) (blue solid) for the transition probability $p = 10^{-4}$. The dotted curves show the single pulse excitation probability for comparison.

5.3.2.2 Asymmetric sequence of pulses

The most general three-pulse composite sequence has the form

$$A3: (A_1)_0(A_2)_{\phi_2}(A_3)_{\phi_3}. \quad (5.22)$$

Although the composite sequence (5.22) costs more total pulse area ($\approx 2.44\pi$) than the preceding two, it is accurate to order $O(\epsilon^5)$. The pulse areas and the phases computed numerically are given in Table 5.2.

The performance of the three-pulse sequences is illustrated in Fig. 5.2. Both sequences (5.14) and (5.22) outperform both the conventional single-pulse excita-

tion probability and the two-pulse composite sequences (5.7) and (5.11) of Fig. 5.1. Moreover, the asymmetric sequence A3 of Eq. (5.11), which is of error order $O(\epsilon^5)$, clearly outperforms the symmetric sequence S3 of Eq. (5.14), which is of error order $O(\epsilon^4)$.

Because the three-pulse sequences seem to be the “sweet spot” in terms of performance (error order and high-fidelity window width) versus cost (total pulse area and control complexity), they deserve some discussion. There are clear advantages and disadvantages of each of these two sequences. The S3 sequence has a nice analytic form and a total pulse area of 2π . However, it has lower error order than A3. The real advantage of the sequence S3 is its analytic form, which makes it very easy to calculate the composite phases for any target transition probability p . The A3 sequence looks less attractive as neither the pulse area nor the phases are rational numbers and they are all numerical, but this sequence has the higher order of error compensation, although at the expense of the larger pulse area of about 2.44π . Its real inconvenience is in the fact that for target transition probabilities not listed in Table 5.2 one has to calculate them numerically, although this is not a very difficult task.

5.3.3 Four-pulse composite sequences

The most general four-pulse composite sequence has the form

$$(A_1)_0(A_2)_{\phi_2}(A_3)_{\phi_3}(A_4)_{\phi_4}. \quad (5.23)$$

We present three sets of four-pulse composite sequences, two symmetric and one asymmetric.

5.3.3.1 Symmetric sequences of pulses

The first symmetric sequence consists of identical nominal $\pi/2$ pulses (but with different phases) [47],

$$S4a : \quad \left(\frac{1}{2}\pi\right)_0\left(\frac{1}{2}\pi\right)_{\frac{1}{2}\pi}\left(\frac{1}{2}\pi\right)_{\frac{3}{2}\pi-\theta}\left(\frac{1}{2}\pi\right)_{\pi-\theta}, \quad (5.24)$$

where $\theta = 2 \arcsin \sqrt{p}$. Its total pulse area is just 2π . The overall transition probability reads

$$P = p[1 - \sin^4(\pi\epsilon/2)]. \quad (5.25)$$

Obviously, it is accurate up to order $O(\epsilon^4)$.

The other symmetric sequence of pulses reads [47]

$$S4b : \quad \left(\frac{1}{2}\pi\right)_0 \pi_{\frac{2}{3}\pi} \pi_{\frac{5}{3}\pi-\theta} \left(\frac{1}{2}\pi\right)_{\pi-\theta}. \quad (5.26)$$

The overall transition probability reads

$$P = p[1 - \sin^6(\pi\epsilon/2)]. \quad (5.27)$$

Obviously, in return to the larger total pulse area of 3π compared to the previous sequence (5.24) it is accurate up to the higher order $O(\epsilon^6)$.

These sequences are very convenient as the availability of exact analytic formulae for the phases allows us to find their values for any value of the transition probability.

5.3.3.2 Asymmetric sequences

The most general three-pulse composite sequence has the form

$$A4 : \quad (A_1)_0 (A_2)_{\phi_2} (A_3)_{\phi_3} (A_4)_{\phi_4}. \quad (5.28)$$

All pulse areas and phases are free control parameters, which allow it to compensate a higher error order. The pulse areas and the phases are computed numerically and are listed in Table 5.3. Although the asymmetric composite sequence (5.28) costs more total pulse area ($\approx 3.44\pi$) than the preceding two sequences S4a and S4b, it is accurate to the higher order $O(\epsilon^7)$.

The performance of the four-pulse sequences is illustrated in Fig. 5.3. All of them significantly outperform the single pulse profile and provide considerable stabilisation at the target transition probability value. The best performance is delivered by the asymmetric sequence A4, which has the error order $O(\epsilon^7)$, followed by S4b, with the error order $O(\epsilon^6)$, and then S4a, with the error order $O(\epsilon^4)$. However, this ranking follows the total pulse area — the cost factor — which is $\approx 3.41\pi$ for A4, 3π for S4b, and 2π for S4a. Note that the error order $O(\epsilon^4)$ for S4a is the same as the one for the three-pulse sequence S3 and one can verify that they generate similar excitation profiles.

5.3.4 Higher number of pulses

Higher number of pulses present the opportunity for an error compensation of a higher order. There exist analytic symmetric composite sequences for arbitrary rotations, which can be used for small p too [47]. They are constructed as follows.

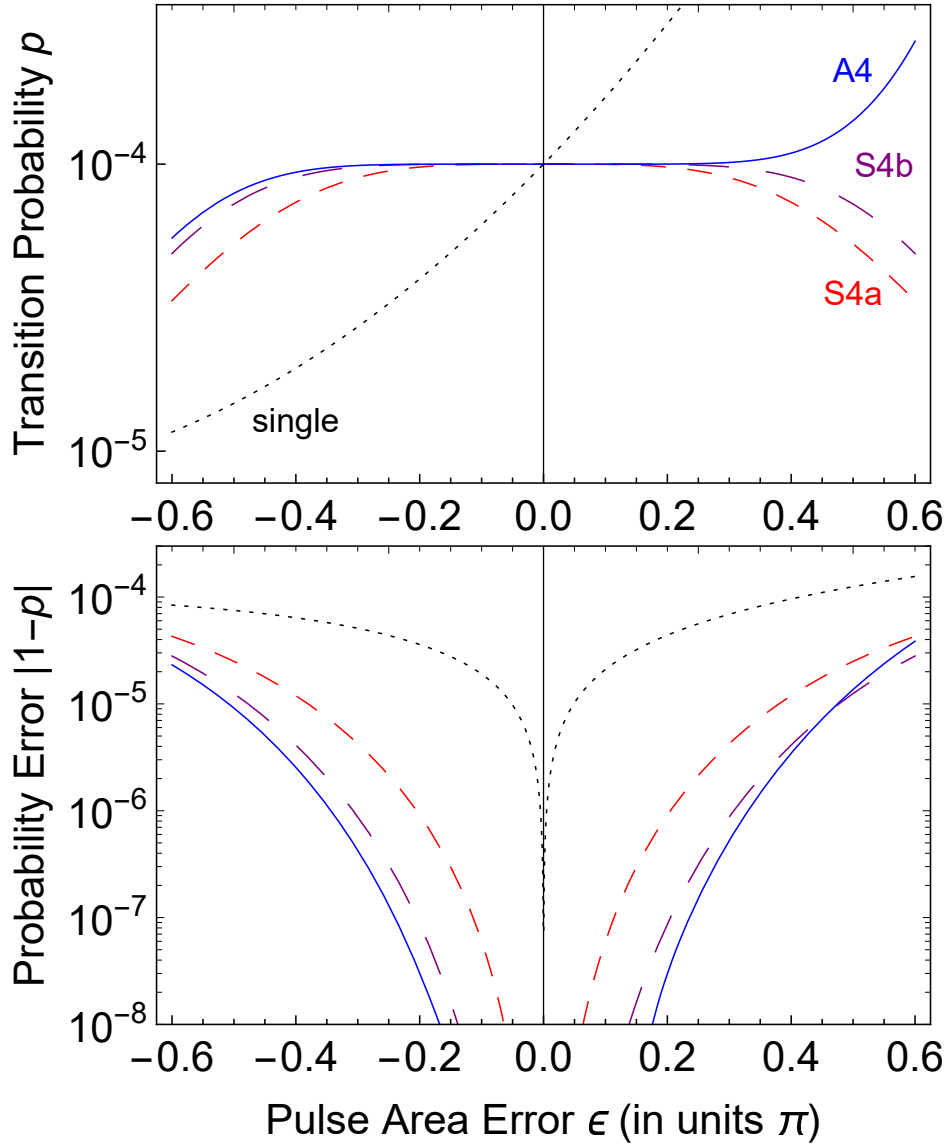


Figure 5.3: Performance of the four-pulse symmetric composite sequences (5.24) (red dashed), (5.26) (purple long-dashed) and the asymmetric sequence (5.28) (blue solid) for the transition probability $p = 10^{-4}$. The dotted curves show the single pulse excitation probability for comparison.

We can use a composite $\pi/2$ pulse to derive a composite θ -pulse by applying a composite $\pi/2$ pulse sequence C , followed by the composite sequence C_θ^R , which is the time-reversed sequence C , with all its phases shifted by the same phase shift θ ,

$$C_0 C_\theta^R, \quad (5.29)$$

an idea introduced by Levitt and Ernst [88]. Moreover, if the sequence C has the error order $O(\epsilon^n)$ then the composite θ sequence (5.29) has the error order $O(\epsilon^{2n})$ [47]. A few examples follow.

p	A_1	A_2	A_3	A_4	ϕ_2	ϕ_3	ϕ_4
10^{-2}	0.5367	1.1586	1.1360	0.5833	0.8499	1.5547	0.4360
10^{-3}	0.8685	1.0434	0.3702	0.5174	1.0634	0.8847	0.0128
10^{-4}	0.8165	0.9044	0.5579	0.6423	1.0362	0.9682	0.0146
10^{-5}	0.7854	0.8335	0.6433	0.6905	1.0207	0.9856	0.0090
10^{-6}	0.7669	0.7937	0.6875	0.7141	1.0118	0.9926	0.0052
10^{-7}	0.7551	0.7698	0.7108	0.7255	0.9933	1.0042	1.9972
10^{-8}	0.7494	0.7578	0.7244	0.7328	0.9962	1.0022	1.9984

Table 5.3: Pulse areas and phases (in units of π) for the composite sequences of 4 pulses (5.28). All composite sequences have the error order $O(\epsilon^7)$.

The composite sequence S2 of Eq. (5.7) becomes a composite $\pi/2$ pulse for $\theta = \pi/2$, which can be used in the twinning construction (5.29),

$$\left(\frac{1}{2}\pi\right)_0 \left(\frac{1}{2}\pi\right)_{\frac{1}{2}\pi} \left(\frac{1}{2}\pi\right)_{\frac{3}{2}\pi-\theta} \left(\frac{1}{2}\pi\right)_{\pi-\theta}, \quad (5.30)$$

which is the same as the sequence S4a of Eq. (5.24). Because the sequence S2 has the error order $O(\epsilon^2)$ then the composite sequence S4a has the error order $O(\epsilon^4)$, as found in the previous section.

The composite sequence S3 of Eq. (5.14) for $\theta = \pi/4$ reads

$$\left(\frac{1}{2}\pi\right)_0 \pi_{\frac{3}{4}\pi} \left(\frac{1}{2}\pi\right)_{\pi}, \quad (5.31)$$

and it has the error order $O(\epsilon^4)$. By using the twinning construction (5.29) we find a θ composite sequence of order $O(\epsilon^8)$,

$$\left(\frac{1}{2}\pi\right)_0 \pi_{\frac{3}{4}\pi} \left(\frac{1}{2}\pi\right)_{\pi} \left(\frac{1}{2}\pi\right)_{2\pi-\theta} \pi_{\frac{7}{4}\pi-\theta} \left(\frac{1}{2}\pi\right)_{\pi-\theta}. \quad (5.32)$$

One can build θ composite sequences of arbitrary length and arbitrary error order compensation by twinning the $\pi/2$ composite sequences [47]

$$\left(\pi/2\right)_0 \pi_{\phi_2} \pi_{\phi_3} \cdots \pi_{\phi_{N-1}} \left(\pi/2\right)_{\phi_N}, \quad (5.33)$$

composed of a sequence of $N - 2$ nominal π pulses, sandwiched by two pulses of areas $\pi/2$, with phases given by the analytic formula

$$\phi_k = \frac{(k-1)^2}{2(N-1)}\pi \quad (k = 1, 2, \dots, N). \quad (5.34)$$

It is easy to verify that the sequences (5.30) and (5.32) (after trivial population-preserving transformation of the phases) belong to such a family of sequences.

Because the sequence (5.33) has the error order $O(\epsilon^{2(N-1)})$ the corresponding twinned sequence (5.29) will have the error order $O(\epsilon^{4(N-1)})$.

Another, asymmetric family of $\pi/2$ composite sequences can be used too [47],

$$(\pi/2)_0 \pi_{\phi_2} \pi_{\phi_3} \cdots \pi_{\phi_{N-1}} (\pi)_{\phi_N}, \quad (5.35)$$

composed of a sequence of $N - 1$ nominal π pulses, preceded by a nominal $\pi/2$ pulse, with phases given by the analytic formula

$$\phi_k = \frac{2(k-1)^2}{2N-1} \pi \quad (k = 1, 2, \dots, N). \quad (5.36)$$

It has the error order $O(\epsilon^{2N-1})$. Hence the twinning method (5.29) generates θ sequences of the error order $O(\epsilon^{2(2N-1)})$. For instance, for $N = 3$ we find by twinning the θ sequence

$$\left(\frac{1}{2}\pi\right)_0 \pi_{\frac{2}{5}\pi} (\pi)_{\frac{8}{5}\pi} (\pi)_{\frac{3}{5}\pi-\theta} \pi_{\frac{7}{5}\pi-\theta} \left(\frac{1}{2}\pi\right)_{\pi-\theta}, \quad (5.37)$$

which has the error order $O(\epsilon^{10})$.

Regarding the asymmetric composite sequences of 2, 3 and 4 pulses, presented above and derived numerically, it is computationally much harder to derive similar sequences for more than 4 pulses. Moreover, the advantage they deliver in terms of error order compensation for a given number of pulses compared to the symmetric sequences seems to decrease with the number of pulses N and approach the point when the results do not repay the labour.

5.4 QUANTUM GATES FOR ULTRASMALL ROTATIONS

Ultrasmall rotation gates are more demanding to construct due to the necessity to have both the probabilities and the phases error-compensated. Mathematically, this is equivalent to expanding the propagator of the gate in a Taylor-Maclaurin series versus the error ϵ and set to zero the first few terms to the same error order $O(\epsilon^m)$ in all propagator matrix elements. Below we present several sequences, which produce high-fidelity rotation gates, two of which are known in the literature and one is derived here.

5.4.1 First-order error compensation

The three-pulse rotation gate has been derived by Wimperis [89],

$$W3 : \quad \theta_0 \pi_{\phi} \pi_{3\phi}, \quad (5.38)$$

Rotation gate G3: $(\frac{1}{2}\pi + x)_{\phi_1} \pi_{\pi+y} (\frac{1}{2}\pi + x)_{\phi_1}$			
p	x	ϕ_1	y
10^{-2}	2.5×10^{-3}	2.492×10^{-2}	5.672×10^{-2}
10^{-3}	2.5×10^{-4}	7.904×10^{-3}	1.797×10^{-2}
10^{-4}	2.5×10^{-5}	2.500×10^{-3}	5.683×10^{-3}
10^{-5}	2.5×10^{-6}	7.906×10^{-4}	1.797×10^{-3}
10^{-6}	2.5×10^{-7}	2.500×10^{-4}	5.684×10^{-4}

Table 5.4: Parameters of the composite sequence G3 of Eq. (5.39) for different transition probabilities p .

with $\theta = \arccos(1 - 2p) = 2 \arcsin \sqrt{p}$ and $\phi = \arccos(-\theta/(2\pi)) \approx \frac{1}{2}\pi + \sqrt{p}$. It is accurate up to order $O(\epsilon^2)$. It is a phase-distortionless sequence and hence suitable for a rotation gate.

Another three-pulse rotation gate has the form [48]

$$G3 : \quad \alpha_{\phi_1} \pi_{\phi_2} \alpha_{\phi_1}, \quad (5.39)$$

where α is determined from the equation

$$\frac{\pi \sin(\alpha)}{\alpha} = 2 \cos(\theta/2). \quad (5.40)$$

Given α , we can find ϕ_1 and ϕ_2 from

$$2\alpha \cos(\phi_1 - \phi_2) + \pi = 0, \quad (5.41a)$$

$$\sin(\phi_1 - \phi_2) = \sin(\theta/2) \cos(\phi_1). \quad (5.41b)$$

This composite sequence is related to the SCROFULOUS composite pulse [169] and it is accurate to the error order $O(\epsilon^2)$.

The values of the pulse area and the composite phases are given in Table 5.4.

5.4.2 Second-order error compensation

A well-known composite sequence, which compensates the second-order error is the BB1 sequence of Wimperis [3],

$$BB1 = (\pi/2)_0 \pi_{\chi} (2\pi)_{3\chi} \pi_{\chi}, \quad (5.42)$$

with $\chi = \arccos(-\theta/4\pi)$. It produces arbitrary phase-distortionless rotations at the angle θ with the error order $O(\epsilon^3)$

5.5 CONCLUSIONS

We presented a solution to the problem of generating well-defined very small excitation of a two-state quantum transition. The method uses composite pulse sequences of two, three, four and more pulses. Both symmetric and asymmetric, analytic and numeric classes of sequences have been presented and analyzed in detail.

The results in this paper can be useful in application such as single-photon generation by a cold atomic ensemble of N atoms. A composite sequence producing a transition probability of $1/N$ will make sure that only one excitation is shared within the ensemble, to be subsequently released by a scheme like DLCZ. Another possible application is fine tuning of quantum gates, in which accurate small adjustments of the rotation angle are needed in order to reach high fidelity. Yet another application is the generation of huge Dicke states in cold atomic ensembles or trapped ions by global collective addressing.

COMPOSITE PULSES FOR ULTRAROBUST OR ULTRASENSITIVE CONTROL

Composite pulses, which produce ultrabroadband and ultranarrowband rotations on the Bloch-Poincaré spheres, are presented. The first class plays a role for design of achromatic polarization retarders, when the second class corresponds to chromatic polarization filters.

6.1 INTRODUCTION AND MOTIVATION

In comparison to the other quantum control methods, CPs is efficient and versatile as follows from the first classification into broadband (BB), narrowband (NB) and passband (PB) classes [3].

All the artillery of ultrahigh-fidelity (flat-top), broadband, constant rotation (full SU(2) matrix optimized) CPs is shown in [48], where well-known BB1 from Wimperis is one of the representatives of this subclass. CPs of this subclass, in contrast to altering-top BB2, maintain 99.99% fidelity (ultrahigh), viz. infidelity is below 10^{-4} error of quantum computation benchmark required in QC and QI. On the contrary, in PO, ultrabroadness is more important than ultrahigh-fidelity. Nevertheless, CPs in [48] can be used also to design achromatic ultrahigh-fidelity constant half-, quarter- and arbitrary-wave plates with an arbitrary phase retardation.

Based on this concept of CPs for rotations on the Bloch space, Ardavan proposed to use the so-called BB1 or BB2 sequences for polarization retarders (i.e., rotations on the Poincaré sphere) [170]. He already found that these stacked composite retarders in almost all cases outperform the conventional compound-type retarders. Existence of BB2 and NB2 sequences leads to the idea of altering CPs, which improve the feature (BB or NB) of the pulse at the expense of precision due to alternations (inflection points) on the top (BB) or on the bottom (NB) of the errant transition probability. We call these new subclasses of CPs as ultrabroadband and ultranarrowband respectively.

With novel method (see Sec. 6.3) we have derived ultrabroadband and ultranarrowband CPs [61], when $\theta = \pi$. These CPs are useful in the applications, where high-accuracy (about 90%) is enough (although higher precision can be achieved increasing number of pulses, due to the novel method). Besides PO, they can be used for high-fidelity ultrarobust (QC) or ultrasensitive (local addressing of trapped ions and atoms in QS) population transfer. The five-pulse (with the same run-time $T = 5\pi$) ultra-BB and ultra-NB CPs outperform well-known BB2 and NB2 pulses respectively, which were expected as the number of alternations is higher in the case of our CPs.

Originally, CPs are derived for θ rotations (x -, y -rotations or mixed rotations with arbitrary ϕ). Here, we took into account z -rotations on the Bloch sphere, which we call as phasal ζ CPs (composite phase gates). We applied our novel method for derivation of ultra-BB rotational θ and phasal composite ζ pulses.

6.2 JONES MATRICES AND ON THE QUANTUM-CLASSICAL ANALOGY

The Poincaré sphere shares much in common with the Bloch sphere: both the evolution matrix of quantum two-state system and Jones matrix for a retarder in LR polarization basis (with a phase shift φ , and rotated at an angle η) represent rotations on the Bloch-Poincaré spheres.

Jones polarization matrix for a retarder with a phase shift φ (the phase shift applied between the ordinary and the extraordinary ray passing through the retarder) and rotated at an angle η (the rotation angle of the retarder's optical axis) is given as (in the left-right circular polarization basis)

$$\mathbf{J}_\eta(\varphi) = \begin{bmatrix} \cos\left(\frac{\varphi}{2}\right) & i \sin\left(\frac{\varphi}{2}\right) e^{2i\eta} \\ i \sin\left(\frac{\varphi}{2}\right) e^{-2i\eta} & \cos\left(\frac{\varphi}{2}\right) \end{bmatrix}, \quad (6.1)$$

note, that here, η in PO differs from θ rotation parameter in NMR and QC.

For example, half- and quarter-wave plates rotated at an angle η , i.e. $(\lambda/2)_\eta$, $(\lambda/4)_\eta$, are described by $\mathbf{J}_\eta(\pi)$ and $\mathbf{J}_\eta(\pi/2)$ respectively.

Ideal half-, quarter- and arbitrary-wave plates are described with Jones polarization matrix $\mathbf{J}_0(\varphi)$ in the LR basis (up to a global phase factor):

$$\mathbf{J}_0(\varphi) = \begin{bmatrix} \cos\left(\frac{\varphi}{2}\right) & i \sin\left(\frac{\varphi}{2}\right) \\ i \sin\left(\frac{\varphi}{2}\right) & \cos\left(\frac{\varphi}{2}\right) \end{bmatrix} \quad (6.2)$$

$$\mathbf{J}_0(\pi) = \begin{bmatrix} 0 & i \\ i & 0 \end{bmatrix} \quad (6.3)$$

$$\mathbf{J}_0(\pi/2) = \frac{1}{\sqrt{2}} \begin{bmatrix} 1 & i \\ i & 1 \end{bmatrix} \quad (6.4)$$

Jones matrix for a rotator in the LR basis represents

$$\mathbf{J}_\eta = \begin{bmatrix} e^{i\eta} & 0 \\ 0 & e^{-i\eta} \end{bmatrix}. \quad (6.5)$$

Due to symmetry $i \rightarrow -i$, and transformations $\varphi \rightarrow \theta$, $\eta \rightarrow \phi/2$ from [PO](#) to [NMR QC](#), we have deal with the same mathematical framework

- Polarization retarder is equivalent to x-rotation or quantum rotation gate, and
- Polarization rotator is equivalent to z-rotation or quantum phase gate.
- Thus, one can apply the results from [QC](#) into the [PO](#) and vice versa, especially to use quantum control techniques and share knowledge between different areas. We see quantum-classical analogy of the rotations on the Bloch-Poincaré spheres. [CPs](#) (composite rotations) is interdisciplinary technique.
- To adapt the results from [NMR QC](#) to [PO](#), it is necessary to use $A_i \rightarrow \varphi_i$ and to change $\eta_i \rightarrow \varphi_i$ and $\phi_i \rightarrow \pm 2\eta_i$ in expressions (5.1) and (6.1) (sign is arbitrary as the composite phases with negative sign are also solutions in symmetric sequences). So, halfed composite phases are necessary to use for η_i -s in the [PO](#).

Henceforward, we will use [NMR QC](#) terminology and notation, and the results for [PO](#) can be obtained by abovementioned way.

6.3 DERIVATION METHOD

So, errant overall propagator is SU(2) matrix

$$\mathbf{U}_n(\epsilon) = \begin{bmatrix} \mathcal{U}_{11}(\epsilon) & \mathcal{U}_{12}(\epsilon) \\ -\mathcal{U}_{12}^*(\epsilon) & \mathcal{U}_{11}^*(\epsilon) \end{bmatrix}, \quad (6.6)$$

where $\mathcal{U}_{11}(\epsilon)$ and $\mathcal{U}_{12}(\epsilon)$ are the complex-valued Cayley-Klein parameters satisfying $|\mathcal{U}_{11}(\epsilon)|^2 + |\mathcal{U}_{12}(\epsilon)|^2 = 1$. We set their zero-error values to the target values,

$$\mathcal{U}_{11}(0) = \cos(\theta/2), \quad \mathcal{U}_{12}(0) = -i \sin(\theta/2) \exp(i\phi), \quad (6.7)$$

for rotational θ pulses, or

$$\mathcal{U}_{11}(0) = \exp(-i\zeta/2), \quad \mathcal{U}_{12}(0) = 0, \quad (6.8)$$

for phasal ζ pulses.

Taking Eqs. (6.7) and (6.8) as a guide, let's consider the general form for general composite rotation

$$\mathbf{U}_n(\epsilon) = \begin{bmatrix} \exp(-i\zeta_\epsilon/2) \cos(\theta_\epsilon/2) & -i \sin(\theta_\epsilon/2) \exp(i\phi_\epsilon) \\ -i \sin(\theta_\epsilon/2) \exp(-i\phi_\epsilon) & \exp(i\zeta_\epsilon/2) \cos(\theta_\epsilon/2) \end{bmatrix}, \quad (6.9)$$

where θ_ϵ is errant rotation angle and arranges x - or y -rotations, i.e. rotational θ pulses or rotation gates, ϕ_ϵ is errant relative phase angle and provides the turns from x - to y -rotation, ζ_ϵ is errant phase-shift angle (sometimes called geometric phase angle) and arranges z -rotations or phase-shift gate up to global phase in the case of phasal ζ pulses and also corresponds to Berry phase (originally examined in cyclic adiabatic processes) alternative in conventional CPs or rotations, i.e. rotational θ pulses. For rotational θ pulses parameters follows $\theta_{\epsilon=0} = \theta$, $\zeta_{\epsilon=0} = 0$ and $\phi_{\epsilon=0} = \phi$ ($\phi = 0$ is the case for ideal θ pulse), and for phasal ζ pulses parameters are equal $\zeta_{\epsilon=0} = \zeta$, $\theta_{\epsilon=0} = 0$ and $\phi_{\epsilon=0} = \text{const}$.

A single resonant pulse is errant linearly $\theta_\epsilon = \theta(1 + \epsilon)$, when for general composite rotation the particular forms of dependences on pulse area error ϵ of the three parameters are generally unknown and related to the structure of CPs, i.e. to the choice of pulse areas and composite phases for the certain number of pulses.

Phasal ζ CPs belong to the case $\theta = 0$ and $\phi = \text{const}$. At least two CPs are required to obtain single phasal ζ pulse.

Note that derivation method presented in Subsec. 6.3.1 does not care about rotation angle, geometric and relative phase stabilities. Here, we have deal with alternating CPs, which make the feature (robustness/sensitivity or both) of the pulse more powerful, sometimes called *ultra*, at the expense of precision due to alternations (at the center/ on the wings or both).

6.3.1 Ultra-BB, ultra-NB and ultra-PB

6.3.1.1 Case of rotational θ pulses

Let's maximize the population transfer area (6.10) at the whole-range of the error bandwidth, i.e. from $\epsilon = -1$ to $\epsilon = 1$ (ultrabroadband θ pulses)

$$\sum_{b,n} \triangleq \int_{-1}^1 p(\epsilon) d\epsilon, \quad (6.10)$$

or minimize it (ultranarrowband θ pulses). Here $p(\epsilon) = 1 - |\mathcal{U}_{11}(\epsilon)|^2 = |\mathcal{U}_{12}(\epsilon)|^2 = \sin^2(\theta_\epsilon/2)$ is errant transition probability.

In (6.10) $p(\epsilon = 0) = p(\theta = \pi) = \sin^2 \theta/2|_{\theta=\pi} = 1$, at the center of bandwidth, is transition probability in QC: when pulse area error is zero, the qubit-state completely transfers from $|0\rangle$ to $|1\rangle$ due to π -rotation on the Bloch sphere. In PO this is mathematically equivalent (see Subsec. 6.2) to the conversion of the polarization state from $|L\rangle$ to $|R\rangle$ (or $|H\rangle$ to $|V\rangle$) due to π -rotation on the Poincaré sphere

$$\int_0^{2\pi} I(\varphi') d\varphi' = \int_0^{2\pi} |\mathcal{U}_{12}(\varphi')|^2 d\epsilon, \quad (6.11)$$

and $I(\varphi')$ describes the conversion efficiency of the half-wave plate $I(\varphi' = \pi) = 1$.

Note that for rotational θ pulses, the target matrix is

$$\mathbf{U}_n = \begin{bmatrix} \cos(\theta/2) & -i \sin(\theta/2) \exp(i\phi) \\ -i \sin(\theta/2) \exp(-i\phi) & \cos(\theta/2) \end{bmatrix}, \quad (6.12)$$

and in the case of $\theta = \pi$ and $\phi = 0$ is equivalent to x-rotation on the Bloch sphere representing $\mathbf{R}_x(\pi)$ rotation gate in the QC (see (1.5)). On the Poincaré sphere it maps to the Jones matrix for a half-waveplate $\mathbf{J}_0(\pi)$ in the PO (see (6.3)).

6.3.1.2 Case of phasal ζ pulses

Let's maximize the phase shifting area (6.13) at the whole-range of the error bandwidth, i.e. from $\epsilon = -1$ to $\epsilon = 1$ (ultrabroadband ζ pulses)

$$\sum \triangleq \int_{-1}^1 z(\epsilon) d\epsilon. \quad (6.13)$$

Here the phase shifting $z(\epsilon) = (\mathcal{U}_{11}(\epsilon) - \mathcal{U}_{11}^*(\epsilon)) / (2i)$ is equal to the trace fidelity in our case $\zeta = \pi$

$$\mathcal{F}_T = \frac{1}{2} \text{Tr} [\mathbf{U}_n(\epsilon) \mathbf{U}_n^\dagger] = \cos \left(\frac{\zeta - \zeta\epsilon}{2} \right)_{\zeta=\pi} \cos \left(\frac{\theta_\epsilon}{2} \right) = \sin \left(\frac{\zeta\epsilon}{2} \right) \cos \left(\frac{\theta_\epsilon}{2} \right), \quad (6.14)$$

and the target matrix is

$$\mathbf{U}_n = \left[\begin{array}{cc} \exp(-i\zeta/2) & 0 \\ 0 & \exp(i\zeta/2) \end{array} \right]_{\zeta=\pi} = \left[\begin{array}{cc} -i & 0 \\ 0 & i \end{array} \right], \quad (6.15)$$

which corresponds to the z-rotation on the Bloch sphere acting as **Z** phase gate in the **QC** (see (1.14)). On the Poincaré sphere it matches with the Jones matrix for a polarization rotator \mathbf{J}_π in the **PO** (see (6.5)).

6.4 ULTRABROADBAND ROTATIONAL $\theta = \pi$ PULSES

The most convenient way to construct ultrabroadband rotational π pulses is the symmetric design consisting of nominal π pulses

$$\pi_{\phi_1} \pi_{\phi_2} \dots, \pi_{\phi_{k/2}} \pi_{\phi_{k/2+1}} \pi_{\phi_{k/2}} \dots \pi_{\phi_2} \pi_{\phi_1}, \quad (6.16)$$

where $k = N - 1$ is the number of inflection points in the errant transition probability vs the pulse area error plot (the number of alternations of the plot). Since the relative constituent phases play a significant role in the calculation, the first and the last phases can be taken as zero $\phi_1 = 0$.

Ultrabroadband rotational $\theta = \pi$ **CPs**, derived by the method Subsec. 6.3.1, have maximum state transfer area for the certain number of **CPs**, hence are unique. For example, five-pulse sequence UB5 with 4 alternations is better than the well-known BB2 sequence with 2 alternations. We have derived up to eleven sequences, which increase the broadness range of the original rotational sequence (a single pulse) more than four times (from 20.5% to 87.7%), and the transition probability area is increased by 83.(3)% by the eleven- π UB11 sequence. Composite phases for the ultrabroadband rotational pulses are shown in the Table 6.1, and the transition probability is plotted in Figure 6.1. For comparison, our five- π UB5 **CP** sequence has the transition probability area equal to $\frac{5}{3} = 1.(6)$, which is smaller than the area of about $\frac{1}{8}(11 + \sqrt{2}) \approx 1.552$ of the well-known five- π BB2 sequence, i.e. by about 0.115. Error robustness range of UB5 is equal to 75.2% and is broader than the range of 64.4% of BB2 sequence.

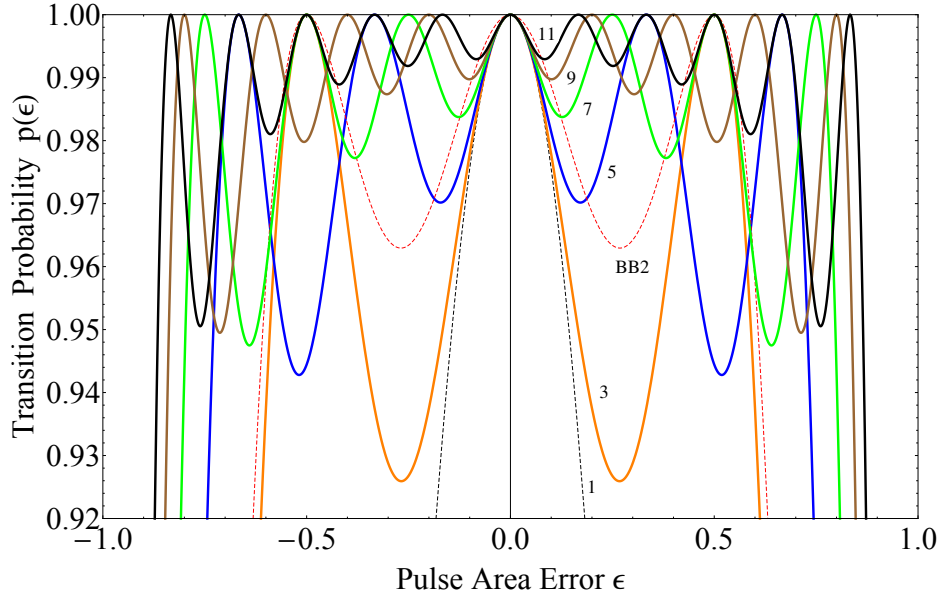


Figure 6.1: Transition probability $p(\epsilon)$ of ultrabroadband rotational π pulses. The numbers N on the curves refer to CP sequences UBN listed in the Table 6.1. As noted above, the curves have $k = N - 1$ alternations on the top of the plot, unlike the BB2 sequence, which has 2 alternations, so it's worse than our five- π UB5.

6.5 ULTRANARROWBAND ROTATIONAL $\theta = \pi$ PULSES

Since NB pulses are asymmetric in composite phases, to construct ultranarrowband rotational π pulses we choose the antisymmetric design consisting of nominal π pulses

$$\pi_{\phi_1} \pi_{\phi_2} \dots, \pi_{\phi_{k/2}} \pi_{\phi_{k/2+1}} \pi_{-\phi_{k/2}} \dots \pi_{-\phi_2} \pi_{-\phi_1}, \quad (6.17)$$

where $k = N - 1$ is the number of inflection points in the errant transition probability vs the pulse are error plot (the number of alternations of the plot). For convenience, the middle phases can be taken as $\phi_{k/2+1} = \pi$.

Ultranarrowband rotational $\theta = \pi$ CPs, derived by the method Subsec. 6.3.1, have minimum state transfer area for the certain number of CPs, hence are unique. For example, five-pulse sequence UN5 with 4 alternations is better than the well-known NB2 sequence with 2 alternations. We have derived up to eleven sequences, which decrease the narrowness range at 50% of probability, viz. full width at half maximum (FWHM), of the original rotational sequence (a single pulse) about 6.75 times (from 50% to 7.4%), and the transition probability area is decreased by 83.3% by the eleven- π UN11 sequence. Composite phases for the ultranarrowband rotational pulses are shown in the Table 6.2, and the transition probability is plotted in Figure 6.2. For comparison, our five- π UN5 CP sequence has the trans-

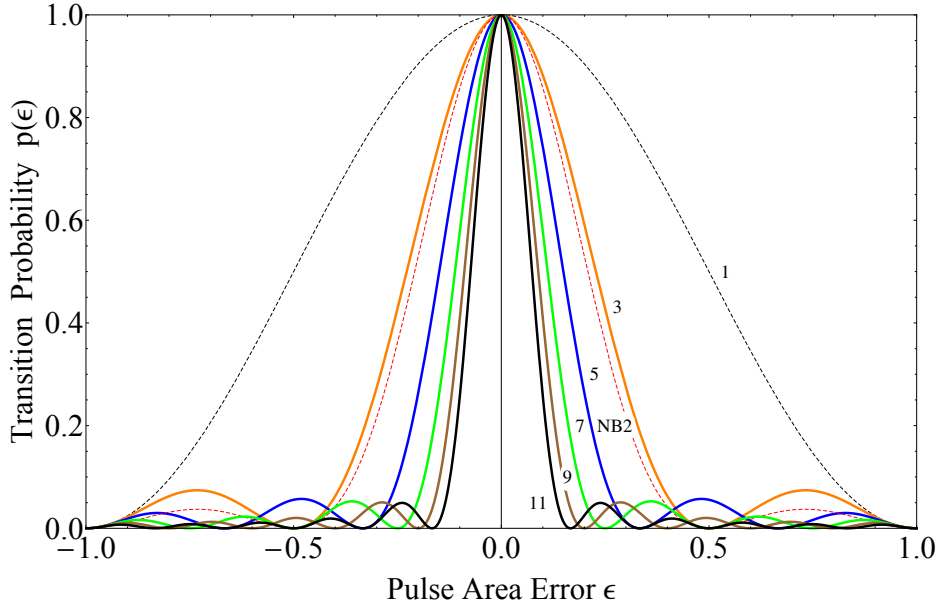


Figure 6.2: Transition probability $p(\epsilon)$ of ultranarrowband rotational π pulses. The numbers N on the curves refer to CP sequences UN N listed in the Table 6.2. As noted above, the curves have $k = N - 1$ alternations on the bottom of the plot, unlike the NB2 sequence, which has 2 alternations, so it's worse than our five- π UN5.

ition probability area equal to $\frac{1}{3} = 0.(3)$, which is smaller than the area of about $\frac{1}{8}(5 - \sqrt{2}) \approx 0.448$ of the well-known five- π NB2 sequence, i.e. by about 0.115. Error sensitivity range of UN5 at FWHM is equal to 14.9% and is narrower than the FWHM range of 20.8% of NB2 sequence.

6.6 ULTRABROADBAND PHASAL $\zeta = \pi$ PULSES

As usual (cf. (3.3)), we construct ultrabroadband phasal π pulses with asymmetric design consisting of nominal π pulses

$$\pi_{\phi_1} \pi_{\phi_2} \dots \pi_{\phi_{k/2+1}} \cdot \pi_{\phi_1 + \frac{1}{2}\pi} \pi_{\phi_2 + \frac{1}{2}\pi} \dots \pi_{\phi_{k/2+1} + \frac{1}{2}\pi}, \quad (6.18)$$

where $k = N - 2$ is the number of inflection points in the trace fidelity vs the pulse are error plot (the number of alternations of the plot). Careful analysis shows that the first few phases can be taken as zero in the calculation (cf. Table 6.3).

Ultrabroadband phasal $\zeta = \pi$ CPs, derived by the method Subsec. 6.3.1, have maximum trace fidelity area for the certain number of CPs, hence are unique. We have derived up to fourteen sequences, which increase the broadness range of the original phasal sequence (two pulses) about four times (from 20.5% to 81.5%), and the trace fidelity area is increased by the 75% by the fourteen- π UBPh14 sequence.

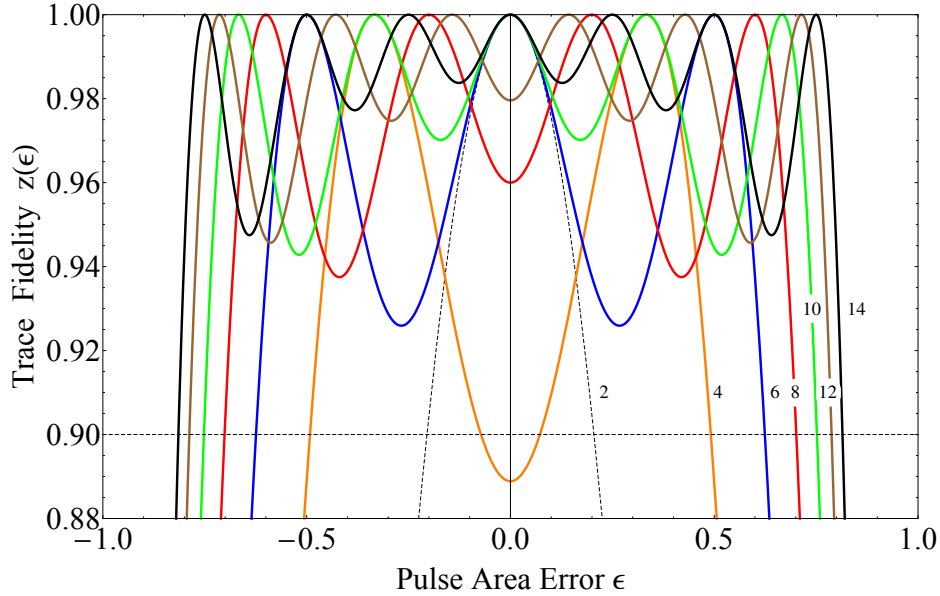


Figure 6.3: Trace fidelity $z(\epsilon)$ of ultrabroadband phasal π pulses. The numbers N on the curves refer to CP sequences UBPh N listed in the Table 6.3. As noted above, the curves have $k = N - 2$ alternations on the top of the plot.

Composite phases for the ultrabroadband phasal pulses are shown in the Table 6.3, and the trace fidelity is plotted in Figure 6.3¹.

6.7 COMMENTS AND CONCLUSIONS

We presented a number of CP sequences consisting of π pulses for transition of the quantum state from $|0\rangle$ to $|1\rangle$ in ultrarobust and ultrasensitive manners, according to the pulse area deviation ϵ . Using quantum-classical analogy, we presented a number of sequences of half-wave plates for conversion of the polarization state from $|H\rangle$ to $|V\rangle$ or from $|L\rangle$ to $|R\rangle$ in ultrabroadband and ultranarrowband ways, according to the phase-shift (retardation) deviation $\varphi' - \varphi = \varphi' - \pi$. Our UB5 pulse already outperforms the well-known BB2 pulse in terms of broadness, e.g. UB5 maintains 90% of transition probability (or conversion efficiency) over the broadness (error-correction or retardation deviation) range spanning a width of roughly 1.504π from the whole 2π , approximately by 17% larger than roughly 1.288π , the width of BB2. Our longest UB11 pulse covers approximately 88% of the whole width for the same benchmark. Our UN5 pulse already outperforms the well-known NB2 pulse in terms of narrowness, e.g. FWHM of UN5 is roughly

¹ Four, eight and twelve phasal sequences are below 100% fidelity at the center (errorless case). Moreover, the trace fidelity is slightly less than 90% in the case of the UBPh4 sequence. Note that in some applications where ultrahigh precision is not a mandatory criterion, these violations are minor deviations from the requirements, and these CP sequences can be applied.

0.298π , approximately 1.4 times narrower than FWHM of NB2. Our longest UNB11 pulse covers approximately 21% of the whole width for the same benchmark.

Furthermore, using the similar derivation approach of CPs, we theoretically design ultrarobust Z quantum gate via a number of CP sequences consisting of π pulses, and equivalently ultrabroadband polarization π rotator. Our longest UBPh14 pulse maintains 90% of trace fidelity over a broadness range of roughly 1.63π .

With the choice of the pulse area structure (or the phase-shift structure in PO) of the CP (or combination of wave-plates in PO), one can apply the method of derivation to obtain arbitrary transition (or arbitrary conversion in PO) from the given quantum (or polarization) state to the arbitrary quantum (or polarization) state in ultrabroadband and ultranarrowband manners. Certainly, achieving superposition state $\frac{1}{\sqrt{2}} (|0\rangle \pm i|1\rangle)$ ² (or left-right circular polarization bases $|L\rangle, |R\rangle$) is of interest.

Results are promising for applications in NMR, QS and, especially PO, where the property of robustness/broadness or selectivity/narrowness is more important and ultrahigh-precision is not obligatory as in QC. In this sense, we acknowledge also the future applications that are not on demand due to the absence of the method.

² An ideal $\pi/2$ rotation on the Bloch sphere from $|0\rangle$ or $|1\rangle$ initial states presents these states. Actual superposition states $\frac{1}{\sqrt{2}} (|0\rangle \pm |1\rangle)$ can be obtained with the same fashion targeting $\pi/2$ rotation with phase $\phi = \pi/2$.

Table 6.1: Phases of symmetric, altering, ultrabroadband composite rotational $\theta = \pi$ sequences of $N = k + 1$ nominal π pulses, which produce ultrarobust population transfer in the ultrabroadband pulse area error correction range. The last column gives the high-transition probability range $[\pi(1 - \epsilon_0), \pi(1 + \epsilon_0)]$ of pulse area error compensation wherein the errant transition probability is above the value 0.9.

Name	Pulses	Number of alternations k (inflection points)	\sum_b cf. (6.10)	Phases $\phi_1, \phi_2, \phi_3, \dots, \phi_{k/2}, \phi_{k/2+1}, \phi_{k/2}, \dots, \phi_3, \phi_2, \phi_1$ (in units π) (according to (6.16))	Transition probability $p(\epsilon) = 90\%$ error correction range
single	1	0	1	0	$[0.79517\pi, 1.20483\pi]$
UB3	3	2	1.5	$0, \frac{1}{2}$	$[0.376\pi, 1.624\pi]$
UB5	5	4	1.(6)	$0, 0.5825, 0.3737$	$[0.248\pi, 1.752\pi]$
UB7	7	6	1.75	$0, 0.6230, 0.4918, 0.7558$	$[0.185\pi, 1.815\pi]$
UB9	9	8	1.8	$0, 0.6490, 0.5514, 0.8458, 0.6774$	$[0.148\pi, 1.852\pi]$
UB11	11	10	1.8(3)	$0, 0.6677, 0.5886, 0.9044, 0.7786, 0.9663$	$[0.123\pi, 1.877\pi]$
BB2	5	2	≈ 1.552	$0, \frac{1}{2}, \frac{7}{4}, \frac{7}{4}, \frac{1}{2}$ (all phases in units π)	$[0.356\pi, 1.644\pi]$

Table 6.2: Phases of asymmetric, altering, ultranarrowband composite rotational $\theta = \pi$ sequences of $N = k + 1$ nominal π pulses, which produce ultrasensitive population transfer in the ultranarrowband pulse area error sensitivity range. The last column gives the full width at half maximum range $[\pi(1 - \epsilon_0), \pi(1 + \epsilon_0)]$ of pulse area error sensitivity wherein the errant transition probability is above the value 0.5. Note that the full population transfer occurs at the center for zero pulse area error $p(\epsilon = 0) = 1$.

Name	Pulses	Number of alternations k (inflection points)	\sum_n cf. (6.10)	Phases $\phi_1, \phi_2, \phi_3, \dots, \phi_{k/2}, \phi_{k/2+1}, -\phi_{k/2}, \dots, -\phi_3, -\phi_2, -\phi_1$ (in units π) (according to (6.17))	FWHM of transition probability error sensitivity range
single	1	0	1	0	$[0.5\pi, 1.5\pi]$
UN3	3	2	0.5	$\frac{1}{2}, 1$	$[0.772\pi, 1.228\pi]$
UN5	5	4	0.(3)	0.5896, 0.4104, 1	$[0.851\pi, 1.149\pi]$
UN7	7	6	0.25	0.5193, 0.6121, 0.3671, 1	$[0.889\pi, 1.111\pi]$
UN9	9	8	0.2	0.5451, 0.4880, 0.6235, 0.3340, 1	$[0.911\pi, 1.089\pi]$
UN11	11	10	0.1(6)	0.5173, 0.5562, 0.4690, 0.6312, 0.3209, 1	$[0.926\pi, 1.074\pi]$
NB2	5	2	≈ 0.448	$0, \frac{1}{2}, \frac{5}{4}, \frac{5}{4}, \frac{1}{2}$ (all phases in units π)	$[0.792\pi, 1.208\pi]$

Table 6.3: Phases of asymmetric, altering, ultrabroadband composite phasal $\zeta = \pi$ sequences of $N = k + 2$ nominal π pulses, which produce ultrarobust Z phase gate in the ultrabroadband pulse area error correction range. The last column gives the high-fidelity range $[\pi(1 - \epsilon_0), \pi(1 + \epsilon_0)]$ of pulse area error compensation wherein the trace fidelity is above the value 0.9.

Name	Pulses	Number of alternations k (inflection points)	Σ cf. (6.13)	Phases $\phi_1, \phi_2, \dots, \phi_{k/2+1}, \phi_1 + \frac{1}{2}, \phi_2 + \frac{1}{2}, \dots, \phi_{k/2+1} + \frac{1}{2}$ (in units π) (according to (6.18))	Trace fidelity $z(\epsilon) = 90\%$ error correction range
two	2	0	1	0	$[0.79517\pi, 1.20483\pi]$
UBPh4	4	2	1.(3)	0, 0.6743	$[0.508\pi, 1.492\pi]$
UBPh6	6	4	1.5	0, 0, $\frac{3}{4}$	$[0.376\pi, 1.624\pi]$
UBPh8	8	6	1.6	0, 0, 0.8048, 0.6000	$[0.299\pi, 1.701\pi]$
UBPh10	10	8	1.(6)	0, 0, 0, 0.4129, 1.0871	$[0.248\pi, 1.752\pi]$
UBPh12	12	10	≈ 1.714	0, 0, 0, 0.8624, 0.7142, 0.5696	$[0.212\pi, 1.788\pi]$
UBPh14	14	12	1.75	0, 0, 0, 0, 0.8798, 0.7500, 0.6202	$[0.185\pi, 1.815\pi]$

BROADBAND COMPOSITE NONRECIPROCAL POLARIZATION WAVE PLATES AND OPTICAL ISOLATORS

We provide a technique for a broadband nonreciprocal wave retarder whose quarter-wave plate phase retardation is the same in forward and backward directions. The system is built using a number of sequential nonreciprocal wave plates. The proposed device can also be utilized to create a broadband optical diode, which consists of two achromatic quarter-wave plates, one reciprocal and the other non-reciprocal, that are sandwiched between two polarizers aligned in parallel.

7.1 INTRODUCTION

For decades, reciprocal and broadband (achromatic) polarization retarders have been a topic of intense attention in optics [171–174]. Traditionally, two or more conventional wave plates, of the same or different materials, are combined to make such retarders. West and Makas [5] reported achromatic combinations of plates with various birefringence dispersions as one of the first known ideas. Destriau and Prouteau [6] presented achromatic retarders made out of wave plates of the same material but different thicknesses for two birefringent plates, while Pancharatnam offered three plates for half-wave [7] and quarter-wave [8] retarders. Harris and colleagues later presented achromatic quarter-wave plates with six [9] and ten identical quarter-wave plates [10]. The analogy between the polarization Jones vector and the quantum state vector has recently been used to suggest arbitrarily precise broadband polarization retarders [11, 12, 170].

All of the above achromatic wave plates are reciprocal, in the sense that their function is invariant upon time inversion. However, as recently shown by Al-Mahmoud et. al [175], wave plates retarders can be non-reciprocal whose phase-shift retardation depends on the light propagation direction. For example, a retarder with retardation of $\pi/2$ in the forward direction (quarter-wave plate) and

π in the backward direction (half-wave plate) or other combination of retardance values can be realized. The Al-Mahmoud et. al [175] non-reciprocal elements are based on magneto-optical phenomena like the Faraday effect. The axial (as opposed to polar) structure of the magnetic field and magnetization vectors in this case, as well as the associated invariance upon space inversion, are what cause the non-reciprocity. In Al-Mahmoud et. al [175] experiment, it was shown that a non-reciprocal Faraday rotator combined with a reciprocal rotator made of two half-wave plates sandwiched between crossed quarter-wave plates could be used to realize adjustable non-reciprocal wave retarders with retardation that differed in the forward and backward directions [175].

In this chapter, we theoretically propose novel broadband polarization quarter-wave plates, which are also nonreciprocal, with the potential to be used in broadband optical isolators or/and circulators for telecommunications, industrial, and laboratory research.

7.2 BACKGROUND

The waveplate is a birefringent medium that modifies the polarization state by adding a phase shift of φ between the two orthogonal polarization components. The half-wave plate and quarter-wave plate retarders are the most popular waveplates, with phase shifts of π and $\pi/2$, respectively. The waveplate retarder's Jones matrix, whose axes are aligned with the lab axes, takes the shape of a diagonal matrix,

$$J(\varphi) = \begin{bmatrix} e^{i\varphi/2} & 0 \\ 0 & e^{-i\varphi/2} \end{bmatrix}, \quad (7.1)$$

where $\varphi = 2\pi L(n_s - n_f)/\lambda$ is the phase shift, λ is the wavelength in vacuum, n_f and n_s are the refractive indices along the fast and slow axes respectively, and L is the thickness of the waveplate. When the waveplate retarder's axes are rotated by an angle θ with regard to the lab axes, the Jones matrix $J_\theta(\varphi)$ is given by

$$\begin{aligned} J_\theta(\varphi) &= R(-\theta) J(\varphi) R(\theta) = \\ &= \begin{bmatrix} e^{i\varphi/2} \cos^2(\theta) + e^{-i\varphi/2} \sin^2(\theta) & -i \sin(2\theta) \sin(\varphi/2) \\ -i \sin(2\theta) \sin(\varphi/2) & e^{-i\varphi/2} \cos^2(\theta) + e^{i\varphi/2} \sin^2(\theta) \end{bmatrix}, \end{aligned} \quad (7.2)$$

with rotation matrix $R(\theta)$ in the horizontal-vertical (HV) basis given by

$$R(\theta) = \begin{bmatrix} \cos \theta & -\sin \theta \\ \sin \theta & \cos \theta \end{bmatrix}. \quad (7.3)$$

Another way to realize a retarder is to use a polarization rotator at an angle θ sandwiched in between two quarter-wave plates rotated by angles $-\pi/4$ and $\pi/4$ with respect to the lab reference frame correspondingly [176]. The Jones matrix J for such a sequence can be given by the product of the Jones matrices of the quarter-wave plates and the rotator:

$$J = J_{-\pi/4}(\pi/2) R(\theta) J_{\pi/4}(\pi/2) = \begin{bmatrix} e^{i\theta} & 0 \\ 0 & e^{-i\theta} \end{bmatrix} = J_0(2\theta). \quad (7.4)$$

The last part of Eq. (7.4) demonstrates that the whole sequence can be considered an effective wave plate with an effective retardation $\varphi = 2\theta$. If one uses Faraday rotator (nonreciprocal device) then the effective waveplate is also nonreciprocal [175]. Even though the two quarter-wave plates can be achromatic — an assumption we make from now on — the effective wave plate is not broadband due to the strong wavelength dependence on the Verdet constant. Our objective in the present chapter is to construct broadband nonreciprocal wave plates using a sequence of several nonreciprocal retarders, each with a specific phase shift and rotated by specific angles.

7.3 COMPOSITE WAVE PLATE

Now we will show three different sequences to construct nonreciprocal broadband quarter-wave plates.

- The first approach is to combine two nonreciprocal quarter-wave plates and one nonreciprocal half-wave plate. This composition is described by the Jones matrix

$$\mathcal{J}(\varepsilon) = J_{\alpha_1}(\pi/2 + \varepsilon/2) J_{\alpha_2}(\pi + \varepsilon) J_{\alpha_3}(\pi/2 + \varepsilon/2). \quad (7.5)$$

- The second approach is to combine two nonreciprocal half-wave plates and one nonreciprocal quarter-wave plate, characterized by the Jones matrix

$$\mathcal{J}(\varepsilon) = J_{\alpha_1}(\pi + \varepsilon) J_{\alpha_2}(\pi + \varepsilon) J_{\alpha_3}(\pi/2 + \varepsilon/2). \quad (7.6)$$

- The third approach is to have multiple nonreciprocal wave plates in the sequence, e.g., combining four nonreciprocal half-wave plates and one nonreciprocal quarter-wave plate. The Jones matrix of this structure reads

$$\begin{aligned} \mathcal{J}(\varepsilon) &= J_{\alpha_1}(\pi + \varepsilon) J_{\alpha_2}(\pi + \varepsilon) J_{\alpha_3}(\pi + \varepsilon) \\ &\quad \times J_{\alpha_4}(\pi + \varepsilon) J_{\alpha_5}(\pi/2 + \varepsilon/2). \end{aligned} \quad (7.7)$$

Here ε and $\varepsilon/2$ represent the systematic deviations from the nominal retardation of the half- and quarter-wave plates respectively.

For the above odd number of sequences (7.5)-(7.7) one can easily check that they are nonreciprocal.

The composite retarder's efficiency is evaluated in terms of the fidelity \mathfrak{F} [170],

$$\mathfrak{F}(\varepsilon) = \frac{1}{2} \left| \text{Tr} \left(J_0^{-1} \mathcal{J}(\varepsilon) \right) \right|, \tag{7.8}$$

where $\mathcal{J}(\varepsilon)$ is the achieved and J_0 is the target Jones matrix. $\mathfrak{F} = 1$ if the two operators \mathcal{J} and J_0 are identical, but the fidelity reduces if the two matrices differ. In order to produce broadband nonreciprocal quarter-wave plate we determine the rotation angles of each wave plate in Eqs. (7.5), (7.6) or (7.7) by using the Monte Carlo method. We generate 10^4 sets of random angles $\alpha_1, \alpha_2, \alpha_3, \alpha_4$ and α_5 . We select solutions, which deliver the biggest overall fidelity $\mathfrak{F}(\varepsilon)$ in the interval of $\varepsilon \in [-\pi, \pi]$ and also, ensure a flat top. The angles are presented in the Table 7.1. It is important to note that the parameters given in the Table 7.1 are not the only possible. Obviously, for the wavelength at which the wave plates serve as half or quarter-wave plates, respectively, we have $\varepsilon = 0$ and $\mathfrak{F}(0) = 1$.

Table 7.1: Calculated angles of rotation (in radians) for the three sequences of Eqs. (7.5), (7.6), and (7.7).

sequences	angles ($\alpha_1; \alpha_2; \dots; \alpha_N$)
(7.5)	(3.3; 1.21; 3.1)
(7.6)	(3.6; 1.65; 3.9)
(7.7)	(1.61; 6.48; 6.47; 1.62; 0.78)

7.4 BROADBAND OPTICAL ISOLATOR

Another interesting case is when the sequence serves as a broadband null retarder in one direction and a broadband half-wave plate in the other direction, which can be archived if we combine our nonreciprocal broadband quarter-wave plate with a commercially available broadband but reciprocal quarter-wave plate. In this case, one can build a broadband optical isolator as shown and explained in Figure 7.1.

The working principle of the proposed optical isolator is the following. Any light beam entering through the polarizer I will exit vertically polarized (blue array), after passing through the achromatic reciprocal quarter-wave plate (ARQWP) the light will be circularly polarized, then passing through the achromatic nonreciprocal quarter-wave plate (ANRQWP) it will be again vertically polarized, thus

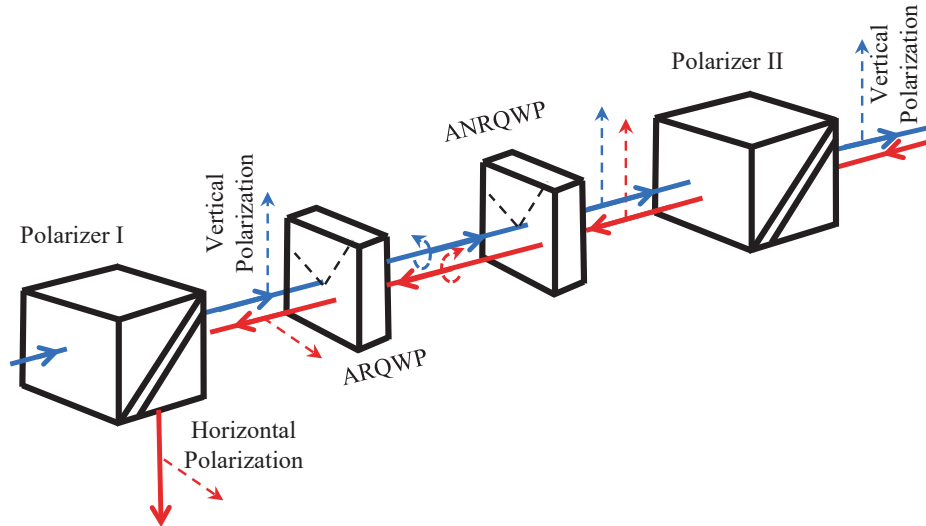


Figure 7.1: Scheme of the broadband optical isolator. ARQWP stands for the achromatic reciprocal quarter-wave plate, while ANRQWP stands for the achromatic non-reciprocal quarter-wave plate.

all light will pass polarizer II. On the way back, if the light re-enters the polarizer II in the backward direction (red array), due to the combined effect of the ANRQWP and ARQWP, the polarization is rotated in such a way (90 degrees) that the whole wave is blocked by the polarizer I, so that no light can exit from right to left.

7.5 NUMERICAL CALCULATIONS

We explained the basic concept of creating broadband nonreciprocal polarization quarter-wave plates and broadband optical isolators in the previous sections. Now, we present numerical simulations to test the effectiveness of the design we have discussed above.

In Figure 7.2 we show the calculation for the fidelity \mathfrak{F} profiles using the three configurations (7.5), (7.6) and (7.7) with rotation angles taken from the Table 7.1. Obviously, the configuration (7.7) outperforms the other configurations and this was expected because configuration (7.7) has five retarders in the series compared to three retarders in case of (7.5) and (7.6). In theory, the fidelity profiles can be made arbitrarily flat by increasing the number of retarders in the series. In practice, it is not clear whether such many-retarders sequences will be useful, due to the many optical elements in the series (Faraday rotators and quarter-wave plates), therefore we limit our investigation to five nonreciprocal quarter-wave plates (five Faraday rotators and ten quarter-wave plates altogether).

For broadband optical isolator simulations in this chapter, we use terbium gallium garnet crystal (TGG) as it is one of the most common crystals for Faraday

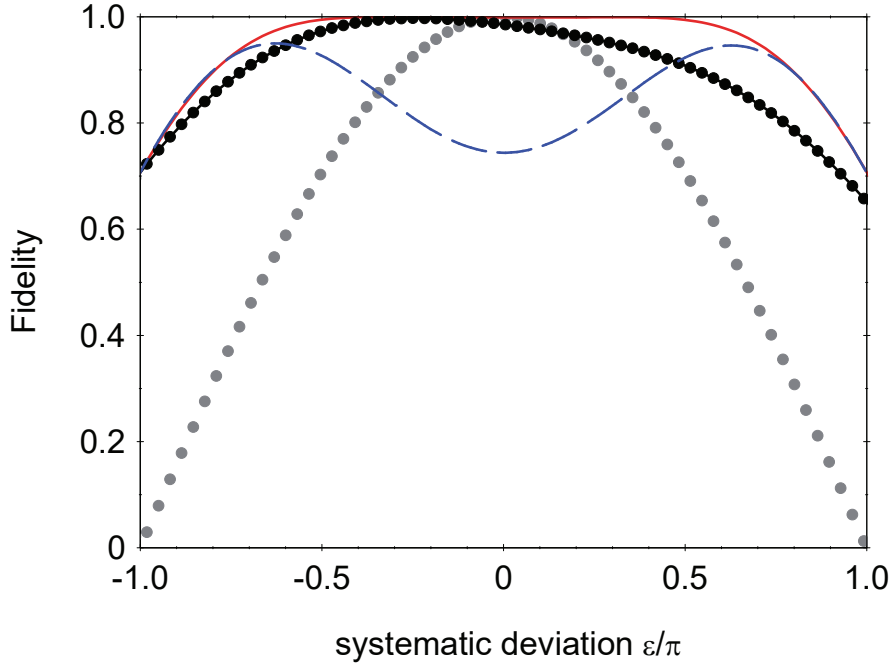


Figure 7.2: Fidelity versus systematic deviation for the composite waveplates designed by using three configurations: Eq. (7.5) is depicted by the blue dashed line, Eq. (7.6) by the black dotted line, and Eq. (7.7) by the red solid line. The gray dotted line is for a quarter-wave plate with a single Faraday rotator for easy reference.

rotators. We fix the applied magnetic field to 1 T, the length of the crystal is considered to be 1 cm for the half-wave plates and 0.5 cm for the quarter-wave plates. Up until now, there has been a lot of research done on the dispersion of the TGG Verdet constant ν [177–179]. It was demonstrated that the following formula can adequately represent the wavelength dependence of this crystal,

$$\nu(\lambda) = \frac{K}{\lambda_0^2 - \lambda^2}, \quad (7.9)$$

where $K = 4.45 \cdot 10^7 \frac{\text{rad} \cdot \text{nm}^2}{\text{T} \cdot \text{m}}$ and $\lambda_0 = 258.2 \text{ nm}$ is the effective transition wavelength. TGG has optimal material properties for the Faraday rotator in the range of 400 – 1100 nm, excluding 470 – 500 nm (the absorption window). For most materials, the Verdet constant decreases (in absolute value) with increasing wavelength: for TGG it is equal to $134 \frac{\text{rad}}{\text{T} \cdot \text{m}}$ at 632 nm and $40 \frac{\text{rad}}{\text{T} \cdot \text{m}}$ at 1064 nm. The operating wavelength range of the Faraday isolator is constrained as a result of this.

The performance of the optical isolators is quantified by its transmission T_f (a portion of the input light's intensity that passes through the isolator), back-transmission T_b (a portion of the back-transmission light's intensity that passes through the isolator in the opposite direction), and isolation D . The light intensity

measured after passing the optical diode in both the forward (I_{forw}) and backward (I_{back}) directions determine these numbers, respectively,

$$T_f = I_{forw}/I_0 = |\mathbf{P}_V \mathbf{J}_f \mathbf{P}_V |in\rangle|^2, \quad (7.10a)$$

$$T_b = I_{back}/I_0 = |\mathbf{P}_V \mathbf{J}_b \mathbf{P}_V |in\rangle|^2, \quad (7.10b)$$

where \mathbf{P}_V stands for vertical polarizers, $|in\rangle$ is the Jones vector for the light entering the isolator, and \mathbf{J}_f and \mathbf{J}_b are Jones matrices for forward and backward wave plates respectively. I_0 has the meaning of the intensity of light at the beginning of the Faraday isolator. The isolation is then determined with the formula [180, 181]

$$D = -10 \log \left[\frac{T_b}{T_f} \right]. \quad (7.11)$$

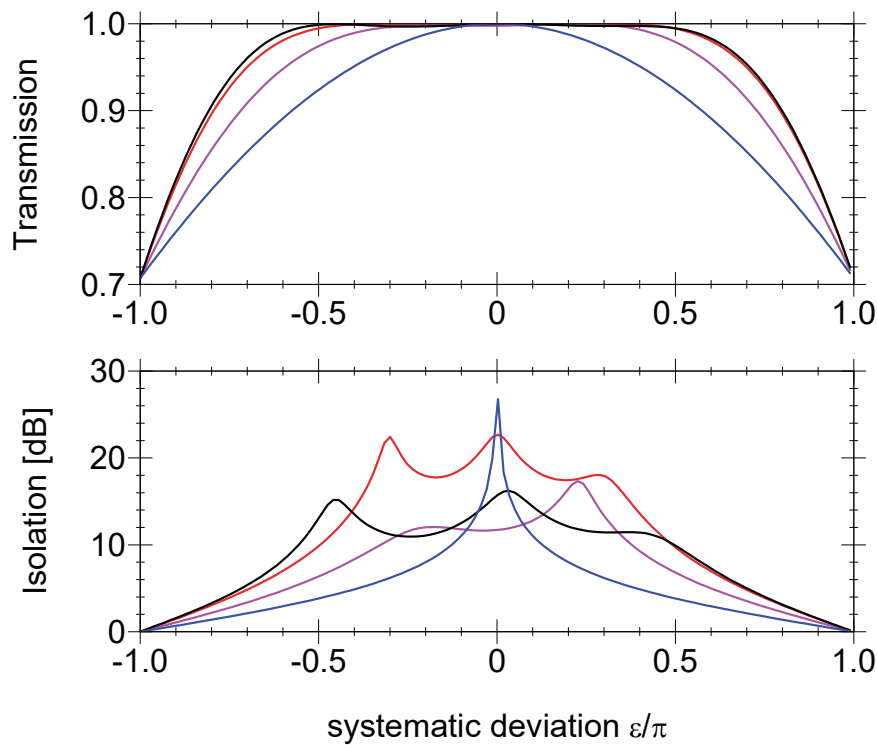


Figure 7.3: Transmission and isolation properties of the optical isolators with different numbers of wave plates in the series, compared to the isolator based on a single rotator (blue line), vs the systematic deviation ε . The other three curves refer to the sequences of Eqs. (7.5) depicted by a purple line, (7.6) by a red line, and (7.7) by a black line.

The transmission and isolation profiles for the three configurations (7.5), (7.6) and (7.7) are shown in Figures 7.3 and 7.4. One can notice that for all these composite isolators both the transmission and isolation are far more efficient than that of isolators using a single rotator (blue curve). Figure 7.3 shows the performance of

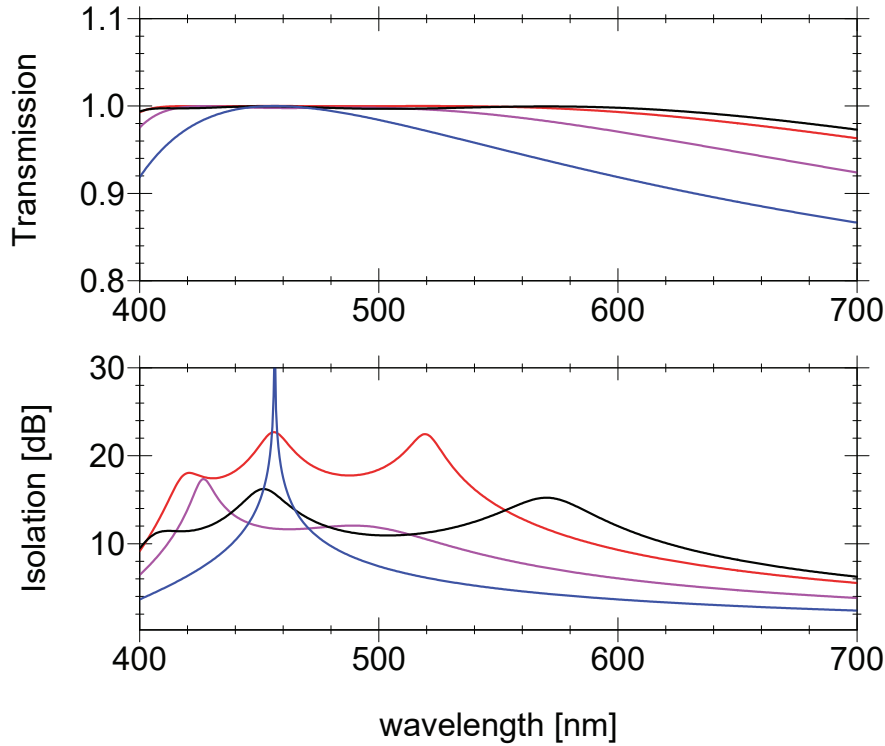


Figure 7.4: The same as Figure 7.3 but instead of systematic deviation ε we use the wavelength parameter.

the optical isolators under study with respect to the systematic deviation ε of the Faraday rotators, whereas in Figure 7.4 the analogous dependence on wavelength is presented. The long tail asymmetry seen in Figure 7.4 stems from the fact that the Faraday rotation angle depends non-linearly on the wavelength (as seen in Eq. (7.9)). The isolation above 10 dB over a region of 200 nm can be seen from Figure 7.4, and it is a much broader spectral range compared to the case of using just a single Faraday rotator (about 20 nm on the level of 10 dB).

We emphasize that the transmission and isolation curves were calculated under the assumption of no losses in realistic realizations. Insertion losses and reflections from the surfaces of the optical elements are the primary causes of the reduced transmission. Losses resulting from optical element propagation would not be as significant.

7.6 CONCLUSIONS

We have presented a novel way to construct broadband nonreciprocal polarization quarter-wave plates. The concept is based on combination of several nonreciprocal waveplates with the optical axis of each rotated by appropriate angles. In addition, the proposed broadband nonreciprocal polarization quarter-wave plate can

be used in combination with a broadband reciprocal polarization quarter-wave plate to build a broadband optical isolator. The isolation bandwidth (isolation of more than 10 dB) is almost 200 nm while the transmission bandwidth is beyond 200 nm. This isolator has the benefit of being resistant to changes in temperature, crystal length, and magnetic field. With the available optical components, an experimental implementation should be feasible.

GENERAL CONCLUSIONS AND PERSPECTIVES

Composite pulses, the powerful quantum control technique from nuclear magnetic resonance, and its wide applications have been explored in this thesis, which are novel or have not been reported in the literature hitherto. The dissertation exhibits the delicate susceptibility of the method to mathematically different kinds of target problems. The prime purpose of the thesis is to encourage a wide range of researchers in both classical and quantum physics to leverage this magical and versatile technique to their research tasks. Thesis addresses several specialized applications, namely in quantum computing and quantum information, quantum information processing (quantum cryptography and quantum networks), quantum sensing, and polarization optics.

As is known, from the point of view of quantum operations, composite pulses act as rotations on the Bloch sphere. Rotation gates tend to have experimental errors in amplitude and pulse duration, which reduces accuracy. In this sense, broadband-type composite pulses are of interest to eliminate the pulse area error. Furthermore, a subclass of constant rotations, being independent of the choice of initial state, are candidates for universal operations on the Bloch sphere. We presented a number of this kind of broadband phase-distortionless composite pulse sequences for three basic quantum gates — the X gate, the Hadamard gate and arbitrary rotation gates in Chapter 2. The composite sequences contain up to 17 pulses and can compensate up to eight orders of experimental errors maintaining ultrahigh-fidelity, equivalent to the quantum computation benchmark.

In the same fashion, we presented a number of broadband phase-distortionless composite pulse sequences for four basic quantum gates — the Z gate, the S gate, the T gate and arbitrary phase gates in Chapter 3. The composite sequences contain up to 18 pulses and can compensate up to eight orders of experimental errors maintaining ultrahigh-precision required for quantum computation. Thus, we close the topic of single-qubit gates via composite pulses in quantum computation and quantum information.

From the other hand, narrowband-type composite pulses provide selective and local spatial addressing of trapped ions or atoms in optical lattices by tightly focused laser beams in quantum sensing. Furthermore, polarization retarder sequences constructed by these composite parameters are the candidates for optical filters in polarization optics, and also this kind of composite pulses are suitable for spatial localization in *in vivo* nuclear magnetic resonance spectroscopy. Passband-type composite pulses ensure both selectivity on the edges and robustness at the center of precision measure (fidelity, transition probability or other). We derived narrowband and passband composite rotational quantum gates — the X gate, the Hadamard gate and arbitrary rotation gates in Chapter 4. Two optimization methods have been used for that purpose — a strict SU(2) approach, the same scenario as in Chapter 2, and a flexible regularization approach. This completes the package of three main classes of composite pulses for rotation gates.

Robust ultrasmall transition probability composite pulses, which are the subject of Chapter 5, allow to construct deterministic and highly efficient single-photon source. This kind of composite pulses can have applications in quantum information processing, to improve the ensemble-based protocols. We examined their application in DLCZ protocol.

Ultrabroadband-type (ultrarobust) or ultranarrowband-type (ultrasensitive) control of quantum or classical systems is important primarily from the point of view of the natural capabilities of the device, and what level of property can be achieved with a given number of pulses. Derivation methodology and capabilities of these types of composite pulses is presented in Chapter 6.

Another interesting application, now in classical physics, is the polarization optics. Interestingly, quantum-classical analogy works, since rotations on the Bloch and Poincaré spheres are mathematically the same, and Jones matrices represent rotation matrices similar to experimental quantum gates. In Chapter 7 we presented a novel way to construct broadband nonreciprocal polarization quarter-wave plates via composite pulse parameters. Broadband nonreciprocal polarization plate is designed via the sequence of nonreciprocal waveplates with the optical axes rotated by certain angles (composite phases), where each nonreciprocal waveplate can be constructed using two conventional (reciprocal) quarter-wave plates and a Faraday rotator in the middle. Furthermore, this new apparatus can be used in combination with a broadband reciprocal polarization quarter-wave plate to build a broadband optical isolator. Isolation of more than 10 dB is maintained in almost 200 nm wavelength-bandwidth, and the transmission bandwidth is beyond 200 nm. The advantage of these kind of isolators is their resistance to changes in temperature, crystal length and magnetic field.



PUBLICATIONS AND PRESENTATIONS

A.1 PUBLICATIONS

1. Hayk L. Gevorgyan and Nikolay V. Vitanov, “**Ultrahigh-fidelity composite rotational quantum gates**” published in *Physical Review A*, **104** (1), 012609 (2021), DOI: [10.1103/physreva.104.012609](https://doi.org/10.1103/physreva.104.012609).
2. Hayk L. Gevorgyan and Nikolay V. Vitanov, “**Ultrahigh-fidelity composite quantum phase gates**”, arXiv:2306.10340 [quant-ph], DOI: [10.48550/arXiv.2306.10340](https://doi.org/10.48550/arXiv.2306.10340).
3. Hayk L. Gevorgyan and Nikolay V. Vitanov, “**Deterministic generation of arbitrary ultrasmall excitation of quantum systems by composite pulse sequences**”, arXiv:2306.13209 [quant-ph], DOI: [10.48550/arXiv.2306.13209](https://doi.org/10.48550/arXiv.2306.13209).
4. Hayk L. Gevorgyan and Nikolay V. Vitanov, “**Narrowband and passband composite rotational quantum gates**”, to be submitted for publication.
5. Hayk L. Gevorgyan, “**Ultrabroadband and Ultranarrowband Composite Polarization Half-Waveplates**” published in *Optica High-brightness Sources and Light-driven Interactions Congress 2022*, Technical Digest Series (Optica Publishing Group, 2022), paper EF3A.5, DOI: [10.1364/EUVXRAY.2022.EF3A.5](https://doi.org/10.1364/EUVXRAY.2022.EF3A.5).
6. Hayk L. Gevorgyan, Andon A. Rangelov and Nikolay V. Vitanov, “**Broadband composite nonreciprocal polarization wave plates and optical isolators**”, arXiv:2305.06431 [physics.optics], DOI: [10.48550/arXiv.2305.06431](https://doi.org/10.48550/arXiv.2305.06431), submitted for publication.

A.2 PRESENTATIONS

1. H. L. Gevorgyan, N. V. Vitanov, “**High-Fidelity Composite Rotation Gates**”, Control of Quantum Dynamics of Atoms, Molecules, and Ensembles by Light, CAMEL-XV, June 2019, Nessebar, Bulgaria.

2. H. L. Gevorgyan, N. V. Vitanov, "**Ultrahigh-Fidelity Composite Rotation Gates**", Gordon Research Conference "Quantum Control of Light and Matter", **GRC**, August 2019, Salve Regina University, New Port, RI, USA.
3. H. L. Gevorgyan, N. V. Vitanov, "**Ultrahigh-Fidelity Composite Rotation Gates**", MSCA-ITN: Light-Matter Interfaces for Quantum Enhanced Technologies, **LIMQUET-2019**, September 2019, Nessebar, Bulgaria.
4. H. L. Gevorgyan, N. V. Vitanov, "**Composite pulses for ultrahigh-precision applications: quantum computing and more**", MSCA-ITN: Light-Matter Interfaces for Quantum Enhanced Technologies, **LIMQUET-2021**, September 2021, Oxford, UK.
5. H. L. Gevorgyan, N. V. Vitanov, "**Ultrabroadband (bat) and ultranarrowband (snake) composite π pulses**", The 9th International Symposium "Optics & its applications 2022", **Optics-2022**, January 2022, Yerevan – Ashtarak, Armenia.
6. H. L. Gevorgyan, N. V. Vitanov, "**Ultrahigh-fidelity robust composite quantum phase gates**", The 9th International Symposium "Optics & its applications 2022", **Optics-2022**, January 2022, Yerevan – Ashtarak, Armenia.
7. H. L. Gevorgyan, N. V. Vitanov, "**Ultrabroadband and Ultranarrowband Composite Polarization Half-Waveplates**", High-Brightness Sources and Light-Driven Interactions Congress, **OPTICA**, March 2022, Budapest, Hungary.

BIBLIOGRAPHY

- [1] G. Chen, D. A. Church, B. G. Englert, C. Henkel, B. Rohwedder, M. O. Scully and M. S. Zubairy, *Quantum Computing Devices: Principles, Designs, and Analysis*. CRC, 2006.
- [2] M. A. Nielsen and I. L. Chuang, *Quantum Computation and Quantum Information*. Cambridge University Press, 2000.
- [3] S. Wimperis, 'Broadband, narrowband, and passband composite pulses for use in advanced NMR experiments', *Journal of Magnetic Resonance, Series A*, vol. 109, no. 2, pp. 221–231, 1994. doi: <https://doi.org/10.1006/jmra.1994.1159>.
- [4] D. Maslov, 'Basic circuit compilation techniques for an ion-trap quantum machine', *New Journal of Physics*, vol. 19, no. 2, pp. 023035, 1–15, 2017. doi: <https://doi.org/10.1088/1367-2630/aa5e47>.
- [5] C. D. West and A. S. Makas, 'The spectral dispersion of birefringence, especially of birefringent plastic sheets', *Journal of the Optical Society of America*, vol. 39, no. 9, pp. 791–794, 1949. doi: <https://doi.org/10.1364/JOSA.39.000791>.
- [6] M. G. Destriau and J. Prouteau, 'Réalisation d'un quart d'onde quasi achromatique par juxtaposition de deux lames cristallines de même nature', *Le Journal de Physique et le Radium*, vol. 10, no. 2, pp. 53–55, 1949. doi: <https://doi.org/10.1051/jphysrad:0194900100205300>.
- [7] S. Pancharatnam, 'Achromatic combinations of birefringent plates. Part i: An achromatic circular polarizer', *Proceedings of the Indian Academy of Sciences, Section A*, vol. 41, no. 4, pp. 130–136, 1955. [Online]. Available: <https://doi.org/10.1007/bf03047097>.
- [8] S. Pancharatnam, 'Achromatic combinations of birefringent plates. Part ii: An achromatic quarter-wp', *Proceedings of the Indian Academy of Sciences*, vol. 41, no. 4, pp. 137–144, 1955. [Online]. Available: <https://doi.org/10.1007/BF03047098>.
- [9] S. E. Harris, E. O. Ammann and I. C. Chang, 'Optical network synthesis using birefringent crystals. i. Synthesis of lossless networks of equal-length crystals', *Journal of the Optical Society of America*, vol. 54, no. 10, pp. 1267–1279, 1964. doi: <https://doi.org/10.1364/JOSA.54.001267>.
- [10] C. M. McIntyre and S. E. Harris, 'Achromatic wave plates for the visible spectrum', *Journal of the Optical Society of America*, vol. 58, no. 12, pp. 1575–1580, 1968. doi: <https://doi.org/10.1364/JOSA.58.001575>.
- [11] T. Peters, S. S. Ivanov, D. Englisch, A. A. Rangelov, N. V. Vitanov and T. Halfmann, 'Variable ultrabroadband and narrowband composite polarization retarders', *Applied Optics*, vol. 51, no. 31, pp. 7466–7474, 2012. doi: <https://doi.org/10.1364/AO.51.007466>.
- [12] S. S. Ivanov, A. A. Rangelov, N. V. Vitanov, T. Peters and T. Halfmann, 'Highly efficient broadband conversion of light polarization by composite retarders', *Journal of the Optical Society of America A*, vol. 29, no. 3, pp. 265–269, 2012. doi: <https://doi.org/10.1364/JOSAA.29.000265>.
- [13] E. S. Dimova, S. S. Ivanov, G. S. Popkirov and N. V. Vitanov, 'Highly efficient broadband polarization retarders and tunable polarization filters made of composite stacks of ordinary wave plates', *Journal of the Optical Society of America A*, vol. 31, no. 5, pp. 952–956, 2014. doi: <https://doi.org/10.1364/JOSAA.31.000952>.
- [14] B. W. Shore, A. Rangelov, N. V. Vitanov and K. Bergmann, 'Piecewise adiabatic passage in polarization optics: An achromatic polarization rotator', *Advances in Chemical Physics*, vol. 159, pp. 219–234, 2016. doi: <https://doi.org/10.1002/9781119096276.ch5>.

- [15] S. Gulde, M. Riebe, G. P. T. Lancaster, C. Becher, J. Eschner, H. Häffner, F. Schmidt-Kaler, I. L. Chuang and R. Blatt, 'Implementation of the Deutsch–Jozsa algorithm on an ion-trap quantum computer', *Nature (London)*, vol. 421, no. 6918, pp. 48–50, 2003. doi: <https://doi.org/10.1038/nature01336>.
- [16] F. Schmidt-Kaler, H. Häffner, M. Riebe, S. Gulde, G. P. T. Lancaster, T. Deuschle, C. Becher, C. F. Roos, J. Eschner and R. Blatt, 'Realization of the Cirac–Zoller controlled-NOT quantum gate', *Nature (London)*, vol. 422, no. 6930, pp. 408–411, 2003. doi: <https://doi.org/10.1038/nature01494>.
- [17] H. Häffner, C. F. Roos and R. Blatt, 'Quantum computing with trapped ions', *Physics Reports*, vol. 469, no. 4, pp. 155–203, 2008. doi: <https://doi.org/10.1016/j.physrep.2008.09.003>.
- [18] N. Timoney, V. Elman, S. Glaser, C. Weiss, M. Johanning, W. Neuhauser and C. Wunderlich, 'Error-resistant single-qubit gates with trapped ions', *Physical Review A*, vol. 77, no. 5, pp. 052334, 1–7, 2008. doi: <https://doi.org/10.1103/PhysRevA.77.052334>.
- [19] T. Monz, K. Kim, W. Hänsel, M. Riebe, A. S. Villar, P. Schindler, M. Chwalla, M. Hennrich and R. Blatt, 'Realization of the quantum Toffoli gate with trapped ions', *Physical Review Letters*, vol. 102, no. 4, pp. 040501, 1–4, 2009. doi: <https://doi.org/10.1103/PhysRevLett.102.040501>.
- [20] G. Zarantonello, H. Hahn, J. Morgner, M. Schulte, A. Bautista-Salvador, R. F. Werner, K. Hammerer and C. Ospelkaus, 'Robust and resource-efficient microwave near-field entangling ${}^9\text{Be}^+$ gate', *Physical Review Letters*, vol. 123, no. 26, pp. 260503, 1–6, 2019. doi: <https://doi.org/10.1103/PhysRevLett.123.260503>.
- [21] C. M. Shappert, J. T. Merrill, K. R. Brown, J. M. Amini, C. Volin, S. C. Doret, H. Hayden, C.-S. Pai, K. R. Brown and A. W. Harter, 'Spatially uniform single-qubit gate operations with near-field microwaves and composite pulse compensation', *New Journal of Physics*, vol. 15, no. 8, pp. 083053, 1–12, 2013. doi: <https://doi.org/10.1088/1367-2630/15/8/083053>.
- [22] E. Mount, C. Kabytayev, S. Crain, R. Harper, S.-Y. Baek, G. Vrijsen, S. T. Flammia, K. R. Brown, P. Maunz and J. Kim, 'Error compensation of single-qubit gates in a surface-electrode ion trap using composite pulses', *Physical Review A*, vol. 92, no. 6, pp. 060301, 1–5, 2015. doi: <https://doi.org/10.1103/PhysRevA.92.060301>.
- [23] W. Rakreungdet, J. H. Lee, K. F. Lee, B. E. Mischuck, E. Montano and P. S. Jessen, 'Accurate microwave control and real-time diagnostics of neutral-atom qubits', *Physical Review A*, vol. 79, no. 2, pp. 022316, 1–9, 2009. doi: <https://doi.org/10.1103/PhysRevA.79.022316>.
- [24] D. Schraft, T. Halfmann, G. T. Genov and N. V. Vitanov, 'Experimental demonstration of composite adiabatic passage', *Physical Review A*, vol. 88, no. 6, pp. 063406, 1–9, 2013. doi: <https://doi.org/10.1103/PhysRevA.88.063406>.
- [25] G. T. Genov, D. Schraft, N. V. Vitanov and T. Halfmann, 'Arbitrarily accurate pulse sequences for robust dynamical decoupling', *Physical Review Letters*, vol. 118, no. 3, pp. 133202, 1–5, 2017. doi: <https://doi.org/10.1103/PhysRevLett.118.133202>.
- [26] A. Bruns, G. T. Genov, M. Hain, N. V. Vitanov and T. Halfmann, 'Experimental demonstration of composite stimulated Raman adiabatic passage', *Physical Review A*, vol. 98, no. 5, pp. 053413, 1–10, 2018. doi: <https://doi.org/10.1103/PhysRevA.98.053413>.
- [27] X. Wang, L. S. Bishop, J. P. Kestner, E. Barnes, K. Sun and S. D. Sarma, 'Composite pulses for robust universal control of singlet–triplet qubits', *Nature Communications*, vol. 3, pp. 997, 1–7, 2012. doi: <https://doi.org/10.1038/ncomms2003>.
- [28] J. P. Kestner, X. Wang, L. S. Bishop, E. Barnes and S. D. Sarma, 'Noise-resistant control for a spin qubit array', *Physical Review Letters*, vol. 110, no. 14, pp. 140502, 1–5, 2013. doi: <https://doi.org/10.1103/PhysRevLett.110.140502>.
- [29] X. Wang, L. S. Bishop, E. Barnes, J. P. Kestner and S. D. Sarma, 'Robust quantum gates for singlet–triplet spin qubits using composite pulses', *Physical Review A*, vol. 89, no. 2, pp. 022310, 1–20, 2014. doi: <https://doi.org/10.1103/PhysRevA.89.022310>.

- [30] C. Zhang, R. E. Throckmorton, X.-C. Yang, X. Wang, E. Barnes and S. D. Sarma, 'Randomized benchmarking of barrier versus tilt control of a singlet-triplet qubit', *Physical Review Letters*, vol. 118, no. 21, pp. 216802, 1–6, 2017. doi: <https://doi.org/10.1103/PhysRevLett.118.216802>.
- [31] G. T. Hickman, X. Wang, J. P. Kestner and S. D. Sarma, 'Dynamically corrected gates for an exchange-only qubit', *Physical Review B*, vol. 88, no. 16, pp. 161303, 1–5, 2013. doi: <https://doi.org/10.1103/PhysRevB.88.161303>.
- [32] K. Eng *et al.*, 'Isotopically enhanced triple-quantum-dot qubit', *Science Advances*, vol. 1, no. 4, e1500214, 1–7, 2015. doi: <https://doi.org/10.1126/sciadv.1500214>.
- [33] X. Rong, J. Geng, F. Shi, Y. Liu, K. Xu, W. Ma, F. Kong, Z. Jiang, Y. Wu and J. Du, 'Experimental fault-tolerant universal quantum gates with solid-state spins under ambient conditions', *Nature Communications*, vol. 6, pp. 8748, 1–7, 2015. doi: <https://doi.org/10.1038/ncomms9748>.
- [34] T. Zanon-Willette, R. Lefevre, R. Metzдорff, N. Sillitoe, S. Almonacil, M. Minissale, E. de Clercq, A. V. Taichenachev, V. I. Yudin and E. Arimondo, 'Composite laser-pulses spectroscopy for high-accuracy optical clocks: A review of recent progress and perspectives', *Reports on Progress in Physics*, vol. 81, pp. 094401, 1–35, 2018. doi: <https://doi.org/10.1088/1361-6633/aac9e9>.
- [35] D. L. Butts, K. Kotru, J. M. Kinast, A. M. Radojevic, B. P. Timmons and R. E. Stoner, 'Efficient broadband Raman pulses for large-area atom interferometry', *Journal of the Optical Society of America B*, vol. 30, no. 4, pp. 922–927, 2013. doi: <https://doi.org/10.1364/JOSAB.30.000922>.
- [36] A. Dunning, R. Gregory, J. Bateman, N. Cooper, M. Himsworth, J. A. Jones and T. Freegarde, 'Composite pulses for interferometry in a thermal cold atom cloud', *Physical Review A*, vol. 90, no. 3, pp. 033608, 1–10, 2014. doi: <https://doi.org/10.1103/PhysRevA.90.033608>.
- [37] P. Berg, S. Abend, G. Tackmann, C. Schubert, E. Giese, W. P. Schleich, F. A. Narducci, W. Ertmer and E. M. Rasel, 'Composite-light-pulse technique for high-precision atom interferometry', *Physical Review Letters*, vol. 114, no. 6, pp. 063002, 1–5, 2015. doi: <https://doi.org/10.1103/PhysRevLett.114.063002>.
- [38] G. Demeter, 'Composite pulses for high-fidelity population inversion in optically dense, inhomogeneously broadened atomic ensembles', *Physical Review A*, vol. 93, no. 2, pp. 023830, 1–8, 2016. doi: <https://doi.org/10.1103/PhysRevA.93.023830>.
- [39] C. D. Aiello, M. Hirose and P. Cappellaro, 'Composite-pulse magnetometry with a solid-state quantum sensor', *Nature Communications*, vol. 4, pp. 1419, 1–6, 2013. doi: <https://doi.org/10.1038/ncomms2375>.
- [40] C. Ventura-Velázquez, B. J. Ávila, E. Kyoseva and B. M. Rodríguez-Lara, 'Robust optomechanical state transfer under composite phase driving', *Scientific Reports*, vol. 9, no. 1, pp. 4382, 1–10, 2019. doi: <https://doi.org/10.1038/s41598-019-40492-y>.
- [41] R. Tycko, 'Broadband population inversion', *Physical Review Letters*, vol. 51, no. 9, pp. 775–777, 1983. doi: <https://doi.org/10.1103/physrevlett.51.775>.
- [42] H. K. Cummins, G. Llewellyn and J. A. Jones, 'Tackling systematic errors in quantum logic gates with composite rotations', *Physical Review A*, vol. 67, no. 4, pp. 042308, 1–6, 2003. doi: <https://doi.org/10.1103/PhysRevA.67.042308>.
- [43] R. Tycko, H. M. Cho, E. Schneider and A. Pines, 'Composite pulses without phase distortion', *Journal of Magnetic Resonance*, vol. 61, no. 1, pp. 90–101, 1985. doi: [https://doi.org/10.1016/0022-2364\(85\)90270-7](https://doi.org/10.1016/0022-2364(85)90270-7).
- [44] M. H. Levitt, 'Composite pulses', *Progress in Nuclear Magnetic Resonance Spectroscopy*, vol. 18, no. 2, pp. 61–122, 1986. doi: [https://doi.org/10.1016/0079-6565\(86\)80005-x](https://doi.org/10.1016/0079-6565(86)80005-x).
- [45] M. H. Levitt, 'Composite pulses', *Encyclopedia of Magnetic Resonance*, pp. 1–16, 2007. doi: <https://doi.org/10.1002/9780470034590.emrstm0086>.

- [46] J. T. Merrill and K. R. Brown, 'Progress in compensating pulse sequences for quantum computation', *Advances in Chemical Physics: Quantum Information and Computation for Chemistry*, vol. 154, pp. 241–294, 2014. DOI: <https://doi.org/10.1002/9781118742631.ch10>.
- [47] B. T. Torosov and N. V. Vitanov, 'Arbitrarily accurate variable rotations on the Bloch sphere by composite pulse sequences', *Physical Review A*, vol. 99, no. 1, pp. 013402, 1–10, 2019. DOI: <https://doi.org/10.1103/PhysRevA.99.013402>.
- [48] H. L. Gevorgyan and N. V. Vitanov, 'Ultrahigh-fidelity composite rotational quantum gates', *Physical Review A*, vol. 104, no. 1, pp. 012609, 1–12, 2021. DOI: <https://doi.org/10.1103/PhysRevA.104.012609>.
- [49] K. R. Brown, A. W. Harrow and I. L. Chuang, 'Arbitrarily accurate composite pulse sequences', *Physical Review A*, vol. 70, no. 5, pp. 052318, 1–4, 2004. DOI: <https://doi.org/10.1103/PhysRevA.70.052318>.
- [50] T. Ichikawa, M. Bando, Y. Kondo and M. Nakahara, 'Geometric aspects of composite pulses', *Philosophical Transactions of The Royal Society A*, vol. 370, no. 1976, pp. 4671–4689, 2012. DOI: <https://doi.org/10.1098/rsta.2011.0358>.
- [51] Y. Kondo and M. Bando, 'Geometric quantum gates, composite pulses, and trotter-suzuki formulas', *Journal of the Physical Society of Japan*, vol. 80, no. 5, pp. 054002, 1–4, 2011. DOI: <https://doi.org/10.1143/jpsj.80.054002>.
- [52] A. Y. Kitaev, A. H. Shen and M. N. Vyalyi, *Classical and Quantum Computation*. American Mathematical Society: Graduate Studies in Mathematics Series, 2002.
- [53] S. Odedra and S. Wimperis, 'Use of composite refocusing pulses to form spin echoes', *Journal of Magnetic Resonance*, vol. 214, pp. 68–75, 2012. DOI: <https://doi.org/10.1016/j.jmr.2011.10.006>.
- [54] S. Wimperis, 'Iterative schemes for phase-distortionless composite 180° pulses', *Journal of Magnetic Resonance*, vol. 93, no. 1, pp. 199–206, 1999. DOI: [https://doi.org/10.1016/0022-2364\(91\)90043-s](https://doi.org/10.1016/0022-2364(91)90043-s).
- [55] S. Husain, M. Kawamura and J. A. Jones, 'Further analysis of some symmetric and antisymmetric composite pulses for tackling pulse strength errors', *Journal of Magnetic Resonance*, vol. 230, pp. 145–154, 2013. DOI: <https://doi.org/10.1016/j.jmr.2013.02.007>.
- [56] S. Odedra and S. Wimperis, 'Improved background suppression in ¹H MAS NMR using composite pulses', *Journal of Magnetic Resonance*, vol. 221, pp. 41–50, 2012. DOI: <https://doi.org/10.1016/j.jmr.2012.05.010>.
- [57] G. H. Low, T. J. Yoder and I. L. Chuang, 'Methodology of resonant equiangular composite quantum gates', *Physical Review X*, vol. 6, no. 4, pp. 041067, 1–13, 2016. DOI: <https://doi.org/10.1103/PhysRevX.6.041067>.
- [58] M. Bando, T. Ichikawa, Y. Kondo and M. Nakahara, 'Concatenated composite pulses compensating simultaneous systematic errors', *Journal of the Physical Society of Japan*, vol. 82, no. 1, pp. 014004, 1–7, 2013. DOI: <https://doi.org/10.7566/JPSJ.82.014004>.
- [59] M. Bando, T. Ichikawa, Y. Kondo, N. Nemoto, M. Nakahara and Y. Shikano, 'Concatenated composite pulses applied to liquid-state nuclear magnetic resonance spectroscopy', *Scientific Reports*, vol. 10, no. 1, pp. 2126, 1–10, 2020. DOI: <https://doi.org/10.1038/s41598-020-58823-9>.
- [60] H. L. Gevorgyan and N. V. Vitanov, 'Ultrahigh-fidelity composite quantum phase gates', *arXiv:2306.10340 [quant-ph]*, 2023. DOI: <https://doi.org/10.48550/arXiv.2306.10340>.
- [61] H. L. Gevorgyan, 'Ultrabroadband and ultranarrowband composite polarization half-waveplates', in *Compact EUV & X-ray Light Sources, Optica High-brightness Sources and Light-driven Interactions Congress*, Technical Digest Series (Optica Publishing Group), 2022, EF3A–5, 1–2. DOI: <https://doi.org/10.1364/EUVXRAY.2022.EF3A.5>.
- [62] H. L. Gevorgyan, A. A. Rangelov and N. V. Vitanov, 'Broadband composite nonreciprocal polarization wave plates and optical isolators', *arXiv:2305.06431 [physics.optics]*, 2023. DOI: <https://doi.org/10.48550/arXiv.2305.06431>.

- [63] L. M. K. Vandersypen and I. L. Chuang, 'NMR techniques for quantum control and computation', *Reviews of Modern Physics*, vol. 76, no. 4, pp. 1037–1069, 2005. doi: <https://doi.org/10.1103/revmodphys.76.1037>.
- [64] J. A. Jones, 'Quantum computing with NMR', *Progress in Nuclear Magnetic Resonance Spectroscopy*, vol. 59, no. 2, pp. 91–120, 2011. doi: <https://doi.org/10.1016/j.pnmrs.2010.11.001>.
- [65] N. V. Vitanov, T. Halfmann, B. W. Shore and K. Bergmann, 'Laser-induced population transfer by adiabatic passage techniques', *Annual Review of Physical Chemistry*, vol. 52, no. 1, pp. 763–809, 2001. doi: <https://doi.org/10.1146/annurev.physchem.52.1.763>.
- [66] L. D. Landau, 'Zur theorie der energieubertragung ii', *Physikalische Zeitschrift der Sowjetunion*, vol. 2, pp. 46–51, 1932.
- [67] E. Majorana, 'Atomi orientati in campo magnetico variabile', *Il Nuovo Cimento (1924-1942)*, vol. 9, no. 2, pp. 43–50, 1932. doi: <https://doi.org/10.1007/BF02960953>.
- [68] E. C. G. Stückelberg, 'Theorie der unelastischen Stösse zwischen Atomen', *Helvetica Physica Acta*, vol. 5, p. 369, 1932.
- [69] C. Zener, 'Non-adiabatic crossing of energy levels', *Proceedings of the Royal Society A: Mathematical, Physical and Engineering Sciences*, vol. 137, no. 833, pp. 696–702, 1932. doi: <https://doi.org/10.1098/rspa.1932.0165>.
- [70] L. P. Yatsenko, N. V. Vitanov, B. W. Shore, T. Rickes and K. Bergmann, 'Creation of coherent superpositions using Stark-chirped rapid adiabatic passage', *Optics Communications*, vol. 204, no. 1-6, pp. 413–423, 2002. doi: [https://doi.org/10.1016/S0030-4018\(02\)01303-2](https://doi.org/10.1016/S0030-4018(02)01303-2).
- [71] N. V. Vitanov and B. W. Shore, 'Stimulated Raman adiabatic passage in a two-state system', *Physical Review A*, vol. 73, no. 5, pp. 053402, 1–4, 2006. doi: <https://doi.org/10.1103/physreva.73.053402>.
- [72] R. Yamazaki, K.-i. Kanda, F. Inoue, K. Toyoda and S. Urabe, 'Robust generation of superposition states', *Physical Review A*, vol. 78, no. 2, pp. 023808, 1–6, 2008. doi: <https://doi.org/10.1103/physreva.78.023808>.
- [73] K. N. Zlatanov and N. V. Vitanov, 'Adiabatic generation of arbitrary coherent superpositions of two quantum states: Exact and approximate solutions', *Physical Review A*, vol. 96, no. 1, pp. 013415, 1–10, 2017. doi: <https://doi.org/10.1103/physreva.96.013415>.
- [74] J. Randall, A. M. Lawrence, S. C. Webster, S. Weidt, N. V. Vitanov and W. K. Hensinger, 'Generation of high-fidelity quantum control methods for multilevel systems', *Physical Review A*, vol. 98, no. 4, pp. 043414, 1–9, 2018. doi: <https://doi.org/10.1103/physreva.98.043414>.
- [75] N. V. Vitanov, A. A. Rangelov, B. W. Shore and K. Bergmann, 'Stimulated Raman adiabatic passage in physics, chemistry, and beyond', *Reviews of Modern Physics*, vol. 89, no. 1, pp. 015006, 1–66, 2017. doi: <https://doi.org/10.1103/revmodphys.89.015006>.
- [76] K. N. Zlatanov and N. V. Vitanov, 'Generation of arbitrary qubit states by adiabatic evolution split by a phase jump', *Physical Review A*, vol. 101, no. 1, pp. 013426, 1–9, 2020. doi: <https://doi.org/10.1103/physreva.101.013426>.
- [77] P. Marte, P. Zoller and J. L. Hall, 'Coherent atomic mirrors and beam splitters by adiabatic passage in multilevel systems', *Physical Review A*, vol. 44, no. 7, pp. R4118–R4121, 1991. doi: <https://doi.org/10.1103/physreva.44.r4118>.
- [78] M. Weitz, B. C. Young and S. Chu, 'Atomic interferometer based on adiabatic population transfer', *Physical Review Letters*, vol. 73, no. 19, pp. 2563–2566, 1994. doi: <https://doi.org/10.1103/PhysRevLett.73.2563>.
- [79] N. V. Vitanov, K. A. Suominen and B. W. Shore, 'Creation of coherent atomic superpositions by fractional stimulated Raman adiabatic passage', *Journal of Physics B: Atomic, Molecular and Optical Physics*, vol. 32, no. 18, pp. 4535–4546, 1999. doi: <https://doi.org/10.1088/0953-4075/32/18/312>.

- [80] R. Unanyan, M. Fleischhauer, B. W. Shore and K. Bergmann, 'Robust creation and phase-sensitive probing of superposition states via stimulated Raman adiabatic passage (STIRAP) with degenerate dark states', *Optics Communications*, vol. 155, no. 1-3, pp. 144–154, 1998. doi: [https://doi.org/10.1016/S0030-4018\(98\)00358-7](https://doi.org/10.1016/S0030-4018(98)00358-7).
- [81] H. Theuer, R. G. Unanyan, C. Habscheid, K. Klein and K. Bergmann, 'Novel laser controlled variable matter wave beamsplitter', *Optics Express*, vol. 4, no. 2, pp. 77–83, 1999. doi: <https://doi.org/10.1364/oe.4.000077>.
- [82] F. Vewinger, M. Heinz, R. G. Fernandez, N. V. Vitanov and K. Bergmann, 'Creation and measurement of a coherent superposition of quantum states', *Physical Review Letters*, vol. 91, no. 21, pp. 213001, 1–4, 2003. doi: <https://doi.org/10.1103/physrevlett.91.213001>.
- [83] P. A. Ivanov, B. T. Torosov and N. V. Vitanov, 'Navigation between quantum states by quantum mirrors', *Physical Review A*, vol. 75, no. 1, pp. 012323, 1–9, 2007. doi: <https://doi.org/10.1103/physreva.75.012323>.
- [84] B. Rousseaux, S. Guérin and N. V. Vitanov, 'Arbitrary qudit gates by adiabatic passage', *Physical Review A*, vol. 87, no. 3, pp. 032328, 1–4, 2013. doi: <https://doi.org/10.1103/physreva.87.032328>.
- [85] M. H. Levitt and R. Freeman, 'NMR population inversion using a composite pulse', *Journal of Magnetic Resonance (1969)*, vol. 33, no. 2, pp. 473–476, 1979. doi: [https://doi.org/10.1016/0022-2364\(79\)90265-8](https://doi.org/10.1016/0022-2364(79)90265-8).
- [86] R. Freeman, S. P. Kempell and M. H. Levitt, 'Radiofrequency pulse sequences which compensate their own imperfections', *Journal of Magnetic Resonance (1969)*, vol. 38, no. 3, pp. 453–479, 1980. doi: [https://doi.org/10.1016/0022-2364\(80\)90327-3](https://doi.org/10.1016/0022-2364(80)90327-3).
- [87] M. H. Levitt, 'Symmetrical composite pulse sequences for NMR population inversion. i. Compensation of radiofrequency field inhomogeneity', *Journal of Magnetic Resonance (1969)*, vol. 48, no. 2, pp. 234–264, 1982. doi: [https://doi.org/10.1016/0022-2364\(82\)90275-X](https://doi.org/10.1016/0022-2364(82)90275-X).
- [88] M. H. Levitt and R. R. Ernst, 'Composite pulses constructed by a recursive expansion procedure', *Journal of Magnetic Resonance (1969)*, vol. 55, no. 2, pp. 247–254, 1983. doi: [https://doi.org/10.1016/0022-2364\(83\)90236-6](https://doi.org/10.1016/0022-2364(83)90236-6).
- [89] S. Wimperis, 'Broadband and narrowband composite excitation sequences', *Journal of Magnetic Resonance (1969)*, vol. 86, no. 1, pp. 46–59, 1990. doi: [https://doi.org/10.1016/0022-2364\(90\)90210-z](https://doi.org/10.1016/0022-2364(90)90210-z).
- [90] S. Wimperis, 'Iterative schemes for phase-distortionless composite 180° pulses', *Journal of Magnetic Resonance (1969)*, vol. 93, no. 1, pp. 199–206, 1991. doi: [https://doi.org/10.1016/0022-2364\(91\)90043-s](https://doi.org/10.1016/0022-2364(91)90043-s).
- [91] B. T. Torosov and N. V. Vitanov, 'Smooth composite pulses for high-fidelity quantum information processing', *Physical Review A*, vol. 83, no. 5, pp. 053420, 1–7, 2011. doi: <https://doi.org/10.1103/physreva.83.053420>.
- [92] B. T. Torosov, S. Guérin and N. V. Vitanov, 'High-fidelity adiabatic passage by composite sequences of chirped pulses', *Physical Review Letters*, vol. 106, no. 23, pp. 233001, 1–4, 2011. doi: <https://doi.org/10.1103/PhysRevLett.106.233001>.
- [93] G. T. Genov, D. Schraft, T. Halfmann and N. V. Vitanov, 'Correction of arbitrary field errors in population inversion of quantum systems by universal composite pulses', *Physical Review Letters*, vol. 113, no. 4, pp. 043001, 1–5, 2014. doi: <https://doi.org/10.1103/physrevlett.113.043001>.
- [94] R. Tycko and A. Pines, 'Iterative schemes for broad-band and narrow-band population inversion in NMR', *Chemical Physics Letters*, vol. 111, no. 4-5, pp. 462–467, 1984. doi: [https://doi.org/10.1016/0009-2614\(84\)85541-4](https://doi.org/10.1016/0009-2614(84)85541-4).
- [95] R. Tycko, A. Pines and J. Guckenheimer, 'Fixed point theory of iterative excitation schemes in NMR', *The Journal of Chemical Physics*, vol. 83, no. 6, pp. 2775–2802, 1985. doi: <https://doi.org/10.1063/1.449228>.

- [96] A. J. Shaka and R. Freeman, 'Spatially selective radiofrequency pulses', *Journal of Magnetic Resonance (1969)*, vol. 59, no. 1, pp. 169–176, 1984. doi: [https://doi.org/10.1016/0022-2364\(84\)90297-x](https://doi.org/10.1016/0022-2364(84)90297-x).
- [97] N. V. Vitanov, 'Arbitrarily accurate narrowband composite pulse sequences', *Physical Review A*, vol. 84, no. 6, pp. 065404, 1–4, 2011. doi: <https://doi.org/10.1103/physreva.84.065404>.
- [98] S. S. Ivanov and N. V. Vitanov, 'High-fidelity local addressing of trapped ions and atoms by composite sequences of laser pulses', *Optics Letters*, vol. 36, no. 7, pp. 1275–1277, 2011. doi: <https://doi.org/10.1364/ol.36.001275>.
- [99] B. T. Torosov, S. S. Ivanov and N. V. Vitanov, 'Narrowband and passband composite pulses for variable rotations', *Physical Review A*, vol. 102, no. 1, pp. 013105, 1–6, 2020. doi: <https://doi.org/10.1103/physreva.102.013105>.
- [100] H. M. Cho, R. Tycko, A. Pines and J. Guckenheimer, 'Iterative maps for bistable excitation of two-level systems', *Physical Review Letters*, vol. 56, no. 18, pp. 1905–1908, 1986. doi: <https://doi.org/10.1103/PhysRevLett.56.1905>.
- [101] H. Cho, J. Baum and A. Pines, 'Iterative maps with multiple fixed points for excitation of two level systems', *The Journal of Chemical Physics*, vol. 86, no. 6, pp. 3089–3106, 1987. doi: <https://doi.org/10.1063/1.452020>.
- [102] S. Wimperis, 'Composite pulses with rectangular excitation and inversion profiles', *Journal of Magnetic Resonance (1969)*, vol. 83, no. 3, pp. 509–524, 1989. doi: [https://doi.org/10.1016/0022-2364\(89\)90346-6](https://doi.org/10.1016/0022-2364(89)90346-6).
- [103] E. Kyoseva and N. V. Vitanov, 'Arbitrarily accurate passband composite pulses for dynamical suppression of amplitude noise', *Physical Review A*, vol. 88, no. 6, pp. 063410, 1–7, 2013. doi: <https://doi.org/10.1103/PhysRevA.88.063410>.
- [104] E. Stoyanova, M. Al-Mahmoud, H. Hristova, A. Rangelov, E. Dimova and N. V. Vitanov, 'Achromatic polarization rotator with tunable rotation angle', *Journal of Optics*, vol. 21, no. 10, pp. 105403, 1–5, 2019. doi: <https://doi.org/10.1088/2040-8986/ab40fc>.
- [105] M. Al-Mahmoud, V. Coda, A. Rangelov and G. Montemezzani, 'Broadband polarization rotator with tunable rotation angle composed of three wave plates', *Physical Review Applied*, vol. 13, no. 1, pp. 014048, 1–10, 2020. doi: <https://doi.org/10.1103/PhysRevApplied.13.014048>.
- [106] S. Odedra, M. J. Thrippleton and S. Wimperis, 'Dual-compensated antisymmetric composite refocusing pulses for NMR', *Journal of Magnetic Resonance*, vol. 225, pp. 81–92, 2012. doi: <https://doi.org/10.1016/j.jmr.2012.10.003>.
- [107] J. A. Jones, 'Designing short robust NOT gates for quantum computation', *Physical Review A*, vol. 87, no. 5, pp. 052317, 1–11, 2013. doi: <https://doi.org/10.1103/physreva.87.052317>.
- [108] J. A. Jones, 'Nested composite NOT gates for quantum computation', *Physics Letters A*, vol. 377, no. 40, pp. 2860–2862, 2013. doi: <https://doi.org/10.1016/j.physleta.2013.08.040>.
- [109] B. T. Torosov and N. V. Vitanov, 'High-fidelity error-resilient composite phase gates', *Physical Review A*, vol. 90, no. 1, pp. 012341, 1–5, 2014. doi: <https://doi.org/10.1103/physreva.90.012341>.
- [110] J. A. Jones, 'Robust Ising gates for practical quantum computation', *Physical Review A*, vol. 67, no. 1, pp. 012317, 1–3, 2003. doi: <https://doi.org/10.1103/physreva.67.012317>.
- [111] J. A. Jones, 'Suppressing weak Ising couplings: Tailored gates for quantum computation', *Physics Letters A*, vol. 316, no. 1-2, pp. 24–28, 2003. doi: [https://doi.org/10.1016/s0375-9601\(03\)01130-7](https://doi.org/10.1016/s0375-9601(03)01130-7).
- [112] L. Xiao and J. A. Jones, 'Robust logic gates and realistic quantum computation', *Physical Review A*, vol. 73, no. 3, pp. 032334, 1–5, 2006. doi: <https://doi.org/10.1103/physreva.73.032334>.
- [113] W. G. Alway and J. A. Jones, 'Arbitrary precision composite pulses for NMR quantum computing', *Journal of Magnetic Resonance*, vol. 189, no. 1, pp. 114–120, 2007. doi: <https://doi.org/10.1016/j.jmr.2007.09.001>.

- [114] C. D. Hill, 'Robust controlled-NOT gates from almost any interaction', *Physical Review Letters*, vol. 98, no. 18, pp. 180501, 1–4, 2007. DOI: <https://doi.org/10.1103/PhysRevLett.98.180501>.
- [115] M. J. Testolin, C. D. Hill, C. J. Wellard and L. C. L. Hollenberg, 'Robust controlled-NOT gate in the presence of large fabrication-induced variations of the exchange interaction strength', *Physical Review A*, vol. 76, no. 1, pp. 012302, 1–8, 2007. DOI: <https://doi.org/10.1103/PhysRevA.76.012302>.
- [116] S. S. Ivanov and N. V. Vitanov, 'Composite two-qubit gates', *Physical Review A*, vol. 92, no. 2, pp. 022333, 1–8, 2015. DOI: <https://doi.org/10.1103/PhysRevA.92.022333>.
- [117] S. S. Ivanov and N. V. Vitanov, 'Scalable uniform construction of highly conditional quantum gates', *Physical Review A*, vol. 84, no. 2, pp. 022319, 1–5, 2011. DOI: <https://doi.org/10.1103/physreva.84.022319>.
- [118] B. T. Torosov and N. V. Vitanov, 'Composite pulses with errant phases', *Physical Review A*, vol. 100, no. 2, pp. 023410, 1–9, 2019. DOI: <https://doi.org/10.1103/PhysRevA.100.023410>.
- [119] A. A. Rangelov and E. Kyoseva, 'Broadband composite polarization rotator', *Optics Communications*, vol. 338, pp. 574–577, 2015. DOI: <https://doi.org/10.1016/j.optcom.2014.11.037>.
- [120] M. Steffen, J. M. Martinis and I. L. Chuang, 'Accurate control of Josephson phase qubits', *Physical Review B*, vol. 68, no. 22, pp. 224518, 1–9, 2003. DOI: <https://doi.org/10.1103/physrevb.68.224518>.
- [121] B. T. Torosov and N. V. Vitanov, 'Experimental demonstration of composite pulses on IBM's quantum computer', *Physical Review Applied*, vol. 18, no. 3, p. 034062, 2022. DOI: <https://doi.org/10.1103/PhysRevApplied.18.034062>.
- [122] S. S. Ivanov, B. T. Torosov and N. V. Vitanov, 'High-fidelity quantum control by polychromatic pulse trains', *Physical Review Letters*, vol. 129, no. 24, p. 240505, 2022. DOI: <https://doi.org/10.1103/PhysRevLett.129.240505>.
- [123] A. Abraham, *The Principles of Nuclear Magnetism*. Clarendon, Oxford, 1961.
- [124] R. Freeman, *Spin choreography: Basic steps in high resolution nmr*, 1997.
- [125] R. S. Said and J. Twamley, 'Robust control of entanglement in a nitrogen-vacancy center coupled to a ^{13}C nuclear spin in diamond', *Physical Review A*, vol. 80, no. 3, pp. 032303, 1–7, 2009. DOI: <https://doi.org/10.1103/physreva.80.032303>.
- [126] E. Collin, G. Ithier, A. Aassime, P. Joyez, D. Vion and D. Esteve, 'NMR-like control of a quantum bit superconducting circuit', *Physical Review Letters*, vol. 93, no. 15, pp. 157005, 1–4, 2004. DOI: <https://doi.org/10.1103/PhysRevLett.93.157005>.
- [127] C. M. Collins, Z. Wang, W. Mao, J. Fang, W. Liu and M. B. Smith, 'Array-optimized composite pulse for excellent whole-brain homogeneity in high-field MRI', *Magnetic Resonance in Medicine*, vol. 57, no. 3, pp. 470–474, 2007. DOI: <https://doi.org/10.1002/mrm.21172>.
- [128] H. K. Cummins and J. A. Jones, 'Use of composite rotations to correct systematic errors in NMR quantum computation', *New Journal of Physics*, vol. 2, no. 1, 6.1–6.12, 2000. DOI: <https://doi.org/10.1088/1367-2630/2/1/006>.
- [129] M. Riebe, H. Häffner, C. F. Roos, W. Hänsel, J. Benhelm, G. P. T. Lancaster, T. W. Körber, C. Becher, F. Schmidt-Kaler, D. F. V. James *et al.*, 'Deterministic quantum teleportation with atoms', *Nature*, vol. 429, no. 6993, pp. 734–737, 2004. DOI: <https://doi.org/10.1038/nature02570>.
- [130] M. D. Barrett, J. Chiaverini, T. Schaetz, J. Britton, W. M. Itano, J. D. Jost, E. Knill, C. Langer, D. Leibfried, R. Ozeri *et al.*, 'Deterministic quantum teleportation of atomic qubits', *Nature*, vol. 429, no. 6993, pp. 737–739, 2004. DOI: <https://doi.org/10.1038/nature02608>.
- [131] N. F. Scherer, R. J. Carlson, A. Matro, M. Du, A. J. Ruggiero, V. Romero-Rochin, J. A. Cina, G. R. Fleming and S. A. Rice, 'Fluorescence-detected wave packet interferometry: Time resolved molecular spectroscopy with sequences of femtosecond phase-locked pulses', *The Journal of Chemical Physics*, vol. 95, no. 3, pp. 1487–1511, 1991. DOI: <https://doi.org/10.1063/1.461064>.

- [132] X.-C. Yang, M.-H. Yung and X. Wang, 'Neural-network-designed pulse sequences for robust control of singlet-triplet qubits', *Physical Review A*, vol. 97, no. 4, pp. 042324, 1–9, 2018. doi: <https://doi.org/10.1103/PhysRevA.97.042324>.
- [133] B. W. Shore, *The Theory of Coherent Atomic Excitation*. Wiley, 1990.
- [134] B. W. Shore, *Manipulating Quantum Structures Using Laser Pulses*. Cambridge University Press, 2011.
- [135] D. Guéry-Odelin, A. Ruschhaupt, A. Kiely, E. Torrontegui, S. Martínez-Garaot and J. G. Muga, 'Shortcuts to adiabaticity: Concepts, methods, and applications', *Reviews of Modern Physics*, vol. 91, no. 4, pp. 045001, 1–54, 2019. doi: <https://doi.org/10.1103/revmodphys.91.045001>.
- [136] L.-M. Duan, M. D. Lukin, J. I. Cirac and P. Zoller, 'Long-distance quantum communication with atomic ensembles and linear optics', *Nature*, vol. 414, no. 6862, pp. 413–418, 2001. doi: <https://doi.org/10.1038/35106500>.
- [137] A. I. Lvovsky, B. C. Sanders and W. Tittel, 'Optical quantum memory', *Nature Photonics*, vol. 3, no. 12, pp. 706–714, 2009. doi: <https://doi.org/10.1038/nphoton.2009.231>.
- [138] N. Sangouard, C. Simon, H. de Riedmatten and N. Gisin, 'Quantum repeaters based on atomic ensembles and linear optics', *Reviews of Modern Physics*, vol. 83, no. 1, pp. 33–80, 2011. doi: <https://doi.org/10.1103/revmodphys.83.33>.
- [139] S.-J. Yang, X.-J. Wang, X.-H. Bao and J.-W. Pan, 'An efficient quantum light–matter interface with sub-second lifetime', *Nature Photonics*, vol. 10, no. 6, pp. 381–384, 2016. doi: <https://doi.org/10.1038/nphoton.2016.51>.
- [140] Y.-F. Pu, N. Jiang, W. Chang, H.-X. Yang, C. Li and L.-M. Duan, 'Experimental realization of a multiplexed quantum memory with 225 individually accessible memory cells', *Nature Communications*, vol. 8, pp. 15359, 1–6, 2017. doi: <https://doi.org/10.1038/ncomms15359>.
- [141] C. Laplane, P. Jobez, J. Etesse, N. Gisin and M. Afzelius, 'Multimode and long-lived quantum correlations between photons and spins in a crystal', *Physical Review Letters*, vol. 118, no. 21, pp. 210501, 1–5, 2017. doi: <https://doi.org/10.1103/physrevlett.118.210501>.
- [142] K. Kutluer, M. Mazzera and H. de Riedmatten, 'Solid-state source of nonclassical photon pairs with embedded multimode quantum memory', *Physical Review Letters*, vol. 118, no. 21, pp. 210502, 1–6, 2017. doi: <https://doi.org/10.1103/physrevlett.118.210502>.
- [143] N. Gisin and R. Thew, 'Quantum communication', *Nature Photonics*, vol. 1, no. 3, pp. 165–171, 2007. doi: <https://doi.org/10.1038/nphoton.2007.22>.
- [144] R. Ursin *et al.*, 'Entanglement-based quantum communication over 144 km', *Nature Physics*, vol. 3, no. 7, pp. 481–486, 2007. doi: <https://doi.org/10.1038/nphys629>.
- [145] H. J. Kimble, 'The quantum internet', *Nature*, vol. 453, no. 7198, pp. 1023–1030, 2008. doi: <https://doi.org/10.1038/nature07127>.
- [146] W. Zhang, D.-S. Ding, Y.-B. Sheng, L. Zhou, B.-S. Shi and G.-C. Guo, 'Quantum secure direct communication with quantum memory', *Physical Review Letters*, vol. 118, no. 22, pp. 220501, 1–6, 2017. doi: <https://doi.org/10.1103/physrevlett.118.220501>.
- [147] Y.-A. Chen *et al.*, 'An integrated space-to-ground quantum communication network over 4,600 kilometres', *Nature*, vol. 589, no. 7841, pp. 214–219, 2021. doi: <https://doi.org/10.1038/s41586-020-03093-8>.
- [148] P. Kok, W. J. Munro, K. Nemoto, T. C. Ralph, J. P. Dowling and G. J. Milburn, 'Linear optical quantum computing with photonic qubits', *Reviews of Modern Physics*, vol. 79, no. 1, pp. 135–174, 2007. doi: <https://doi.org/10.1103/revmodphys.79.135>.
- [149] S. Barz, 'Quantum computing with photons: Introduction to the circuit model, the one-way quantum computer, and the fundamental principles of photonic experiments', *Journal of Physics B: Atomic, Molecular and Optical Physics*, vol. 48, no. 8, pp. 083001, 1–25, 2015. doi: <https://doi.org/10.1088/0953-4075/48/8/083001>.

- [150] T. Rudolph, 'Why I am optimistic about the silicon-photon route to quantum computing', *APL Photonics*, vol. 2, no. 3, pp. 030901, 1–19, 2017. doi: <https://doi.org/10.1063/1.4976737>.
- [151] S. Takeda and A. Furusawa, 'Toward large-scale fault-tolerant universal photonic quantum computing', *APL Photonics*, vol. 4, no. 6, pp. 060902, 1–13, 2019. doi: <https://doi.org/10.1063/1.5100160>.
- [152] R. H. Dicke, 'Coherence in spontaneous radiation processes', *Physical Review*, vol. 93, no. 1, pp. 99–110, 1954. doi: <https://doi.org/10.1103/physrev.93.99>.
- [153] S. S. Ivanov, P. A. Ivanov and N. V. Vitanov, 'Simple implementation of a quantum search with trapped ions', *Physical Review A*, vol. 78, no. 3, pp. 030301, 1–4, 2008. doi: <https://doi.org/10.1103/physreva.78.030301>.
- [154] S. S. Ivanov, P. A. Ivanov, I. E. Linington and N. V. Vitanov, 'Scalable quantum search using trapped ions', *Physical Review A*, vol. 81, no. 4, pp. 042328, 1–6, 2010. doi: <https://doi.org/10.1103/physreva.81.042328>.
- [155] I. E. Linington, P. A. Ivanov and N. V. Vitanov, 'Quantum search in a nonclassical database of trapped ions', *Physical Review A*, vol. 79, no. 1, pp. 012322, 1–7, 2009. doi: <https://doi.org/10.1103/physreva.79.012322>.
- [156] G. Tóth, 'Detection of multipartite entanglement in the vicinity of symmetric Dicke states', *Journal of the Optical Society of America B*, vol. 24, no. 2, pp. 275–281, 2007. doi: <https://doi.org/10.1364/josab.24.000275>.
- [157] A. R. U. Devi, R. Prabhu and A. K. Rajagopal, 'Characterizing multiparticle entanglement in symmetric N -qubit states via negativity of covariance matrices', *Physical Review Letters*, vol. 98, no. 6, pp. 060501, 1–4, 2007. doi: <https://doi.org/10.1103/physrevlett.98.060501>.
- [158] J. K. Stockton, J. M. Geremia, A. C. Doherty and H. Mabuchi, 'Characterizing the entanglement of symmetric many-particle spin- $\frac{1}{2}$ systems', *Physical Review A*, vol. 67, no. 2, pp. 022112, 1–17, 2003. doi: <https://doi.org/10.1103/physreva.67.022112>.
- [159] M. Bourennane, M. Eibl, S. Gaertner, N. Kiesel, C. Kurtsiefer and H. Weinfurter, 'Entanglement persistency of multiphoton entangled states', *Physical Review Letters*, vol. 96, no. 10, pp. 100502, 1–4, 2006. doi: <https://doi.org/10.1103/physrevlett.96.100502>.
- [160] W. Dür, 'Multipartite entanglement that is robust against disposal of particles', *Physical Review A*, vol. 63, no. 2, pp. 020303, 1–4, 2001. doi: <https://doi.org/10.1103/physreva.63.020303>.
- [161] J. K. Stockton, R. van Handel and H. Mabuchi, 'Deterministic dicke-state preparation with continuous measurement and control', *Physical Review A*, vol. 70, no. 2, pp. 022106, 1–11, 2004. doi: <https://doi.org/10.1103/physreva.70.022106>.
- [162] C. Thiel, J. von Zanthier, T. Bastin, E. Solano and G. S. Agarwal, 'Generation of symmetric Dicke states of remote qubits with linear optics', *Physical Review Letters*, vol. 99, no. 19, pp. 193602, 1–4, 2007. doi: <https://doi.org/10.1103/physrevlett.99.193602>.
- [163] H. Häffner *et al.*, 'Scalable multiparticle entanglement of trapped ions', *Nature*, vol. 438, no. 7068, pp. 643–646, 2005. doi: <https://doi.org/10.1038/nature04279>.
- [164] D. B. Hume, C. W. Chou, T. Rosenband and D. J. Wineland, 'Preparation of Dicke states in an ion chain', *Physical Review A*, vol. 80, no. 5, pp. 052302, 1–5, 2009. doi: <https://doi.org/10.1103/physreva.80.052302>.
- [165] I. E. Linington and N. V. Vitanov, 'Robust creation of arbitrary-sized Dicke states of trapped ions by global addressing', *Physical Review A*, vol. 77, no. 1, pp. 010302(R), 1–4, 2008. doi: <https://doi.org/10.1103/physreva.77.010302>.
- [166] S. S. Ivanov, N. V. Vitanov and N. V. Korolkova, 'Creation of arbitrary Dicke and NOON states of trapped-ion qubits by global addressing with composite pulses', *New Journal of Physics*, vol. 15, no. 2, pp. 023039, 1–11, 2013. doi: <https://doi.org/10.1088/1367-2630/15/2/023039>.

- [167] X. Zou, K. Pahlke and W. Mathis, 'Generation of arbitrary superpositions of the Dicke states of excitons in optically driven quantum dots', *Physical Review A*, vol. 68, no. 3, pp. 034306, 1–4, 2003. DOI: <https://doi.org/10.1103/physreva.68.034306>.
- [168] N. Kiesel, C. Schmid, G. Toth, E. Solano and H. Weinfurter, 'Experimental observation of four-photon entangled Dicke state with high fidelity', *Physical Review Letters*, vol. 98, no. 6, pp. 063604, 1–4, 2007. DOI: <https://doi.org/10.1103/physrevlett.98.063604>.
- [169] H. K. Cummins, G. Llewellyn and J. A. Jones, 'Tackling systematic errors in quantum logic gates with composite rotations', *Physical Review A*, vol. 67, no. 4, pp. 042308, 1–7, 2003. DOI: <https://doi.org/10.1103/physreva.67.042308>.
- [170] A. Ardavan, 'Exploiting the Poincaré-Bloch symmetry to design high-fidelity broadband composite linear retarders', *New Journal of Physics*, vol. 9, no. 2, pp. 24, 1–8, 2007. DOI: <https://doi.org/10.1088/1367-2630/9/2/024>.
- [171] E. Hecht, *Optics (4th Edition)*. Addison Wesley, 2002.
- [172] M. Born and E. Wolf, *Principles of Optics: Electromagnetic Theory of Propagation, Interference and Diffraction of Light*. Pergamon, 1975.
- [173] M. A. Azzam and N. M. Bashara, *Ellipsometry and Polarized Light*. North Holland, 1977.
- [174] D. Goldstein and E. Collett, *Polarized Light*. CRC, 2003.
- [175] M. Al-Mahmoud, H. Hristova, V. Coda, A. A. Rangelov, N. V. Vitanov and G. Montemezzani, 'Non-reciprocal wave retarder based on optical rotators combination', *OSA Continuum*, vol. 4, no. 10, pp. 2695–2702, 2021. DOI: <https://doi.org/10.1364/OSAC.439325>.
- [176] A. Messaadi, M. M. Sánchez-López, A. Vargas, P. García-Martínez and I. Moreno, 'Achromatic linear retarder with tunable retardance', *Optics Letters*, vol. 43, no. 14, pp. 3277–3280, 2018. DOI: <https://doi.org/10.1364/OL.43.003277>.
- [177] A. B. Villaverde, D. A. Donatti and D. G. Bozinis, 'Terbium gallium garnet verdet constant measurements with pulsed magnetic field', *Journal of Physics C: Solid State Physics*, vol. 11, no. 12, pp. L495–L498, 1978. DOI: <https://doi.org/10.1088/0022-3719/11/12/004>.
- [178] X. Chen, B. Lavorel, J. P. Boquillon, R. Saint-Loup and M. Jannin, 'Optical rotary power at the resonance of the terbium ${}^7F_6 \rightarrow {}^5D_4$ line in terbium gallium garnet', *Solid-State Electronics*, vol. 42, no. 9, pp. 1765–1766, 1998. DOI: [https://doi.org/10.1016/S0038-1101\(98\)00163-4](https://doi.org/10.1016/S0038-1101(98)00163-4).
- [179] H. Yoshida, K. Tsubakimoto, Y. Fujimoto, K. Mikami, H. Fujita, N. Miyanaga, H. Nozawa, H. Yagi, T. Yanagitani, Y. Nagata *et al.*, 'Optical properties and Faraday effect of ceramic terbium gallium garnet for a room temperature Faraday rotator', *Optics Express*, vol. 19, no. 16, pp. 15 181–15 187, 2011. DOI: <https://doi.org/10.1364/OE.19.015181>.
- [180] J. S. Kim and J. K. Chang, 'Achromatic polarization rotator and circular polarizer consisting of two wave plates of the same material', *Journal of the Korean Physical Society*, vol. 48, no. 1, pp. 51–55, 2006.
- [181] L. Weller, K. Kleinbach, M. A. Zentile, S Knappe, I. Hughes and C. Adams, 'Optical isolator using an atomic vapor in the hyperfine Paschen-Back regime', *Optics Letters*, vol. 37, no. 16, pp. 3405–3407, 2012. DOI: <https://doi.org/10.1364/OL.37.003405>.

